UNDERSTANDING THE MECHANISMS OF MUSCLE ATROPHY

A DISSERTATION

SUBMITTED TO THE FACULTY OF

UNIVERSITY OF MINNESOTA

BY

HAIMING LIU

IN PARTIAL FULFILLMENT OF THE REQUIREMENTS

FOR THE DEGREE OF

DOCTOR OF PHILOSOPHY

DR. LADORA V. THOMPSON

JUNE, 2016

ACKNOWLEDGEMENTS

I would like to express my deepest gratitude to my academic advisor Dr. LaDora Thompson for her guidance and support during the past several years. Dr. LaDora Thompson has mentored me closely and patiently, instructing me in all the essential skills of being an independent researcher in academia, such as research design, data interpretation, lab management, scientific writing, presentations and teaching. With her guidance, I have been able to overcome all the challenging situations faced in the path to completing my doctoral study and finishing my dissertation work.

I also would like to give my sincerest thanks to Dr. Deborah Ferrington. As an expert in biochemistry and the study of the immunoproteasome, she taught me a great deal on the subject, and lent a depth of knowledge necessary for constructing the background of my dissertation study. Also, as a co-author and a committee member, she shared a wealth of technical resources, gave me valuable advice on my research, its design, problem-solving, structuring the discussion of results and in composing the manuscript in Chapter III.

Further, I would like to give thanks to all the other committee members, Drs. Dawn Lowe, LeAnn Snow and Edgar Arriaga, all of whom have giving me valuable advice since the very beginning of my dissertation study. Particularly, I am thankful to Dr. Dawn Lowe for providing me with his additional technical support and guidance.

I would like to thank the following co-authors, who collaborated on the manuscripts within this dissertation, and acknowledge their contributions: Drs. LaDora Thompson (the guarantor and the corresponding author for all these studies), Deborah Ferrington (research design, interpretation of results, and scientific review for Chapter III), Cory Baumann (scientific review for Chapter III; the primary author on the paper in Chapter IV), Ted Graber (data interpretation and scientific review for Chapter V), and Lisa Ferguson-Stegall (scientific review for Chapter V). Also, I would like to thank Drs. Dongmin Kwak and Russell Rogers for their review of the manuscript in Chapter IV.

I would like to thank and acknowledge the following individuals who also contributed to the studies demonstrated in Chapter III and IV, including: Rebecca Kapphahn of the

Ferrington lab for teaching me experimental techniques including qPCR and the proteasome activity assay; Dr. Nathan Schuld for giving me advises on the proteasome-related experiments; Tara Mader of the Lowe Lab for teaching me the tibial nerve transection; and, JingYing Zhang of the Thompson Lab for assistance with the Western blot preparation. Additionally, I'd like to thank Dr. Walter Low of the Department of Neurosurgery for the technical support, and, Briana K. Jones of the Program in Physical Therapy for the data collection of the study in Chapter V. Lastly I would like to thank Christopher Kerr for the review of the acknowledgements part.

DEDICATION

This thesis is dedicated to my family in China, including my dad, Liu Chuyang, my mom, Zhang Zimei, and my grandma, Chen Guanying.

ABSTRACT

Skeletal muscle mass is regulated by protein turnover, the balance between protein synthesis and degradation. Muscle atrophy or a loss of muscle mass occurs when protein degradation exceeds protein synthesis, under conditions such as denervation and aging. Muscle atrophy is usually accompanied with reduced muscle contractility that lead to impaired physical activities and decreased quality of life. As a result, understanding the cellular and molecular mechanisms underlying the protein turnover is important to provide potential interventions and treatments for individuals suffered from muscle atrophy.

In skeletal muscle the majority of the proteins are degraded by the ubiquitin-proteasome system (UPS). The core of this system is called proteasome, which works as a "garbage disposal" for the degradation of the myofibrillar proteins via specific enzymatic activities. The immunoproteasome, an inducible form of proteasome, also has a function of performing proteasome enzymatic activities primarily demonstrated in the immune system (generate peptides for antigen presentation). However, the role of the immunoproteasome during skeletal muscle protein degradation is unknown. Therefore, the *purpose* of the first study was to investigate the role of the standard and immuno-proteasome in denervation-induced protein degradation in skeletal muscle. In this study, wild type (WT) and the immunoproteasome deficient (*lmp7*$^{-/-}$*/mecl-1*$^{-/-}$ double knockout, L7M1) mice were used to test the *hypotheses* that (1) the proteasome system is activated in denervation-induced muscle atrophy and (2) deletion of immunoproteasome subunits attenuates muscle atrophy by altering the proteasome composition and activities. Three major findings were found: following 7 and 14 days of denervation (1) an activation of the proteasome system occurs in conjunction with significant muscle atrophy in the WT mice; (2) the composition of the subunits within the 20S core appears to be influenced by deletion of the two immunoproteasome subunits; (3) however, the immunoproteasome was not essential for protein degradation induced by denervation.

The *purpose* of the next study was to elucidate the physiological properties of skeletal muscle in response to denervation with a *hypothesis* that the UPS is a finely-tuned system

that degrades myofibrillar proteins without impairing the contractility of the intact myosin and actin. We found an activation of the UPS accompanied with decreases in muscle size and force production post 14-day denervation. Importantly, the specific force and power were not impaired in the denervated muscles when compared to the controls. These results suggest that an activation of the UPS is associated with reductions in skeletal muscle quantity rather than quality.

Frailty is a clinical syndrome, which is highly associated with sarcopenia, leads to adverse health outcomes, and increased mortalities. Animal models have the potential to tease out the cellular mechanisms underlying frailty. The *purpose* of the third study in this dissertation is to initiate the development of a Frailty Index in 27- to 28-month-old C57BL/6 mice that matches the established clinical frailty phenotype index in humans (weakness, slow walking speed, low activity level, poor endurance) [1]. A frail or mildly-frail mouse was identified if presented ≥ three or two frailty criteria, respectively. From this study, we showed that one mouse was identified as frail and one was mildly-frail. This prevalence of 9% frailty is consistent with the prevalence of frailty in humans at the same survival age (11% frailty in human at age of 76-84[1]). This work has been published in *The Journals of Gerontology. Series A: Biological Sciences and Medical Sciences.*

TABLE OF CONTENTS

LIST OF TABLES

Chapter II

Chapter III

Chapter IV

Chapter V

LIST OF FIGURES

Chapter II

Interlude I

Chapter III

Interlude II

Chapter IV

Chapter V

CHAPTER I. INTRODUCTION

Skeletal muscle is one of the most important tissues in the human body because of the many diverse functions. The four diverse functions of skeletal muscle include producing movement, supporting organs, maintaining body temperature and storing nutrients. One important characteristic of skeletal muscle is its ability to adapt to stimuli. One obvious adaptation is the muscle's ability to change in size or mass, either increase or decrease. The loss of muscle mass is defined as muscle atrophy, which is also accompanied with a decrease in muscle strength, and leads to impaired physical activities. The major cellular process underlying muscle atrophy is altered protein turnover where the protein degradation exceeds protein synthesis. Understanding how the mechanisms of protein turnover are fine-tuned has potential to provide gene or protein targets to prevent muscle atrophy. The findings from basic biological and physiological studies may assist with the development of translational studies that may impact future clinical practice.

In skeletal muscle there are three major systems that contribute to protein degradation including ubiquitin-proteasome system (UPS), autophagy/lysosomal system, and the Ca^{2+} -dependent calpain system. These systems have been investigated in various conditions of muscle atrophy such as denervation, immobilization and aging. The UPS is known for its role in the degradation of the myofibrillar proteins within the sarcomere. In fact, myosin and actin are first disassembled from the sarcomere and ubiquitinated by E3 ligases (e.g. MuRF1); then transferred to the proteasome and degraded by the catalytic subunits in the 20S core of the proteasome. An inducible form of the proteasome is the immunoproteasome, which has been extensively studied for its immune function. However, the role of the immunoproteasome in skeletal muscle atrophy is not clear. The immunoproteasome deficient mouse model provides an exceptional opportunity to elucidate the role of the immunoproteasome during the process of protein degradation following denervation. Chapter III highlights the role of the immunoproteasome following denervation of 7 days and 14 days.

Because one of the main functions of skeletal muscle is to produce movement Chapter IV describes the contractile properties at 14 days following denervation. At 14 days there is

significant muscle atrophy and the UPS system continues to be activated. Currently, it is unknown if this UPS activation alters skeletal muscle contractile *quality.*

Having a physical therapy and rehabilitation education background, one of my long-term goals is to design rehabilitation and pharmacological interventions with translational potential in humans who suffer from severe muscle atrophy. Sarcopenia is a condition with severe muscle atrophy. Sarcopenia is defined as age-related muscle atrophy and this condition is becoming more critical each day. One of the most important reasons for the criticalness of sarcopenia is that it promotes adverse health outcomes, such as falls and fractures, and enhances the progression of *frailty*. Frailty is a clinical syndrome with several age-related deficits, such as increased vulnerability, declined physiological and physical functions; which finally leads to a higher risk of morbidity and mortality [2,3]. Frailty and sarcopenia are like two evil friends walking hand in hand and come to visit when an individual is getting old and becoming vulnerable.

Because of the deleterious outcomes of sarcopenia and frailty, there is a need to perform interventions or treatments as early as possible. The development of efficacious interventions requires understanding the cellular, molecular, and physiological properties. The mouse model provides the possibility of investigating these properties. In the past decade, the field of frailty lacks a clinically-relevant non-invasive index in mice. Chapter V highlights the development of a mouse Frailty Index that mimics the clinical frailty phenotype index.

To provide the background information for the two major areas within this dissertation (denervation-induced muscle atrophy and Frailty Index for mice), I review the structure, function, and adaptation (atrophy) of skeletal muscle. Then I review Frailty Index in both humans and mice (Chapter II). Chapters III – V contain a manuscript in preparation to be submitted to American Journal of Physiology, a submitted manuscript to Journal of Applied Physiology, and a published article in *The Journals of Gerontology. Series A: Biological Sciences and Medical Sciences*. Finally, I summarize the main findings of these studies and how the findings contribute to the field of muscle atrophy and frailty.

CHAPTER II. BACKGROUND

Skeletal muscle is the most abundant tissue in mammals, which plays a role in producing skeletal movement and storing essential nutrients. A decrease in skeletal muscle mass is called *muscle atrophy*. There are many conditions associated with muscle atrophy, such as disease, aging, inactivity or loss of innervation. Muscle atrophy is usually accompanied with muscle weakness (decreased strength), which leads to deleterious outcomes such as decreased physical activities, increased risk of hospitalization and mortality [4,5]. In turn, these deleterious outcomes may contribute to further muscle atrophy. Understanding how the mechanisms underlying muscle atrophy are fine-tuned has the potential to provide the foundation in developing therapies that potentially restore muscle mass and strength; hence, improve the activities of daily living.

SKELETAL MUSCLE STRUCTURE

STRUCTURE OF A WHOLE SKELETAL MUSCLE

Because muscle atrophy is defined as a decrease in size, a short review of muscle structure is in order. Skeletal muscle (e.g., gastrocnemius muscle) contains several components including muscle fibers, connective tissues, motor nerves, and blood vessels. The muscle fibers, as known as muscle cells, are the basic units of skeletal muscle. The connective tissue is identified into three parts, endomysium, perimysium and epimysium. The endomysium surrounds the cell membrane of each individual muscle fiber, or the sarcolemma. A bundle of muscle fibers is surrounded by the perimysium, which forms the muscle fascicle. Motor neurons and capillaries transverse both the endomysium and perimysium to connect with the individual muscle fibers. Several fascicles are clustered together by the last layer of connective tissue, epimysium (**Figure 1**). The epimysium is continuous with the tendons, which attach the muscle to the skeleton. In addition to the muscle fibers and connective tissues, motor nerves and blood vessels are also essential for the function of a whole muscle. For example, the neural input initiates the voluntary contraction; and the blood vessels provide nutrient supplies, such as oxygen and energy in the form of ATP.

Figure 1. The structure of skeletal muscle.

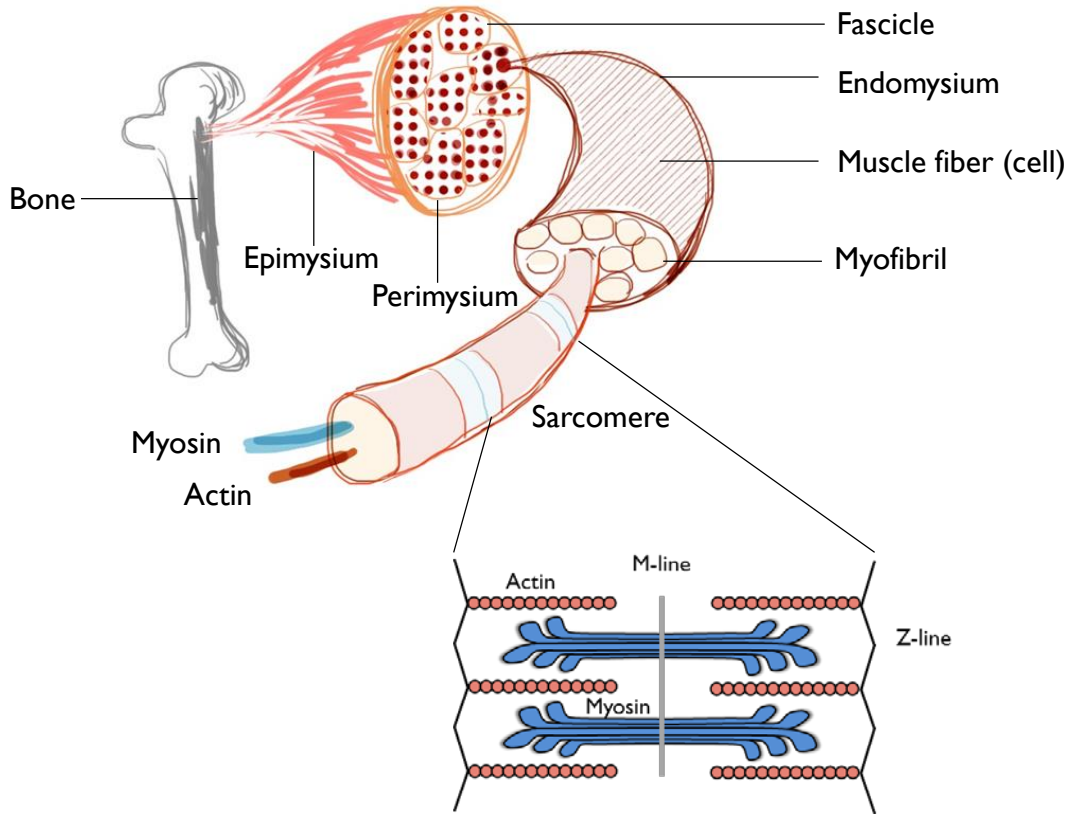

A whole muscle is composed of many fascicles and wrapped by the epimysium. Each fascicle is wrapped by the perimysium and is composed of muscle fibers, which are the cells in skeletal muscle. Each muscle fiber is wrapped by the endomysium and contains many myofibrils. A myofibril is a striated structure made from repeated sarcomeres. The sarcomere is defined from Z-disc to Z-disc and the middle of the sarcomere is defined as the M-line. The sarcomere contains the myosin (thick filament) and actin (thin filament), which make up the majority of the muscle proteins and are required for contractility. The myosins are at the center of the sarcomere; whereas the actins attach to a Z disc at the end of the sarcomere.

MUSCLE FIBERS, SARCOMERE AND CONTRACTILE PROTEINS

A muscle fiber is a striated cell than spans the entire length of the muscle. The muscle fiber contains multiple nuclei all along the surface underneath the sarcolemma. Outside of the sarcolemma, there is a loose collagen network with glycoproteins called basement membrane. Satellite cells are located in between the sarcolemma and the basement membrane. The cytoplasm of muscle fiber is called sarcoplasm. The sarcoplasm contains cellular organelles such as nuclei, mitochondria, endoplasmic reticulum (sarcoplasmic reticulum), proteasome and cytosolic proteins.

Within each muscle fiber, there are hundreds of myofibrils. Myofibril is composed of a repeated structure called the sarcomere, the fundamental unit for muscle contraction (**Figure 1**). The sarcomere is highly organized by overlapping of thick filaments (myosin) and thin filaments (actin). The myosins are at the center of the sarcomere; whereas the actins attach to a Z disc at the end of the sarcomere. Specifically, myosin contains two myosin heavy chains and four light chains. The molecular weight of myosin heavy chain is about 200 kDa. Actin is a 42-kDa protein (G-actin, globular) or is polymerized into double helical strands called F-actin. The actin filaments bind with other regulatory proteins (tropomyosin, troponin I, troponin C, and troponin T). The myosin and actin compose the majority of the muscle proteins. As a result, any loss or modification these proteins would affect the muscle size, may lead to muscle atrophy, and a decrease in strength.

NEUROMUSCULAR JUNCTION (NMJ)

The motor neuron is important for voluntary muscle contraction. The motor neuron provides an action potential, which proceeds muscle contraction. Also, activity of the motor neuron is important for maintaining muscle mass [6]. There is an important connection between the motor neuron and the muscle, the neuromuscular junction (NMJ). In general, the NMJ is composed of three components (**Figure 2**): (1) the presynaptic terminal, which is packed with synaptic vesicles containing the neurotransmitter acetylcholine (Ach); (2) the synaptic cleft, a 50- to 80-nm-gap between the motor neuron and the muscle fiber, filled with basal lamina containing molecules secreted by both nerve and muscle fiber [7]; (3) and the postsynaptic endplate at the muscle fibers, which is

a deeply folded structure with the nicotinic acetylcholine receptors (nAChR). Any interruptions, such as denervation or aging-related junctional loss, will influence the content and the functions of the molecules (such as AchR, HDACs) in any of the three components of the NMJ. Thus, altering muscle mass and muscle contractility.

Figure 2. Neuromuscular junction (NMJ).

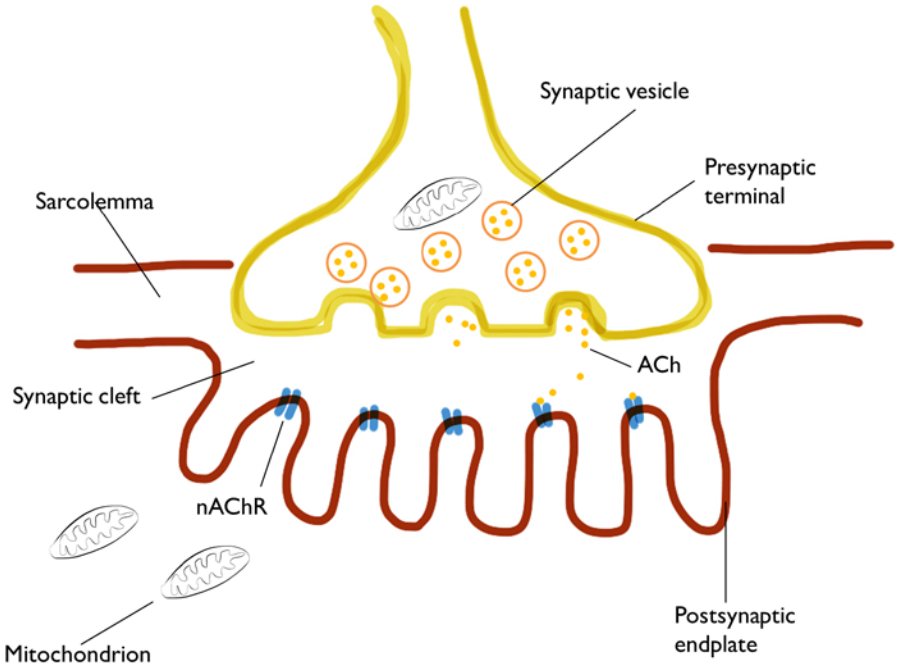

The communication between the alpha motor neuron and the skeletal muscle occurs through the neuromuscular junction (NMJ). The NMJ is composed of the presynaptic terminal, the synaptic cleft, and the postsynaptic endplate. Both the presynaptic terminal and the postsynaptic endplate contain mitochondria. Within the presynaptic terminal, there are synaptic vesicles containing the neurotransmitter acetylcholine (Ach). The Achs are released from the presynaptic terminal and bind to the nicotinic acetylcholine receptors (nAChR) at the postsynaptic endplate.

MUSCLE FUNCTION

MUSCLE PHYSIOLOGY

The process of muscle contraction requires an action potential, which is initiated from the motor neuron through the neuromuscular junction (NMJ). In brief, the action potential at the presynaptic terminal triggers the opening of voltage-dependent calcium channels and induces influx of calcium to the cytosol of the presynaptic neuron. This influx of calcium triggers the release of Ach in the synaptic cleft. The Ach further binds to the nAChR located in the postsynaptic endplate to produce an action potential. This action potential is transmitted to the transverse tubules (T tubules) and subsequently causes the excitation-contraction (EC) coupling, which is essential for force production. As a result, loss of neural input would impair the function of voluntary muscle contraction. **Figure 3** summarizes EC coupling. The action potential at the T-tubules depolarizes the inner side of the muscle fiber and activates the L-type voltage-dependent calcium channels (dihydropyridine receptors, DHPRs), which further activate the ryanodine receptors 1 (RyR1s) located at the sarcoplasmic reticulum (SR). In turn, the RyR1 opens the Ca^{2+} channels on SR and release Ca^{2+}. The Ca^{2+} binds to the troponin C on the thin filament, allowing the myosin binding sites to be exposed. Thus the actin is able to bind to the myosin, creating cross bridges. In the absence of ATP and/or the presence of ADP, the myosin head forms a strong binding with actin; whereas when an ATP presents, the myosin head produces a weak binding [8]. The release of phosphate from myosin allows force generation by changing the structure of the catalytic domain. Thus, muscle function can be altered by any structural or chemical alterations in actin and myosin via affecting the weak-to-strong actomyosin transition [8].

Figure 3. Excitation-contraction (EC) coupling.

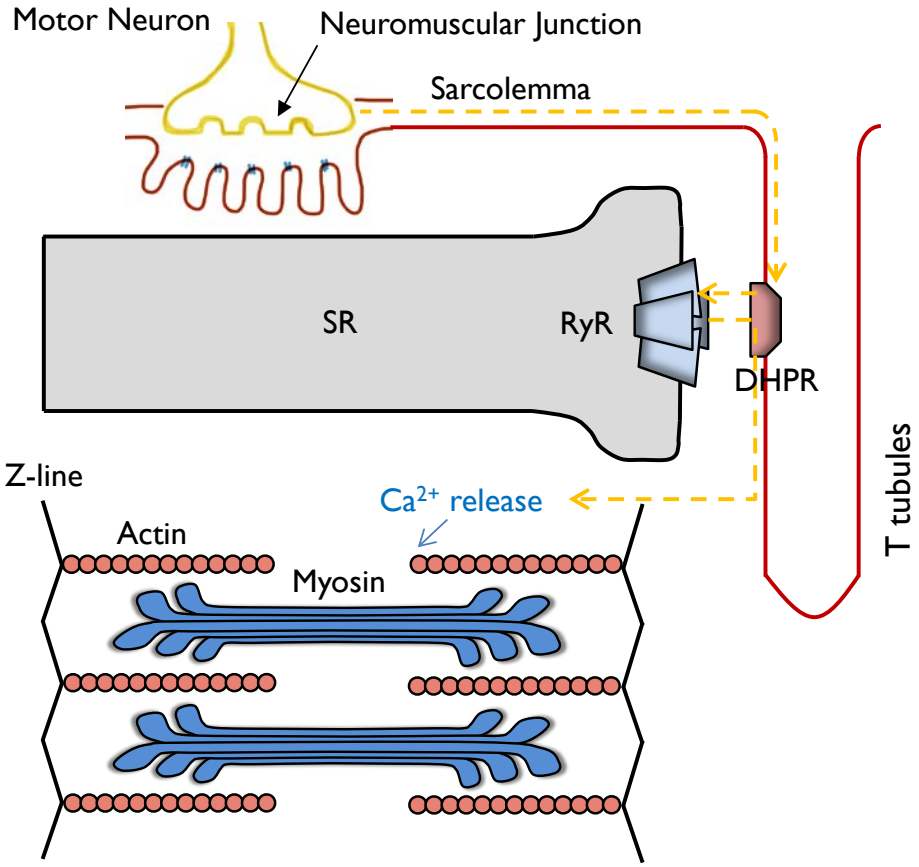

Following binding of Ach to the nAChR an action potential is produced at the motor endplate. This action potential is transmitted to the transverse tubules (T tubules) and subsequently causes the excitation-contraction (EC) coupling. The action potential at the T-tubules depolarizes the inner side of the muscle fiber and activates the dihydropyridine receptors (DHPRs), which further activate the ryanodine receptors 1 (RyR1s) located at the sarcoplasmic reticulum (SR). In turn, the RyR1 opens the Ca^{2+} channels on SR and releases Ca^{2+}. The Ca^{2+} binds to the troponin C on the thin filament, allowing the myosin binding sites to be exposed. Thus the actin is able to bind to the myosin, creating cross bridges.

MUSCLE ATROPHY

A rapid muscle loss (muscle atrophy) occurs under multiple conditions, such as denervation and cachexia [5,9,10]. Muscle atrophy under various catabolic conditions involves an imbalance between protein synthesis and degradation (protein turnover). This imbalance occurs either with a reduction of protein synthesis and/or an increase of protein degradation (**Figure 4**). There are several proteolytic systems involved in muscle atrophy (see next section). Protein synthesis in skeletal muscle is mainly through the Akt (protein kinase B)/mTORC (mammalian target of rapamycin) pathway, which is initiated by growth hormone, insulin-like growth factor 1, and testosterone *etc* [11,12].

Figure 4. Protein turnover.

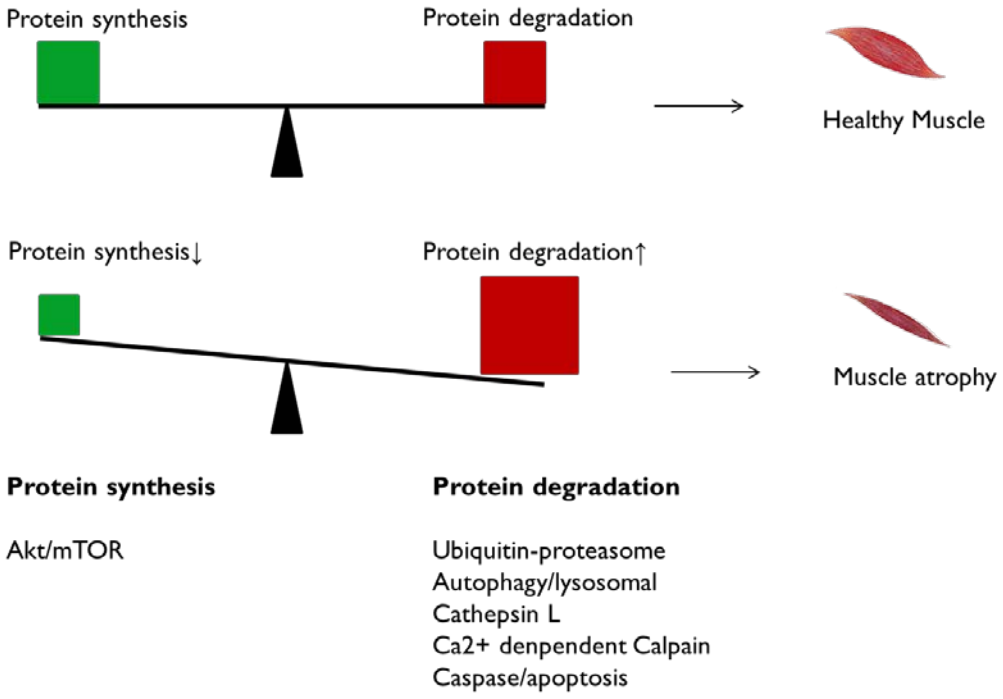

In healthy muscles there is a balance between protein synthesis and protein degradation. When there is a reduction of protein synthesis and/or an increase of protein degradation, muscle atrophy occurs. Protein synthesis in skeletal muscle is mainly through the Akt (protein kinase B)/mTORC (mammalian target of rapamycin) pathway. The protein degradation systems include the ubiquitin-proteasome, autophagy/lysosomal, cathepsin L, Ca^{2+}-dependent calpain, and caspase/apoptosis systems.

PROTEIN DEGRADATION SYSTEMS

Two well-studied systems responsible for muscle protein degradation include the ubiquitin-proteasome system (UPS) and the lysosomal/autophagy pathway. Specifically, the UPS is responsible for degradation of myofibrillar proteins (e.g. myosin and actin); whereas the lysosomal/autophagy plays a role in removing protein aggregates, dysfunctional mitochondria, and endoplasmic reticulum membranes [10,13]. Other catabolic systems required for protein breakdown include Ca^{2+}-dependent calpain system, cathepsin L and caspase-dependent apoptosis [12,14]. Here, I am interested in the UPS because it is the main system for the degradation of the myofibrillar proteins.

UBIQUITIN PROTEASOME SYSTEM (UPS)

It has been reported that UPS degrades most of the muscle proteins [5]. Two important steps in the UPS pathway are highlighted in **Figure 5**. The first step involves three major enzymes (ubiquitin-activating E1 enzymes, ubiquitin-conjugating E2 enzymes, ubiquitin-protein ligases E3), which tag the target-protein with ubiquitins (chains) and bring it to the 26S proteasome. The second step involves leading the target protein to the 26S proteasome. Specifically, the PA700 (19S) complex binds and unfolds the ubiquitin-modified protein so the polyubiquitin chain is broken and the ubiquitins are recycled and the 20S catalytic core further degrades the misfolded proteins [15–17]. In short, enhanced protein degradation in skeletal muscle results from increased muscle-specific ubiquitin E3 ligases and increased proteasome enzymatic activities.

Figure 5. Ubiquitin-proteasome system (UPS).

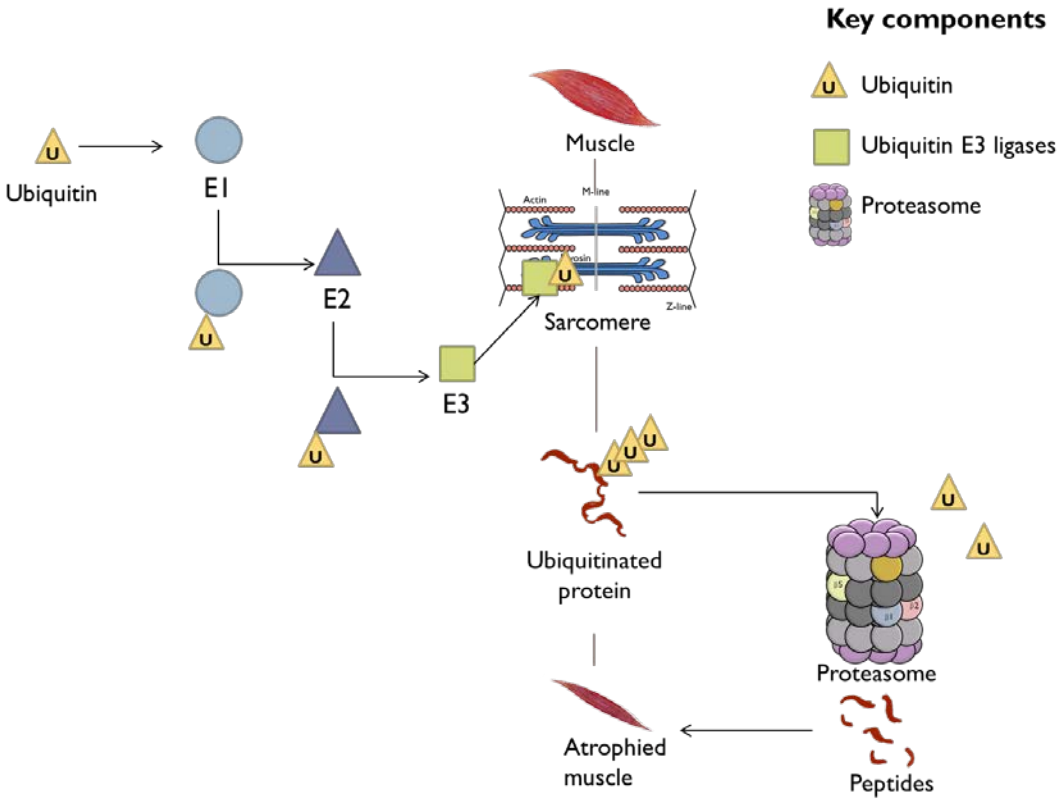

The UPS degrades myofibrillar proteins through two steps: (1) tagging the target protein (e.g. myofibrillar proteins in the sarcomere) with ubiquitins through three major enzymes (ubiquitin-activating E1 enzymes, ubiquitin-conjugating E2 enzymes, ubiquitin-protein ligases E3); (2) The 26S proteasome degrades the protein substrates and the ubiquitins are recycled. The degradation of the myofibrillar proteins in the sarcomere leads to muscle atrophy.

E3 ligases

Several E3 ligases are important for protein degradation, as they play a role in disassembly and ubiquitination of the myofibrillar proteins. For example, Muscle-specific RING-finger 1 (MuRF1) [9,18], and Muscle Atrophy F-Box (MAFbx)/atrogin-1[19] are the most studied E3 ligases that have been found dramatically increased at both gene and protein levels under multiple catabolic conditions, such as cachexia [12,20,21], fasting [9,22], and denervation [5,23–25].

MuRF1: Myosin heavy chain (MyHC), myosin-binding protein C (MyBP-C), Myosin light chain 1 (MLC1), and MLC2 require MurF1 for disassembly [9]. Specifically, with denervation these myofibrillar proteins are ubiquitinated by MuRF1 and degraded by 26S proteasome [5]. It has been reported that MuRF1 binds to titin, a structural protein functioning as a scaffold that links the contractile apparatus to the Z disc [26].

MAFbx/atrogin-1 assists skeletal muscle atrophy by inhibiting protein synthesis and myotube differentiation via the degradation of eukaryotic initiation factor 3f (eIF3f) and MyoD, respectively [27–29]. In brief, muscle mass is maintained by eIF3f [30] through the mTORC1 signaling pathway [28]. During muscle atrophy, eIF3f is ubiquitinated by MAFbx and degraded by proteasome [27,29,31]; whereas MyoD is degraded through a lysine-dependent pathway [24,31]. Lately, it has also been reported that MyHC and the sarcomeric proteins, such as vimentin and desmin are the potential targets of MAFbx [32,33].

26S proteasome

Figure 6 shows the structure of the 26S proteasome. The main site for protein degradation is the 26S proteasome, which contains the 20S catalytic core and the PA700 (19S) regulatory complex. The 20S catalytic core is composed of 28 subunits (four heteroheptameric rings made of seven subunits each). The two outside rings are made of constitutively expressed α-subunits whereas the two inner rings contain the catalytic β-subunits [15,34]. The outer α-subunits interact with the regulatory complex to translocate the ubiquitinated protein substrates into the 20S core, whereas the catalytic β-subunits are responsible for cleavage of protein substrates. Specifically, three pairs of catalytic β-subunits (β1, β2 and β5), perform caspase-like, trypsin-like, and chymotrypsin-like proteolytic activity, for cleavage after acidic, basic, and hydrophobic amino acids,

respectively [35]. The proteasome activities and some of the subunits have been found elevated under different atrophy conditions, such as denervation [22,23,36], cachexia [37], muscular dystrophy [38,39].

Figure 6. The structure of 26S proteasome.

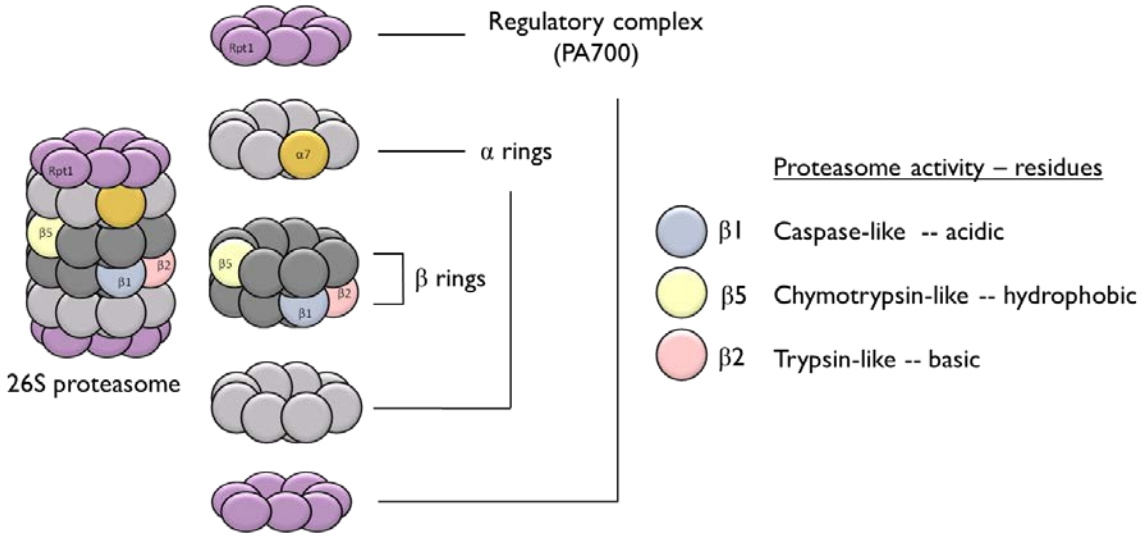

The 26S proteasome is composed of the regulatory complex (PA700/19S) and the 20S core. The 20S catalytic core is composed of four heteroheptameric rings made of seven subunits each. The two outside rings are made of constitutively expressed α-subunits whereas the two inner rings contain the catalytic β-subunits. Specifically, three pairs of catalytic β-subunits (β1, β2 and β5), perform caspase-like, trypsin-like, and chymotrypsin-like proteolytic activity, for cleavage after acidic, basic, and hydrophobic amino acids, respectively.

Immunoproteasome

When the three pairs of subunits (β1, β2 and β5) of the 20S catalytic core are replaced by LMP2 (iβ1), MECL-1 (iβ2), and LMP7 (iβ5), a 20S immunoproteasome (i20S) is formed. The regulatory complex of the i20S can be either the 19S complex (PA700) or 11S complex (PA28αβ), or a combination (**Figure 7** [40]). The immunoproteasome subunits are responsible for proteasome activities for the generation of antigen presentation. LMP7 and MECL-1 conduct the same activities as β5 and β2, whereas LMP2 performs the chymotrypsin-like activity because of the requirement of hydrophobic amino acids in the C-terminal position [35].

Besides the standard 26S proteasome and the immunoproteasome, there are several intermediate forms, with a mixture of the standard and inducible β subunits. Indeed, there are six different subtypes of proteasome. With different combination of the β subunits, they present different levels of proteasome activities.

Figure 7. The structure of immunoproteasome.

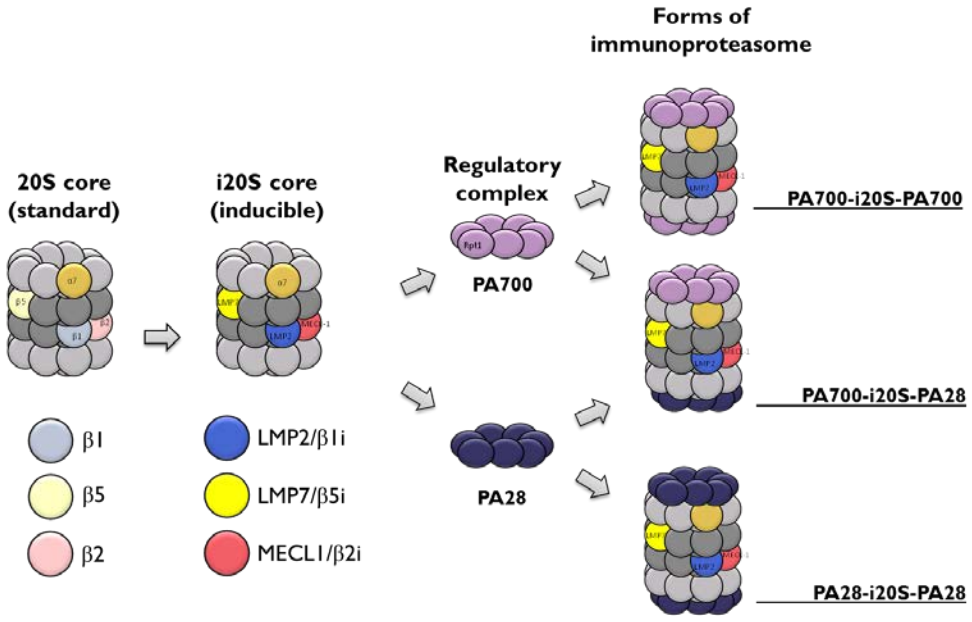

When the three pairs of subunits (β1, β2 and β5) of the 20S catalytic core are replaced by LMP2 (iβ1), MECL-1 (iβ2), and LMP7 (iβ5), a 20S immunoproteasome (i20S) is formed. In an immunoproteasome, the regulatory complex of the i20S can be either the PA700 or PA28, or a combination. As a result, there are three forms of immunoproteasome, PA700-i20S-PA700, PA700-i20S-PA28, and PA28-i20S-PA28.

Functions of the Immunoproteasome – immune

The immunoproteasome has two general functions, immune and non-immune. There are three immune functions, the first is antigenic peptide generation for the major histocompatibility complex class I presentation during inflammation, second is T cell differentiation and survival [41], and third is the regulation of cytokine production, such as TNF-α, interleukin (IL)-6, IL-1β and IFN-α [40]. Some non-immune functions of immunoproteasome have been studied recently, such as muscle remodeling (see more details in the following section), apoptosis [40], anti-oxidative stress [42], and lipid metabolism [43,44].

Functions of the Immunoproteasome – muscle remodeling

There are four lines of evidence in rodents supporting a role of the immunoproteasome during muscle remodeling. First, elevated levels of LMP7 are associated with cardiac atrophy in mice with diabetes. Specifically, Zu *et al* report the protein level of LMP7 increased by 280% in cardiac muscles from the streptozotocin-treated mice, which is a condition that mimics diabetic cardiomyopathy that causes a 30% decrease in left ventricular size. The chymotrypsin-like activity, a corresponding proteasome activity of LMP7 and β5, was also elevated in the diabetic hearts [45]. Second, in skeletal muscle from mice with muscular dystrophy showed an increase in LMP7 levels, too. For instance, the dystrophin/utrophin-deficient (*mdx*$^{-/-}$*:utrn*$^{-/-}$) mice showed a 3-fold increase of LMP7 content and a 200% increase in the chymotrypsin-like activity in the hindlimb muscles in conjunction with muscle atrophy of 36% compared to the WT mice [38]. Third, in the aged muscles, the immunoproteasome subunits are also elevated. For instance, the soleus muscle from 30- to 38-month-old rats exhibited 38% atrophy with 4-fold increase in both LMP2 and LMP7 content compared to the young (5-14 mo) [13]. Similarly, the fast-twitch muscles from the old rats showed 3-fold increase in both LMP2 and LMP7 when compared to the young [16,17]. Fourth, one study also indicated immunoproteasome is also involved in protein degradation in response to denervation. This study will be highlighted in the later section.

Experimental models to investigate Immunoproteasome

The ability to genetically modify mice enables the investigation of the structure-function of the immunoproteasome subunits. In this mouse model, two immunoproteasome

subunits, LMP7 and MECL-1 are knocked out (L7M1 mice). Other models, including human single or double mutations, also enable the structure-function investigations.

In general, various investigations using multiple experimental models have identified the importance of the subunits (both proteasome and immunoproteasome) in the assembly of the 20S core. A brief discussion follows because the results of Chapter III suggest a change in the assembly of the 20S core in the absence of the immunoproteasome subunits under the condition of denervation.

A proteasome assembly defect was noted in lymphoblastoid cell lines from patients with Nakajo-Nishimura syndrome, a human autoinflammatory disease with LMP7 mutation [43] Specifically, this study found an accumulation of immature 20S proteasome precursors, which resulted in a decrease in both 20S and 26S proteasome content and their respective activities [43]. In other experimental models there is evidence for impaired subunit incorporation into the 20S core in the absence of one or two immunoproteasome subunits[46,47]. For instance, when LMP7 and MECL-1 are genetically eliminated, there is a decrease in LMP2 protein content in retina and spleen [48,49]. When LMP7 is genetically eliminated, both LMP2 and MECL-1 protein contents are less [50]. When the LMP2 is absent, the incorporation of MECL-1 is blunted and vice versa. Collectively, it appears the assembly of the 20S core requires the physical interaction between the immunoproteasome subunits [51].

DENERVATION AND MUSCLE ATROPHY

In my graduate study, I chose a model of denervation (tibial nerve transection) to induce atrophy in mice. Tibial nerve transection is an established method to cause rapid gastrocnemius muscle loss by 20% at day 7 and 40% day 14 [52,53], without impairing the mouse's ability to ambulate. Following denervation, both UPS and autophagy system have been activated. Interestingly, some studies also reported elevated mTORC1 following denervation.

DENERVATION AND UPS

Overall, the activation of the UPS following denervation is shown by increased expression of E3 ligases and increased proteasome components (activities and/or

subunits). As a result, in the next paragraphs, I will review the literature focused on the UPS in denervation-induced muscle atrophy and how these key markers respond to loss of neural input.

Denervation and E3 ligases

As aforementioned, E3 ligases are one of the most important proteins in the UPS, which play a role in protein ubiquitination. In the early phase (3 days) of muscle atrophy induced by denervation there is increased mRNA level of MuRF-1 and MAFbx [23]. In addition, knocking out either of these E3 ligases, muscle atrophy induced by denervation is attenuated [18,19] . Other E3 ligases associated with denervation-induced muscle atrophy includes Nedd-4 [6,54], MUSA1 [22,24], and SMART [22].

Denervation and proteasome/immunoproteasome

26S proteasome plays a role in proteolysis for the ubiquitinated proteins as aforementioned. **Table 1** summarizes the literature in the field of proteasome and denervation. Overall, there is an increase in proteasome content and activities following denervation. Gomes *et al* investigated proteasome content and activities at 14 days post denervation. They report an increase of the 20S (α1) and PA700 (19S/Rpt1) protein content and increased proteasome activities (ATP-dependent, 26S) following 14-day denervation [23]. Furuya *et al* investigated some of these proteasome characteristics following 7 day denervation. They report increased protein level of α5, subunits of PA700 (19S/Rpt4, 19S/Rpn10) and catalytic subunit β2 in 7-day denervated soleus muscle, accompanied with 70% increase in the 26S chymotrypsin-like activity [36]. These studies provide rationale that the 26S proteasome plays a role in denervation-associated protein degradation. Interestingly, Gomes *et al* also reported increased protein level of MECL-1 and PA28, which are the important subunits in immunoproteasome. **Table 1** also includes data from my study using wild type mice. Both the Gomes *et al* and my data implicate a potential role of immunoproteasome in denervation-induced protein degradation. Although the previous studies investigate components of proteasome and immune-proteasome, further analysis is needed to understand the fine-tuning of protein degradation.

Table 1. Denervation-induced activation of proteasome system (rationale).

Rationale	DN days	% of atrophy	Measures for proteasome subunits	Proteasome subunits					Proteasome activities (26S)		
				20S proteasome (α)	PA700	PA28	standard β	inducible β	Caspase-like	Chymotrypsin-like	Trypsin-like
Gomes et al., 2012	3 days	n.s.	Protein level *	α1, 50%↑	Rpt1, 280% ↑	PA28α, n.s.		MECL-1, n.s.	20%↑	n.s.	30%↑
			mRNA level (fold change vs. ctrl)	α2: 1.92 α3: 2.18 α4: 2.38	Rpt1: 1.89	PA28α: 0.6	β2: 1.17 β5: 1.96	LMP7: 0.84 LMP2: 0.84 MECL-1: 0.64			
	14 days	41%	Protein level *	α1, 65%↑	Rpt1, 200%↑	PA28α, 10%↑		MECL-1, 13%↑	70%↑	50%↑	50%↑
			mRNA level (fold change vs. ctrl)	α2: 1.35 α3: 1.49 α4: 1.44	Rpt1: 1.22	PA28α: 0.6	β2: 0.86 β5: 1.63	LMP7: 0.41 LMP2: 0.71 MECL-1: 0.54			
Furuya et al., 2014	7 days	20%	Protein level * (fold change vs. ctrl)	α5: 1.6	Rpt4 and Rpn11: n.s.		β2: 1.7				
			mRNA level * (fold change vs. ctrl)	α4: 2.2	Rpt3 and Rpn2: n.s.		β2: 2			70%↑	
Milan et al., 2015	3 days		mRNA level * (fold change vs. ctrl)	α4:~4	Rpt3: ~4 Rpn6: ~3						
Quy et al., 2013	2 days									n.s.	
Liu et al., 2016	7 days	26%	Protein level *	α7, 129%↑	Rpt1, 448% ↑	PA28α, n.s.	β1, 617%↑ β5, 512%↑ β2, 882%↑	LMP2: 83%↑ LMP7: 117%↑ MECL-1: 180%↑	232%↑	209%↑	299%↑
	14 days	39%	Protein level *	α7, 334%↑	Rpt1, 189%↑	PA28α, 112%↑	β1, 307%↑ β5, n.s. B2, 688%↑	LMP2: 93%↑ LMP7: 99%↑ MECL-1: 139%↑	114%↑	140%↑	161%↑

*: report the signficant changes
n.s: no significant difference

Signaling in denervation-induced activation of UPS

It is well established that the alpha motor neuron is critical for muscle mass maintenance and the overall homeostasis of the muscle [55,56]. When a muscle is denervated the neural activity is lost. **Figure 8** shows how loss of neural activity initiates the signaling of UPS that leads to muscle atrophy. Muscle atrophy initiated by loss of neural input is likely associated with the accumulation of histone deacetylases (HDACs). HDAC4 is concentrated at the NMJ when the muscle is innervated. After denervation, HDAC4 is released from NMJ and accumulated in the nuclei of affected muscle due to reduced intracellular calcium level [56,57]. Increased nuclear levels of HDAC4 suppress the Dach2, which is a transcriptional repressor of *Mgn* (myogenin). The upregulation of myogenin further promotes the expression of E3 ligases of MuRF1 and atrogin-1 [58], which leads to skeletal muscle protein degradation through the UPS.

There is indirect evidence showing an up-regulation of immunoproteasome with denervation. Specifically, there is evidence for the HDAC/Mitogen-activated protein kinases (MAPK) cascade, which is associated with denervation-induced muscle atrophy. In fact, transcription factors activator protein 1 (AP1) and specificity protein 1 (Sp1) are increased in gastrocnemius muscle via HDAC4 triggered MAP3 kinase cascade after 3 days of denervation [59]. Similarly, increased AP-1 was demonstrated in 14-day denervated TA muscles and knocking down HDAC4 compromised the elevation of AP-1 isoforms [60]. These transcription factors are also associated with the transcription of the immunoproteasome subunits, LMP2, LMP7 and MECL-1in cells [61,62].

The mTOR-FOXO (forkhead box O) pathway is also activated following denervation, which is responsible for the upregulation of E3 ligases [6,63]. It has reported that the denervation-induced mTORC1 is Akt-independent, which is different from the insulin-like growth factor activated Akt/mTORC1 anabolic signaling. Thus, the activation of FOXO is further induced by activation of mTROC1 through the ribosomal S6K-IRS-Akt* feedback route [63]. Activation of FOXO is likely responsible for the elevated E3 ligases after 3 days of muscle atrophy-induced by denervation.

---

* Abbreviations: S6K, ribosomal S6 kinase; IRS, insulin receptor substrate

The mTOR signaling may contribute to the elevation of the content of standard proteasome subunits and activators by activating the corresponding transcription factors, nuclear factors erythroid-derived 2-related factors (Nrfs) [22,64–66]. Although there is no direct evidence, indirect evidence states both Nrfs and mTOR are elevated after denervation. In addition, one in vitro study reported that mTORC1 was able to activate Nrfs [64]. In the same study, applying rapamycin, which is an inhibitor of mTOR, attenuated the increase in standard proteasome subunits and the activator PA700.

These studies provide support for the upregulation of proteasome subunits and immunoproteasome in response to denervation. Although my thesis study (Chapter III) is focused more on characterizing the downstream changes in the UPS, especially the proteasome and immunoproteasome, understanding the potential upstream markers may help with the design of future studies in identifying the proposed defects in the assembly of the 20S core in the absence of immunoproteasome subunits.

Figure 8. Denervation-initiated activation of UPS.

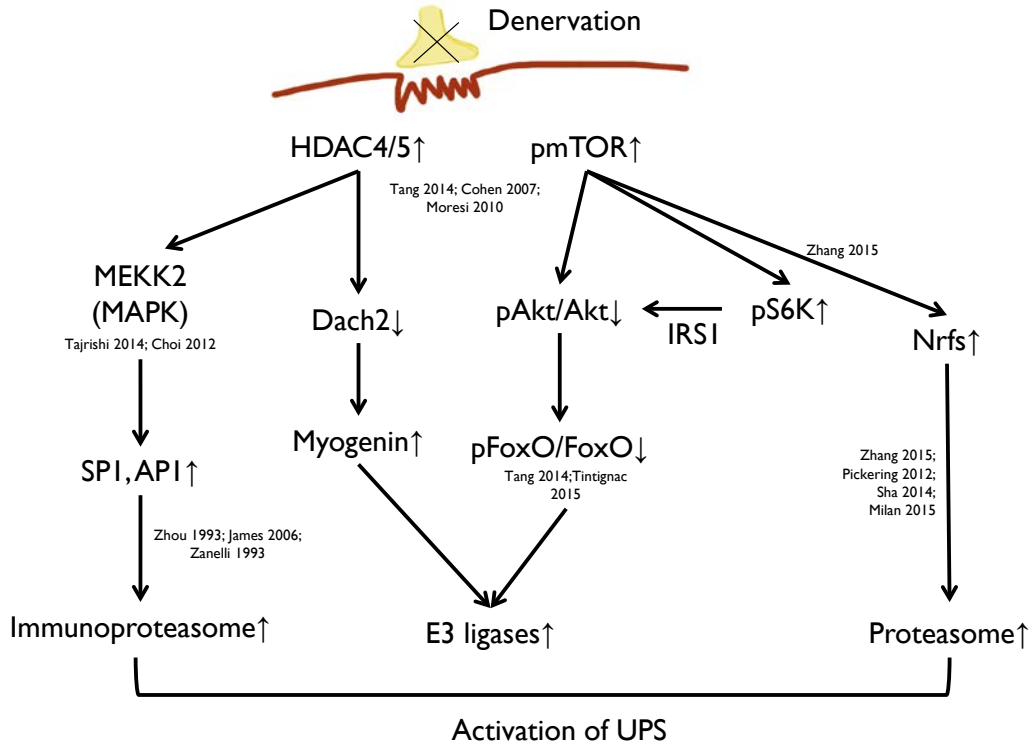

Denervation induces the activation of the UPS by increasing the expression of the key components in the UPS, including the E3 ligases, proteasome and immunoproteasome. There are two major pathways, HDAC and mTOR, that contribute to the upregulation of the transcription factors for these key components. Specifically, the loss of neural activity strongly upregulates HDAC4/5 which ultimately induces E3 ligases via the inhibition of Dach2 and the activation of myogenin. In addition, the upregulation of HDAC4/5 activates transcription factors for immunoproteasome (Sp1 and AP1) via the MAPK cascade. After denervation, mTOR is also activated, the phosphorylation of Akt is decreased via the activation of S6K/IRS. As a result, the transcription factor FOXO is elevated and also contributes to the increased expression of E3 ligases. The increased proteasome transcription factors (Nrfs) are likely associated with the activation of mTOR.

DENERVATION AND OTHER PROTEOLYTIC PATHWAYS

Although my thesis study is focused on one of the protein degradation systems – UPS, we cannot ignore the other proteolytic pathways involved in denervation-induced muscle atrophy. Thus, I will briefly demonstrate their functions in denervation-induced muscle atrophy in the following paragraph.

Autophagy has been extensively investigated in denervation-induced muscle atrophy. Autophagy is important for the selective removal of mitochondria, aggregated proteins, membrane and extracellular proteins, damaged organelles and pathogens [36,67]. Impaired mitochondrial function has been found in denervated muscles and associated with an upregulation of autophagy markers [68]. For example, after 7-day denervation, the tibial anterior muscle had a reduction in subsarcolemmal mitochondrial respiration and the protein levels of the autophagy proteins LC3II, ULK1, ATG7, p62, and Beclin1 were significantly increased [68]. Consistently, the mRNA levels of LC3b and Gabarapl1, Atg4b, and Beclin1 have also been found significantly increased in 7-day denervated TA muscles [69] [a].

There are some shared upstream signaling pathways for both UPS and autophagy under the condition of denervation. For example, HDACs are important for the expression of E3 ligases and proteasome as aforementioned, HDAC1/2 are responsible for transcription of autophagy genes [58,70]. Also, FOXO, which is a transcription factor for E3 ligases, is also responsible for transcription of some autophagy genes[69] (e.g. PINK1[67] [b]). In contrast to protein degradation, the protein synthesis related mTOC1 is a suppressor of autophagy. Taken together, the UPS and autophagy do not work separately in protein degradation. As a result, I have also investigated the response of autophagy marker LC3 following denervation in both WT and immunoproteasome deficient muscles.

Cathepsins, lysosomal proteases, are also important for proteolysis in skeletal muscle [71,72]. The major role of the cathepsins is to degrade membrane proteins, such as receptors,

---

[a] Abbreviations: LC3, microtubule-associated protein light chain 3; ULK1, unc-51-like kinase; Atg7, autophagy-related gene 7; p62, sequestosome 1; Beclin1/Atg6, autophagy-related gene 6;
[b] PINK, PTEN-induced putative kinase 1

ligand, channels and transporters [55,73]. To emphasize the specific targets of cathespins, inhibition of lysosomal proteinase activity does not attenuate myofibrillar protein breakdown [74]. Interestingly, it has been suggested that cathepsin is also directly regulated by FOXO1, which is the transcription factor involved in UPS and autophagy activation [75,76]. There are reports showing Cathepsin L is involved in protein degradation induced by denervation [23,77].

Calpain is another system likely involved in denervation-induced protein degradation. The major role of calpain is disassembly of sarcomeric proteins such as titin, vinculin, C-protein, and nebulin etc. [55,78]. For example, in myoblast cell with accelerated degradation, inhibition of m-calpain decreased protein degradation by 30% and stabilized nebulin [78]. Also, the calpain activities has been found elevated in muscles following 3-day and 14-day denervation [23].

In summary, the UPS, autophagy, Cathepsin L, and calpains have distinct roles in the process of protein degradation in skeletal muscle. Because skeletal muscle is composed of various proteins, these systems work together in order to achieve a reduction in muscle size.

Age-related muscle adaptation

SARCOPENIA

The age-related muscle atrophy is called sarcopenia, which is operationally identified by skeletal muscle mass index (sum of the muscle mass from four limbs (kg)/ hight^2 (m^2)) using the dual energy x-ray absorptiometry (DEXA) scan in the clinic [79]. Sarcopenia is due to a decrease in both fiber size and fiber number. The primary muscle loss occurs in the fast-twitch muscle fibers, with increased fibrosis and adipose tissue [80]. It has been reported that muscle loss is about 1-2% per year after the age of 50 years. The prevalence of sarcopenia under 70 years old is 10%; whereas the prevalence increases to 23% in people above 80 years old [79,81]. Also, by the age of 80, peak muscle mass is reduced by 40% [82].

The etiology and pathology of sarcopenia are multi-factorial. Aging is associated with multiple catabolic conditions, such as decreased activity, denervation, increased oxidative stress, chronic inflammation, age-related hormone changes, and satellite cells [83]. The preferential loss of fast-twitched muscle fibers is likely due to a decline in the number of neuromuscular junctions [84,85]. Age-related upregulation of oxidative stress promotes protein degradation through the UPS and the other proteases, such as caspases and calpains. Increased oxidative stress is also associated with impaired mitochondrial biogenesis, which in turn affects muscle size [86]. Inflammation cytokines, such as interleukin 6, and/or C-reative protein and/or TNFα, have been found elevated in atrophied muscle with aging [87]. Increased expression of cytokines is associated with activation of UPS via the NFκB signaling. In contrast to the conditions that mainly contribute to the catabolism of muscle with aging, the age-related reduction of growth hormone, IGF-1 or testosterone is primarily associated with attenuated protein anabolism [88]. Lastly, satellite cells likely play a role in the etiology of sarcopenia. There is decreased satellite cells and impaired muscle regeneration with aging. For instance, the number of pax7-positive satellite cell in the fast-twitch fibers dramatically decreased by ~50% in vastus lateralis muscle from elderly (76-year old) [89].

DYNAPENIA

Sarcopenia is usually accompanied with decreased muscle strength, which is known as dynapenia [90]. With aging, muscle contractile properties are impaired, including decreased force, power production [91], maximal shortening velocity and fatigue resistance [11]. Dynapenia is due to the deterioration in both muscle quantity and muscle quality. However, with aging, the reduction in muscle quality is more severe than the reduction in muscle quantity, such that specific force (force/muscle cross-sectional area) is 20% lower in aged muscles compared to the young [8]. The factors that contribute to the age-related decrease in muscle quality is likely due to the changes in neurologic and contractile apparatus, including impairments in alpha motor neuron excitability, neuromuscular transmission, E-C coupling, and myosin-actin interaction (decreased strong-binding) [92–94]. These changes are likely due to the increased oxidative stress during aging. For example, age-related oxidation and/or nitrosylation of RyR1 contribute to the impaired muscle quality by affecting the E-C coupling [95,96].

FRAILTY

Frailty is one of the most notable adverse outcomes of sarcopenia, which is a clinical syndrome with impaired physiological and physical functions, increased vulnerability, a higher hospitalization and mortality rate [2,3]. Frailty is highly associated with sarcopenia; however it should be distinguished from sarcopenia. Frailty is more multifaceted than sarcopenia because it involves the biological, physical, and functional components. It has been reported that 9.9% of people aged ≥ 65 years old are frail [97]; and this portion increases to 25%-50% in people aged ≥ 85 years old [3]. Frailty prevention and/or treatment will likely be factorial (e.g., exercise, nutrition supplementation, vitamins, and pharmacological management) [98]. However, it is difficult to identify the optimal interventions for frailty because of its complexity and dynamic features. To date, in the clinical setting there are numerous models to identify frailty. Among these models, the two most recognized and accepted Frailty Indexes are the Frailty Phenotype Index and the Accumulative Deficit Index. I will introduce both indexes in the following sections.

THE FRAILTY PHENOTYPE INDEX

Fried *et al* [1]developed the frailty phenotype index based on a data set from the Cardiovascular Health Study that investigated 5,317 people aged at 65 years and older. The cohort has been evaluated by the frailty phenotype index using five criteria: unintentional weight loss, weakness in grip strength, slowness in walking speed, poor endurance, and low physical activity (summarized in **Table 2**). Frailty was identified if three or more criteria present in an individual; whereas intermediate frailty was identified when two criteria present. With this frailty index, 7% of the cohort was identified as frail and 46% of the cohort was not frail. The prevalence of frailty increased with age in this study. Adverse outcomes, including died, first hospitalization, first fall, worsening activities of daily living (ADL) disability, worsening mobility disability, were evaluated following 3 and 7 years after the identification of frailty phenotype. Most important, the frail individuals had higher incidences of these adverse health outcomes than the intermediate and non-frail subjects in the cohort. Moreover, after 7 years of initial evaluation, the mortality rate in the frail, intermediate, and none individuals were 43%, 23%, and 12%, respectively. Taken together, being frail is bad news. Moreover, the results of this study gave this non-invasive frailty phenotype index validation, standardization, and operation [1].

Table 2. Fried Frailty Phenotype Index [1].

Frailty Criteria	Description of each indicator
Weight loss	Unintentional weight loss
Weakness	Grip strength: lowest 20% in the same gender/body mass index cohort
Poor endurance	Self-reported exhaustion
Slowness	Walking time/15 feet: slowest 20% in the same gender/body mass index cohort
Low activity	Energy expenditure < 383 kcal/week (men); < 270 kcal/week (women)
Presence of Frailty	**Frail: ≥ 3 criteria present** **Intermediate frail: 1 or 2 criteria present**

THE ACCUMULATIVE DEFICIT INDEX

Rockwood *et al* [99] developed a Frailty Index that included 70 clinical deficits and measured a cohort with 2305 old patients who participated in the Canadian Study of Health and Aging. These deficits include the activities of daily living (ADL), current diseases, physical signs, and clinical examinations. To indicate severity, each deficit was scored at a range of 0-1 (score at 0, 0.5, or 1.0; or 0, 0.33, 0.67, or 1.0) and a total score of 7-point Clinical Frailty Scale was generated based the scores from 70 deficits. A higher score indicated a higher possibility that frailty is present. According to the results of the evaluation, individuals are more likely to have adverse health outcomes and higher risk of mortality if they have a higher total score [99].

Lately, the same group developed a biomarker-based frailty index (FI-B) to define frailty [100]. Mitnitski *et al* analyzed baseline data and mortality (up to 7-years) in the Newcastle 85+ Study. The FI-B contains 40 biomarkers, including cellular aging, inflammation, hematology, and immunosenescence. To calculate the FI-B, each biomarker was scored at 0-1 and the final FI equals to the total score divided by the number of the deficits evaluated. If FI = 0, there is no deficit present; whereas FI = 1, it means every deficit presents. According to their results, the FI-B was strongly associated with 7-year mortality. Specifically, an FI-B > 0.33 (median) was associated with a higher mortality [100].

Collectively, these three frailty indexes used clinically with human populations are able to predict adverse health outcomes and mortality. These frailty indexes are able to identify frail individuals; however, the mechanisms underlying frailty still need to be elucidated. Most likely the mechanisms underlying frailty are multifactorial and will require molecular and cellular analyses; hence, animal models of frailty are needed.

FRAILTY INDEX IN MOUSE MODEL

The C57BL/6 mouse is a well-established animal model in biomedical studies. One of the most prominent benefits of using this mouse model is the convenience in transgenic studies. The C57BL/6 mice also exhibit age-related changes that also occur in human, such as sarcopenia, increased inflammation, bone degeneration, and lesions in multiple organs [101,102]. The C57BL/6 mice have a 50% survivorship at age of 28 months which

equivalents to human aged at 80-year-old [103]. Taken together, the C57BL/6 mice can be utilized in frailty studies that would tease out the underlying mechanisms.

In literature, one model to identify frailty in mice is based on the accumulated deficits frailty index, which calculates 31 invasive and noninvasive measures [104]. This Frailty Index is very similar to the human accumulative deficits index, including body composition (fat mass and lean mass), basic metabolic status (level of electrolytes and blood components), physical activities (distance, duration and velocity). To determine frailty in the experiment group, a reference value of each measure was obtained from adult mice first. Then the value from experimental mouse was compared with their corresponding reference value. A frailty value for each measure was designated based on the difference between the experimental mice and the reference. If the difference = 1 standard deviation (*SD*), the frailty score is 0.25; if the different = 2 *SD*, the frailty score is 0.75; if the difference = 3 *SD*, the frailty score is 1, which is the maximum score; if the difference < 1*SD*, the frailty score is 0. The final FI score = total frailty scores/ number of measures. So an animal with no deficit, the FI score is 0; whereas an animal with all possible maximal deficits would have a score of 1. The major finding of this study is that a higher FI score is presented in the older mice and is positively correlated to the age-related cardiac myocyte changes. So far, there are several other frailty models to identify frailty in mice also based on the accumulative deficits [105–107].

In summary, there are two major validated assessment tools of frailty in clinic, the Frailty Phenotype Index and the Accumulative Deficit Index. The Frailty Phenotype Index is a short, non-invasive, and practical index based on five criteria with a clear definition of frail and intermediate frail; whereas the accumulative deficit index is based on 70 deficits in ADLs and clinical examinations. In mouse, an established animal model for intervention studies in the field aging, there are fewer Frailty Indexes and they are based on the Accumulative Deficit Index. However, a clinically-relevant *non-invasive* mouse Frailty Index is still lacking, which drove us to develop a Frailty Index for mice mimics the clinical Frailty Phenotype Index based on the Fried's study.

INTERLUDE I

Peripheral nerve injury induces rapid loss of muscle mass in the denervated muscle. The majority of the reduction in muscle mass is due to myosin and actin degradation. The major proteolytic system for myosin and actin is the ubiquitin-proteasome system. The loss of neural input initiates the transcription factors for key components of this system, including the E3 ligases and the "garbage disposal"- proteasome. Although there are many studies demonstrating an upregulation of the E3 ligases, especially MuRF1 and MAFbx at both protein and mRNA levels following denervation, a limited number of reports assessed multiple components of the proteasome (such as regulatory complex, total proteasome, catalytic subunits) and immunoproteasome (LMP7, MECL-1 and LMP2). To date there is no published study identifying the role of the immunoproteasome in process of muscle protein degradation utilizing an immunoproteasome deficient mouse model. Thus, the first study "Role of the standard and immuno-proteasome in denervation-induced muscle atrophy" described in Chapter III (thesis study) contains two objectives: First, to evaluate the multiple components of the 26S proteasome in skeletal muscle in response to denervation in order to improve our understanding of this system. The second objective is to investigate how immunoproteasome deletion alters the response to denervation to gain insight into immunoproteasome's role in muscle atrophy. To achieve these objectives, we utilized the wild type (WT) and the lmp7$^{-/-}$/mecl-1$^{-/-}$ double knockout (L7M1) mice, which are missing two immunoproteasome subunits. Based on these objectives, the study will test two hypotheses: (1) an activation of the proteasome system occurs in conjunction with significant muscle atrophy following 7 and 14 days of denervation. 2) With immunoproteasome deficiency, the proteasome subunits composition and the proteasome activities are altered and these alterations attenuate muscle atrophy from denervation.

A two-factor experimental design (strain x denervation days) was used in this study to test the hypotheses described above. As shown in **Figure 1**, there were two levels in the strain factor and three levels in the time factor (denervation days). Two strains, WT and L7M1 mice, underwent tibial nerve transection for three time points, 0, 7, and 14 days.

Tibial nerve transection is an established denervation method that eliminates the neural input to the gastrocnemius, soleus, and plantaris muscles. In this study, I used gastrocnemius muscle for analysis because it is the largest muscle among the three muscles and provides enough proteins for the multitude of assays. It has been reported that tibial nerve transection successfully induces progressive muscle atrophy in the gastrocnemius muscle by 20% and 40% at day 7 and 14, respectively [52]. The details in this study including the results and discussion are presented in Chapter III.

Figure1. Research design for the study in Chapter III.

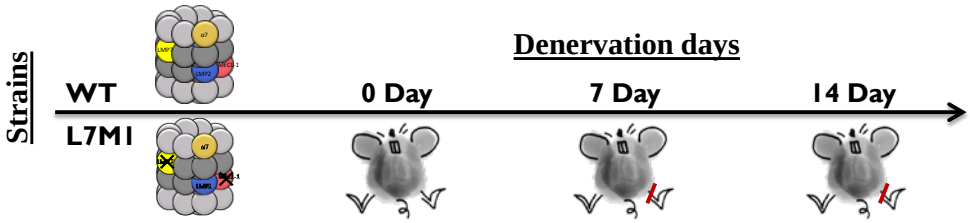

Morphological changes
- Muscle wet weight (n = 7-10)
- Cross-sectional area: H&E stain (n = 5-6)

Proteasome and immunoproteasome subunits
- Western blot (n = 4-10, depends on the antibody)

Proteasome activities
- Assay using fluorogenic peptides (n = 7-10)

Statistics
- Two-way analysis of variance (Two-way ANOVA) was performed followed by the Fisher's least significant difference (LSD) post hoc test

*Gastrocnemius muscles were used for all analyses

CHAPTER III. ROLE OF THE STANDARD AND IMMUNO-PROTEASOME IN DENERVATION-INDUCED MUSCLE ATROPHY

The content in this chapter is from the manuscript prepared to American journal of physiology. Cell physiology.

Role of the Standard and Immuno-proteasome in Denervation-induced Muscle Atrophy

Haiming Liu[1], Deborah A. Ferrington[2], Cory W. Baumann[1], LaDora V. Thompson[1]

Department of Physical Medicine and Rehabilitation[1] and Department of Ophthalmology and Visual Neurosciences [2], University of Minnesota, Minneapolis, Minnesota

CORRESPONDENCE

LaDora V. Thompson, Ph.D.
Department of Physical Medicine and Rehabilitation
University of Minnesota, Medical School, Minneapolis, Minnesota
Phone: 612-626-5271
Email: thomp067@umn.edu

- I was the primary author of the manuscript and I was responsible for the experimental design, data collection and analysis.
- Dr. Deborah Ferrington assisted in study design, data interpretation, scientific review, and providing the mice for the study.
- Dr. Cory Baumann participated in the scientific review on the manuscript.
- Dr. LaDora Thompson was the guarantor of study, assisted in study design and data interpretation, major contribution to manuscript writing, scientific review, and funding.
- I would like to thank Dr. Ted G. Graber for the assistance with tissue collection and JingYing Zhang for her assistance with Western blot preparations.

INTRODUCTION

Denervation in skeletal muscle leads to a loss of muscle mass, decreased strength [6] and impaired mobility [108]. The loss of muscle mass, or muscle atrophy, is primarily due to an imbalance between the protein degradation and synthesis. Activated catabolic pathways involving the ubiquitin-proteasome system and the autophagy/ lysosome pathway are responsible for shifting the balance towards protein degradation. While several studies report that denervation-induced muscle atrophy is associated with increased proteasome activation [23], a comprehensive examination of the multiple components of this pathway has not been done. Thus the goal of this study is focused on the proteasome.

The 26S proteasome is responsible for degradation of the ubiquitinated proteins. This proteolytic complex contains a 20S core particle consisting of four stacked rings of seven subunits each. The outer rings of 20S core contain the constitutively expressed alpha subunits, which associate with the regulatory complex PA700. The two β rings at the center of the 20S core contain three pairs of catalytic β subunits(β1, β5 and β2), which cleave after acidic, hydrophobic, and basic amino acid residues, respectively [15,34]. These catalytic subunits are part of the standard proteasome. The immunoproteasome, which is regulated by PA28, is also present in skeletal muscle, albeit at much lower concentrations. In the immunoproteasome, the β1, β5 and β2 subunits are replaced by the inducible subunits LMP2 (β1i), LMP7 (β5i) and MECL-1 (β2i), respectively. One well-described function of the immunoproteasome is the production of immunogenic peptides as part of immune surveillence[49,109,110]. A few studies have revealed the connections between immunoproteasome and muscle atrophy; increased immunoproteasome subunits have been reported under catabolic conditions in aged rodents [16,35] and muscular dystrophy [38]. However, the contribution of immunoproteasome to the degradation of muscle post-denervation has not been defined.

The purpose of this study is two-fold: First, we evaluated multiple components of the 26S proteasome in skeletal muscle in response to denervation to improve our understanding of this system. The second objective is to investigate how immunoproteasome is altered under the condition of denervation to gain insight into immunoproteasome's role in muscle atrophy. To achieve this objective, we utilized the *lmp7*$^{-/-}$*/mecl-1*$^{-/-}$ double

knockout (L7M1) mice, which are deficient in two immunoproteasome subunits. We analyzed the composition of proteasome subunits and enzymatic activities in gastrocnemius (GAS) muscle from both wild type (WT) and L7M1 mice following tibial nerve transection for 7 or 14 days. Our results show an activation of the proteasome system occurs in conjunction with significant muscle atrophy that was equivalent in both WT and L7M1 mice following 7 and 14 days of denervation. However, in the absence of two immunoproteasome subunits, the composition of proteasome subunits and the proteasome activities were slightly altered post denervation. Thus, while the immunoproteasome influences the composition of the proteasome subunits and the function of the proteasome activity, it does not appear to be essential for protein degradation during denervation-induced atrophy.

METHODS

Animal: Male 5-7 month-old C57BL/6 wild type (WT) and the double knockout *lmp7*$^{-/-}$ *and mecl1*$^{-/-}$ (L7M1) mice on a C57BL/6 genetic background were used in present study. The description of the L7M1 mice has been reported in previous studies [49]. The WT and L7M1 mice were randomly assigned to either innervated (Day 0) or denervation (DN) group. All mice were fed ad libitum and maintained on a 14 hr light/ 10 hr dark cycle at 20 ^{o}C. At the end of the study, mice were deeply anesthetized with intraperitoneal injection of a mixture of ketamine/xylazine (100 mg/kg ketamine, 10 mg/kg xylazine). While under anesthesia, the mice were weighed and dissected for tissue collection. The gastrocnemius (GAS) muscles were divided in half along the sagittal plane during the tissue collection. Each half was flash frozen with liquid nitrogen and saved at -80 ^{o}C freezer for either enriched proteasome preparation or protein extraction. Exsanguination was performed to euthanize the mice after the dissection. All procedures and protocols were approved by the Institutional Animal Care and Use Committee of the University of Minnesota.

Tibial nerve transection: Mice from the DN group underwent tibial nerve transection (modified from [52,53]) on the right hindlimb for either 7 (Day 7) or 14 days (Day 14). In brief, 2.5% inhalation isoflurane was used to put the mouse under deep anesthesia. Next, an incision (1cm) was made from the sciatic notch to the knee followed by cutting through the hamstring muscle. The tibial nerve was then identified and separated from the peroneal and sural nerve branches at the area of the popliteal fossa. One knot was made (8-0 sterile silk suture) on the distal portion of the tibial nerve. To prevent re-innervation, the proximal portion of the tibial nerve (approximately 5 mm above the knot) was sutured to the biceps femoris muscle. A piece of the tibial nerve was removed between the suture site and the knot (≥3 mm segment). The muscle and skin-incision were closed by sutures and glued completely with vet-bond. All surgical procedures were performed under aseptic conditions. After surgery, the mouse was given 0.1ml Buprenorphine (0.03 mg/ml) for analgesia and returned to the cage with soft bedding in the bottom and lying on a heating pad until fully conscience. The incision site was monitored for three days after the surgery. Mice were also monitored for activity, eating/drinking status, urine, and feces production daily for three days.

Enriched proteasome preparation and protein extraction: The enriched proteasome preparation was produced as described previously with a few modifications [16,38]. One half of the frozen GAS muscle was sealed in a pouch and dipped in liquid nitrogen then crushed using a hammer and a pestle. The crushed muscle was first homogenized in buffer (0.1 M KCl, 20 mM MOPS, pH7.0) followed by centrifugation at 4,000 g, 4 ^{o}C for 20 min. The supernatant was collected. This step was repeated (for a total of two times). Next, the supernatants were centrifuged at 1,180 g for 20 min at 4 ^{o}C. The supernatant was removed and centrifuged at 100,000 g for 16 hrs at 4 ^{o}C. The pellet was then homogenized in buffer (50 mM Tris-HCl, 5 mM $MgCl_2$, 0.1% CHAPS, and 0.4% sucrose, pH7.5) and stored at -80 ^{o}C. The other half of the GAS muscle was prepared for detecting protein content of autophagy marker microtubule associated protein light chain 3 (LC3). Briefly, in order to perform this protein extraction, a portion of GAS muscle (~ 35 mg/muscle) was homogenized in 800 μl RIPA buffer (Thermo Scientific, Rockford, IL) with a supplement of 8 μl protease inhibitor cocktail (Thermo Scientific, Rockford, IL). Homogenate was centrifuged at 10,000 g for 15 min at 4 ^{o}C and the supernatant was retained. The protein concentration of both preparations was determined by the Bicinchoninic Acid (BCA) protein assay.

Western blotting. To determine the protein content of proteasome/ immunoproteasome subunits, and LC3, Western blotting was performed with antibodies that recognize these specific proteins. Prior to analyses, the optimal protein load (within the linear range of response) was determined for each antibody. The muscle homogenates described before were diluted with reducing sample buffer (Thermo Scientific, Rockford, IL) and heated at 95 ^{o}C for 4 min. The samples were loaded equally on a 13% sodium dodecyl sulfate (SDS)-polyacrylamide gel and separated by electrophoresis using mini-vertical gel electrophoresis units (BIO-RAD). The proteins were transferred to PVDF membranes using either Trans-blot SD semidry transfer cell (BIO-RAD) at 14 V for 30 min (α7, β1, β5, β2 and LC3) or using Mini Transfer-Blot Cell (BIO-RAD) at 110 V for 1 hr (all of the remaining proteins). After blocking in 5% hipure liquid gelatin (Norland Products, Inc., Cranbury, NJ) or 5% non-fat dry milk in TBS/T at room temperature for one hour, membranes were incubated with primary antibodies at 4 ^{o}C for overnight. Goat anti-

mouse (Thermo Fisher Scientific) or goat anti-rabbit HRP (BIO-RAD) secondary antibody was used at an appropriate concentration. Protein load and antibody information are described in **Table 1**. The membranes were then developed using SuperSignal West Dura Extended Duration chemiluminescence substrate (Pierce). Images were taken by ChemiDoc XRS (BIO-RAD) and densitometry analysis was performed by Quantity One (BIO-RAD). A GAS muscle from a WT mouse was used as a blot control to compare samples on different blots. Final protein content of each individual sample was expressed as a ratio of the intensity of the sample to the blot control probed with the same antibody. Purified 20S proteasome (Boston Biochem, Cambridge, MA) and 20S immunoproteasome (Boston Biochem, Cambridge, MA) were used as positive controls for proteasome and immunoproteasome subunits.

Proteasome activity assay: Proteasome activities were determined using fluorogenic peptide substrates as previously described (Chen et al., 2014). LLE-AMC (Proteasome Substrate II, Fluorogenic, EMDmillipore, Billerica, MA), LLVY-AMC (Proteasome Substrate III, Fluorogenic, EMDmillipore, Billerica, MA) and VGR-AMC (Bz-Val-Gly-Arg-AMC, ENZO) were used for caspase-, chymotrypsin-, and trypsin- like activities, respectively. Peptides were prepared as a 40 mM stock solution in DMSO and diluted in 50 mM Tris pH 7.8 buffer (final concentration: LLE – 200 uM; LLVY – 75 uM; VGR – 150 uM). Enriched proteasome preparations (4 ug/well for caspase- and chymotrypsin-activities; 7.5 ug/well for trypsin-like activity) were incubated in buffer (50 mM Tris pH7.8, 5 mM MgCl2, 20 mM KCl, and 1mM ATP) with or without 0.2 mM MG132 (Z-Leu-Leu-Leu-H, aldehyde, Peptides International, Louisville, KY), which is a proteasome inhibitor, for 30 min at 37 ^{o}C before adding the fluoropeptides. A negative control without any 37luoropeptides was used to determine the background signals. A serial dilution of 7-Amino-4-methylcoumarin (AMC, Sigma- Aldrich, St. Louis, MO) was used to generate a standard curve. Fluorescence was measured at 37 ^{o}C in a CytoFluor 4000 Multiwell Plate Reader (Applied Biosystems, Foster City, CA) / Synergy™ HTX Multi-Mode Microplate Reader (BioTek, Winooski, VT) at a wavelength of 360/40 nm (excitation), 460/40 nm (emission) and a gain of 70 for 2 hr at 5 min intervals. The activities were determined by comparing peptide fluorescence from samples with fluorescence of the standard curve of AMC.

Histology: Cross-sectional area (CSA) of individual fibers from the GAS muscle was determined as previously described [111]. A piece of the frozen GAS muscle was mounted with OCT (Tissue-Tek, Torrance, CA) and sliced at 10 μm using a Cryostat (Leica CM3050S, Nussloch, Germany) at -25 ^{o}C. The muscle sections were dried at room temperature for 30 min, stained with hematoxylin and eosin, and imaged at 20x with a microscope (Nikon Eclipse E400). CSA was determined by circling 200-300 individual myofibers selected randomly per muscle using ImageJ analysis software (National Institutes of Health, http://rsb.info.nih.gov/ij/).

Statistical analysis: Data are presented as means ± SEM. Statistical analysis was performed by IBM SPSS 22. A significant difference was achieved when $p < .05$. To determine the difference between strains over denervation, data was analyzed by two-way ANOVA. If an effect of interaction (strain x DN days, $p < .05$) presented in the two-way ANOVA, data was further analyzed by LSD *post hoc* test. For two of the proteins, LMP7 and MECL-1, one-way analysis of variance (ANOVA) was performed to identify the time effect of denervation in the WT mice.

RESULTS

Immunoproteasome deficiency does not affect GAS atrophy following denervation

To assess the extent of atrophy in the GAS muscles after tibial nerve transection in WT and L7M1 mice, muscle weight (muscle/body weight) and cross-sectional area (CSA) were determined in each experimental group (**Fig. 1**). Both WT and L7M1 mice exhibited a significant time-dependent decrease in normalized muscle weight after denervation (**Fig. 1a**. Two-way ANOVA, time effect: $p < .001$). After 7 days of denervation, the normalized muscle weight decreased 16% in WT and 19% in L7M1 compared to their corresponding day 0 group. At day 14, the muscle loss continued, increasing to 35% and 39% in WT and L7M1, respectively. Importantly, no strain difference in the normalized muscle weight was detected (strain effect: $p = .416$). Consistent with results from whole muscle weight, single skeletal muscle fiber CSA decreased significantly following 14 days of denervation in both strains (**Fig. 1b**. WT: 40% decrease; L7M1: 31% decrease) and there was no evidence of strain difference. (WT: 0d *vs.* 14d, 2005 ± 127 *vs.* 1210 ± 20 μm^2, L7M1: 0d *vs.* 14d, 1708 ± 107 *vs.* 1184 ± 74 μm^2, Two-way ANOVA, time effect: $p < .001$, strain effect: $p = .186$). In examining the fiber size distribution at day 0 and 14 after denervation (**Fig. 1c** and **1d**), there is a shift towards smaller fiber CSA at day 14 in both strains, with a decrease in frequency of large fibers with CSA > 2400 μm^2. Together, immunoproteasome deficiency does not influence the atrophy in GAS muscles from tibial nerve transection at 7 or 14 days.

Protein content of proteasome subunits in response to denervation

To investigate the composition of the proteasome subunits in the absence of LMP7 and MECL-1 following 7 and 14 days of denervation, we detected the protein content of each proteasome subunit in GAS muscles from WT and L7M1 mice in each experimental group. In the enriched-proteasome preparation of the GAS muscle from each mouse, Western blot analysis was performed using specific antibodies for α7, subunits of the regulatory complexes (PA700/Rpt1 and PA28α) and the catalytic β subunits (standard and inducible forms).

Total proteasome content: Because the α-subunits are constitutively expressed in the 20S proteasome the evaluation of the α7 content is a good representative of the total proteasome [48]. With denervation, the α7 content in both strains showed a time-dependent increase in proteasome content ($p < .001$, **Fig. 2b**)

PA700 and PA28: The multi-subunit regulatory complex PA700 binds to the 20S proteasome core to form a 26S proteasome. To estimate PA700 content, we measured Rpt1, one of the subunits of the complex. After denervation, the PA700/Rpt1 content showed a time-dependent increase in both strains (**Fig. 2c**). The ATP-independent regulatory complex, PA28, is associated with immunoproteasome function (such as antigen presentation). In both strains, the content of PA28α increased significantly at day 14 when compared to day 0 (**Fig. 2d**).

β subunits: The β subunits responsible for the proteasome's catalytic activities include the standard subunits (β1, β5, β2) and the inducible subunits (LMP2/β1i, LMP7/β5i, MECL-1/β2i). In general, all standard subunits increased in response to denervation in both strains (**Fig. 3b-d**); however, the denervated muscles from the WT mice exhibited a robust elevation in β1 and β5 content at day 7 compared to L7M1 (**Fig. 3b**. $p = .003$ (LSD); **Fig. 3c**. $p = .002$ (LSD)). Specifically, with 7 days of denervation, the increase in β1 and β5 were 600% and 500% in WT. In contrast, in L7M1, β1 and β5 content only increased 300% and 200%. At day 14, no strain difference in β1 and β5 content was detected. With denervation, the β2 content in both strains showed a time-dependent increase at day 7 and day 14 (**Fig. 3d**, $p < .001$).

Fig. 4 highlights the LMP7, MECL-1, and LMP2 content in denervated muscles from WT and L7M1 mice. As expected, we did not detect any protein expression of LMP7 or MECL-1 in the L7M1 muscles **(Fig. 4a),** which confirms the genetic knockout of these subunits. In WT mice, LMP7 and MECL-1 content increased at day 7 and this increase was sustained through day 14 after denervation (**Fig. 4b-c**). Lastly, the LMP2 content, which is the only inducible subunit in L7M1 mice, was increased in both strains following denervation. However, the WT showed a higher overall content compared to the L7M1 mice (**Fig. 4d**, strain effect: $p = .003$).

In summary, in both strains, the subunits in the proteasome system, including α7, regulatory complexes, the standard β and the inducible subunits were elevated in the denervated muscle. However, the change in composition of the subunits in both strains did not parallel one another. Under the condition of denervation, there was a robust increase in β1 and β5 content in WT mice at day 7. However, the mice without immunoproteasome subunits LMP7 and MECL-1 had attenuated response for β1 and β5. Also, lower content of LMP2 was observed in L7M1 muscles.

Proteasome activities

To determine whether the genetic elimination of the two inducible subunits LMP7 and MECL-1 influences the function of the proteasome, the caspase-, chymotrypsin- and trypsin- like activities were monitored using fluorogenic peptide substrates with or without the proteasome inhibitor, MG132, to measure proteasome-specific activity **(Fig. 5)**. With denervation, both strains showed a significant increase in all three proteasome activities. The rate-limiting proteasome activity, chymotrypsin-like activity, showed an interaction between time and strain (**Fig. 5a**, $p = .041$). Specifically, the chymotrypsin-like activity in WT mice was greater than the L7M1 mice after 7 days of denervation. Similarly, an interaction was observed in the trypsin-like activity. At day 14, the trypsin-like activity in L7M1 mice was greater than the WT (**Fig. 5b**, at day 14, WT *vs.* L7M1: $p = .027$). In contrast to the chymotrypsin-like and trypsin-like activities, the caspase-like activity did not show an interaction; however, there was a strain effect. Specifically, L7M1 mice showed greater caspase-like activity at baseline and across the denervation period compared to the WT (**Fig. 5c**, strain effect: $p = .001$). Taken together, immunoproteasome deficiency altered the proteasome activities.

Autophagy markers

Autophagy is an alternative protein degradation pathway that is activated in denervation-induced muscle atrophy [112]. Although the autophagic flux is the most accurate means to estimate the autophagy degradation activity, these measures require the application of lysosomal inhibitors, which cannot be done in whole muscle [113]. However, Western blot analysis is still suitable to report the overall change of autophagic protein levels in a

tissue, so we assessed the protein levels of the autophagic marker LC3 in the skeletal muscles from both strains of mice **(Fig. 6)**. During the process of autophagy, LC3I conjugates with phosphatidylethanolamine to convert to LC3II during the formation of the autophagosome [114]. These two species can be distinguished on Western blotting by their different mobility on an SDS-PAGE gel. Therefore, we probed for both LC3I and LC3II content in order to estimate the activation of the autophagy pathway. The content of both LC3I and LC3II increased **(Fig. 6b-c)** after denervation in both strains. These results indicate autophagy was activated in skeletal muscle and immunoproteasome deficiency did not alter the process of autophagy following denervation.

DISCUSSION

The current study investigated multiple components of the proteasome system in skeletal muscle in response to denervation, which to date has not been comprehensively evaluated. This is also the first study to investigate the role of immunoproteasome in muscle protein degradation in the *lmp7*$^{-/-}$*/mecl-1*$^{-/-}$ double knockout mice. The major findings include: activation of the proteasome system occurs in conjunction with significant muscle atrophy in the WT and L7M1 mice following 7 and 14 days of denervation. However, the immunoproteasome deficient mice presented a different composition of proteasome subunits post-denervation and slightly altered enzymatic proteasome activities compared to WT mice. Interestingly, atrophy in the gastrocnemius muscles was not affected by the genetic ablation of LMP7 and MECL-1. In summary, the immunoproteasome influences the composition of the proteasome subunits and the function of the proteasome but does not appear to be essential for protein degradation during denervation-induced atrophy.

Activation of the 26S proteasome, β-subunits, and autophagy following denervation in WT mice

The ubiquitin-proteasome system is known to degrade sarcomeric proteins, such as myosin, actin, and troponin under conditions of muscle atrophy [67]. One of the key components of this system is the 26S proteasome, which is composed of the regulatory complex PA700 and the 20S core. The ubiquitin-conjugated proteins (sarcomeric proteins) are recognized, deubiquitinated and transferred to the 20S proteasome core via the ATP-dependent PA700 complex [115]. As we expected, in the WT mice, a significant time-dependent increase was found in the content of the total 20S proteasome and the PA700 complex after denervation. These findings are consistent with two previous studies reporting an upregulation of both total proteasome and its regulatory complexes in denervated muscles following the same two periods of denervation that resulted in 20% and 41% muscle atrophy at day 7 [36] and day 14 [23], respectively. Moreover, increased α1 and PA700 (Rpt1) were found within a very short period of muscle denervation (3-day) and with a longer period of denervation (14-day) [23]. Similar findings were noted in mouse soleus muscle in an intermediate period of denervation (7 days post-denervation) with increased protein content of α5 and PA700 (Rpt4, Rpn10) [36]. We also monitored the

content of the regulatory complex PA28α, which is an ATP-independent and associated with the immunoproteasome related functions, such as generation of antigenic peptides [116]. Our data and that of others [23] show PA28 is upregulated with denervation, which suggests that PA28 complex is involved in muscle degradation following denervation.

In addition to the total content of proteasome and the activators, the composition of the catalytic β-subunits is also important for protein degradation. The β-subunits are located at the center of the 20S core to form the β-rings. Three catalytic β-subunits, β1, β2, and β5, as well as their inducible counterpart, LMP2 (β1i), MECL-1(β2i), and LMP7 (β5i) are able to perform distinct proteasome activities for cleavage after certain amino acids. The up-regulation in multiple proteasome subunits is as expected because following denervation there is extensive degradation of the sarcomeric proteins resulting in muscle atrophy. Similarly, upregulation of the catalytic subunits was noted in two previous studies that investigated similar durations of denervation [23,36].

In addition to the ubiquitin-proteasome system, another important catabolic pathway in denervation-induced muscle atrophy is the autophagy/lysosome pathway. It is known that autophagy functions to maintain the homeostasis in skeletal muscle by removing protein aggregates, dysfunctional mitochondria, and endoplasmic reticulum membranes [10,13]. Consistent with others [22,117], we observed an accumulation of the autophagy marker LC3 in the denervated muscles from the WT mice suggesting autophagy activation.

In order to have an understanding of the cellular mechanisms responsible for the up-regulation of the proteasome in WT mice it is important to elucidate the triggers that occur with denervation. One of the cellular triggers is activation of mammalian target of rapamycin (mTOR) [56,57] , which is known for negatively regulating the autophagy pathway [36,118]. However, mTOR also regulates the proteasome system. Specifically, mTOR signaling may contribute to the increased content of standard proteasome subunits and PA700 by activating the transcription factors, nuclear factors erythroid-derived 2-related factors (Nrfs). The link between Nrfs and mTOR has been clearly established in cultured cells. For instance, application of rapamycin, which is an inhibitor of mTOR, attenuated the increase in standard proteasome subunits and the activator PA700 [64]. Also,

in vivo studies have demonstrated that both Nrfs and mTOR are elevated after denervation [36,117].

Another trigger for protein degradation that occurs with denervation is HDAC/Mitogen-activated protein kinases (MAPK) cascade. In fact, transcription factors activator protein 1 (AP1) and specificity protein 1 (Sp1) are increased via HDAC4 triggered MAP3 kinase cascade after denervation [59,60]. These transcription factors are associated with the transcription of the immunoproteasome subunits, LMP2, LMP7 and MECL-1 in cells [61,62].

In summary, the denervation-related increase in standard and immune-proteasome subunit content in muscle reported in the current study is likely due to upregulation of transcription factors triggered by the lack of innervation via mTOR and HDAC signaling. Further investigations are needed to substantiate the involvement of these two pathways.

Proteasome activities in response to denervation in the WT mice

In order to have a reduction in muscle cross-sectional area, there are three enzymatic activities of the proteasome functioning together to catalyze the digestion of myofibrillar proteins into peptides, including chymotrypsin-, trypsin- and caspase- like activities. Indeed, our results in the WT mice are similar to the reported literature [23] and we have comprehensively described the three activities at 7 and 14 days after denervation.

Chymotrypsin-like activity is the most dominant proteasome activity, therefore it functions as a rate-limiting step in protein degradation [119–121]. In skeletal muscle, multiple studies report that chymotrypsin-like activity is upregulated by 40% - 70% after denervation [23,36,117,122]. Because the chymotrypsin-like activity is associated with specific proteasome subunits within the 20S core, any changes in subunit composition have potential to influence and subsequently explain the enzymatic activity response. In fact, in the WT mice, the robust response in β5 content at 7 days post-denervation is consistent with its observed increase in activity. Although LMP7 and LMP2 contributes to the chymotrypsin-like activity and their content is increased, their direct contribution to the overall proteolytic function is likely minimal. The minimal contribution is likely due to two reasons. First, in un-manipulated skeletal muscle [123] the immunoproteasome

represents a small percentage (5%) of the total 20S proteasome. Second, with denervation both standard and immunoproteasome content increase; however, the fold increase is greater in the standard subunits.

In contrast to the rate-limiting β5-mediated chymotrypsin-like activity with denervation, the caspase-like and trypsin-like activities appear to be less important in protein degradation. Evidence to support the limited roles of these two activities, include: (1) inhibition of caspases-like activity did not lead to accumulation of the misfolded proteins [119,124]; (2) inhibition of the trypsin-like activity only led to small reduction of protein degradation [125]. Nevertheless, the elevation of caspase-like and trypsin-like activities in response to denervation in the current study is consistent with previous literature in the WT mice [23]. Also, the pattern of change in each activity is comparable to the corresponding standard β subunits and PA700 content.

Taken together, with 7 days and 14 days of denervation, both the ubiquitin-proteasome and the autophagy/lysosome pathways have been activated for protein degradation in the WT mice, which is consistent with the literature. We also observed an upregulation in the standard and inducible catalytic subunits of the proteasome, which was likely due to activation of the upstream transcription factors triggered by denervation. Moreover, this upregulation of the catalytic subunits is likely responsible for the increased proteasome enzymatic activities for protein degradation.

Activation of the 26S proteasome, β-subunits, and autophagy following denervation in Immunoproteasome deficient mice

Overall, there is evidence for proteasome and autophagy activation in immunoproteasome deficient mice; however, there are several notable differences compared with WT mice. Specifically, L7M1 protein content of β1 and β5 did not increase to the same extent as the WT muscle 7 days post denervation. There are some possible explanations for this attenuation in β1and β5 content. One mechanism for the blunted response in β1and β5 in L7M1 is likely due to the impaired incorporation of these subunits into the 20S core [35,47]. For instance, in the presence of MECL-1 it has been reported that β5 was more efficiently incorporated into immunoproteasomes [46]. Also,

there was a decreased ability of the 20S to assemble in immortalized lymphoblastoid cell lines from patients with a LMP7 gene mutation [43]. Similar findings were demonstrated in spleen, retina [48,49], and C2C12 myoblasts [126], where decreased incorporation of LMP2 was noted with deletion or inhibition of LMP7 and/or MECL-1. Together, LMP7 and MECL-1 likely exhibit a role in facilitating the incorporation of the standard proteasome subunits, as well as the inducible subunit LMP2.

The enriched-proteasome preparation used in the current study is an established method to detect the proteasome subunits fully incorporated into the mature 20S core [16,127]. Thus, our data suggests an impaired ability of incorporation of the standard proteasome in the absence of the inducible subunits after denervation. In order to test this possibility, protein content of the unincorporated subunits within the cytosol would require investigation. Although we propose the immunoproteasome deficiency alters subunit incorporation, future research is needed to confirm that these two mice strains have similar responses upstream (e.g., HDAC and mTOR) and gene regulation.

Proteasome activities in response to denervation in Immunoproteasome deficient mice

Similar to the WT, the proteasome enzymatic activities in L7M1 mice were also increased following 7 and 14 days of denervation. However, we have observed strain differences in these proteasome activities. For instance, the chymotrypsin-like activity of the immunoproteasome deficient mice is blunted at 7 days in contrast to the WT. This response is consistent with its subunit composition (lower β5 and LMP2 and no LMP7). The lower content of β5 and LMP2 is likely due to impaired incorporation of these subunits into the proteasome core [46,47].

One interesting finding in the current study involves the time course of the caspase-like and the trypsin-like activities associated with the denervation in the L7M1 mice. The content of β2, MECL1 and β1 within each muscle does not appear to support the observed enzymatic activities. This unexpected finding, lack of a relationship between subunit composition and its activity, may involve the presence of intermediate proteasomes. The intermediate proteasome is a mixture of both standard and inducible subunits in the 20S core, where the inherent quality of the proteasome enzymatic activity

is reported to be quite variable [123]. Therefore, the variability of the trypsin-like and the caspase-like activities in the current study may be due to presence of the intermediate proteasomes [35,48,123].

Despite these notable differences in the proteasome subunit content and activities between the two strains, the overall extent of muscle atrophy was the same. It seems likely, the same extent muscle atrophy was due to the major contribution of chymotrypsin-like activity and the autophagy pathway. Even with the impaired proteasome assembly in the immunoproteasome deficient mice and the 25% lower chymotrypsin-like activity, there does not seem to be a significant effect on the process of protein degradation.

Conclusion

The current study demonstrated that denervation-induced activation of the proteasome system is associated with significant increases in both content of catalytic subunits and enzymatic activities in skeletal muscle of WT and L7M1 mice. The genetic elimination of the two inducible catalytic subunits, LMP7 and MECL-1, attenuated the elevated chymotrypsin-like activity by potentially suppressing β5 and LMP2 incorporation into the 20S core. Future investigations are required to detect the protein content of the proteasome subunits in the cytosol in order to confirm there are un-incorporated proteasome subunits in the L7M1 mice. In addition, future study is also required to confirm the role of immunoproteasome in affecting the upstream cell signaling (such as HDAC and mTOR signaling) of denervation-induced muscle atrophy.

FIGURES AND TABLES

Figure 1. Atrophy of the GAS muscle and single fibers in WT and L7M1 mice.

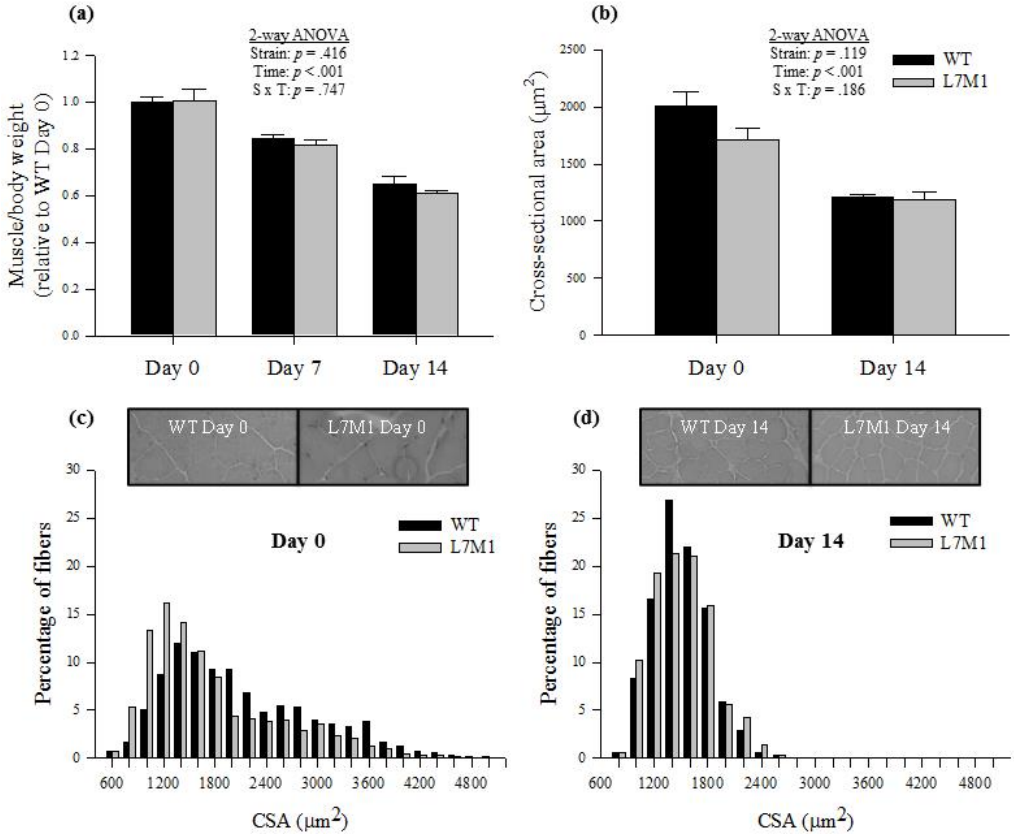

Two-way ANOVA was used to detect the effect of strain (WT *vs.* L7M1) and time (Day 0, 7, and 14). (a) Results of muscle/body weight are expressed relative to the WT Day 0. (b) CSA of individual fibers in GAS muscle (expressed as μm^2). Statistical comparison showed a significant denervation (time) effect in both muscle/body weight and CSA ($p < .001$). No strain effect or interaction was detected in any of these measures. Panels c and d show fiber size distribution of individual fibers of GAS muscle from WT and L7M1 mice at day 0 (c) and at day 14 (d) after denervation. The insert is H&E stain of a section from GAS muscle in WT and L7M1 at day 0 and day 14 after denervation. Values are mean ± SE. Sample size: for muscle/body weight: n = 7-10 per group; for CSA: n = 5-6 per group, 200-300 individual fibers analyzed per animal.

Figure 2. Protein content of α7 and proteasome activators in WT and L7M1 mice with denervation.

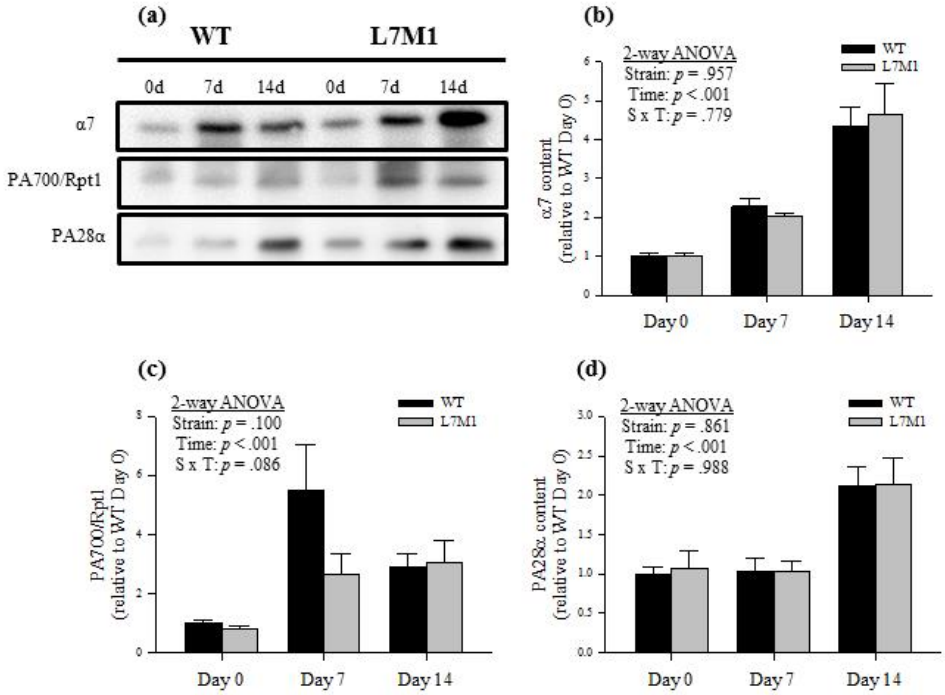

Representative Western blots from GAS muscles of WT and L7M1 mice at 0, 7 and 14 days (0d, 7d, and 14d) of denervation. (b-d) Results of densitometry are presented as the fold change compared to WT 0 Day for each respective protein. Each panel contains results of two-way ANOVA that was used to detect the effect of strain (WT vs. L7M1) and time (Day 0, 7, and 14) for (b) α7, (c) PA700/ Rpt1, and (d) PA28α. Statistical comparison showed a significant denervation (time) effect in all the proteins ($p < .001$). No strain effect was detected in any of these proteins. Values are mean ± SE. Sample size per group: n = 7-10.

Figure 3. Protein content of standard catalytic β subunits in WT and L7M1 mice with denervation.

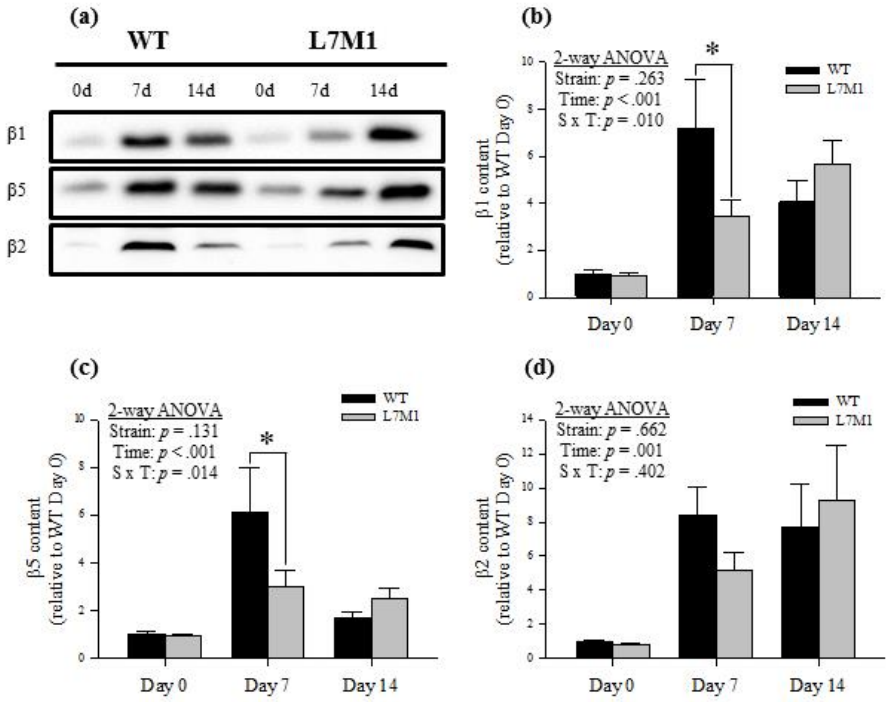

Representative Western blots from GAS muscles of WT and L7M1 mice at 0, 7 and 14 days (0d, 7d, 14d) of denervation. (b-d) Results of densitometry are presented as the fold change compared to WT Day 0 for each respective protein. Each panel contains results of two-way ANOVA that was used to detect the effect of strain (WT vs. L7M1) and time (Day 0, 7, and 14) for (b) β1, (c) β5, and (d) β2. When an effect of interaction was detected, a Fisher's LSD *post-hoc* test was followed to compare differences between strains at each time point (* indicates L7M1 is significant different from WT at that given time point, $p \leq .05$). Statistical comparison showed a significant denervation (time) effect in all the proteins above ($p < .001$). No strain effect was detected in any of these proteins. (b) β1 was significantly higher at day 7 in the WT compared to L7M1 (S x T, $p = .01$, LSD *post-hoc* test: $p = .003$). (c) β5 was significantly higher at day 7 in the WT compared to L7M1 (S x T, $p = .01$, LSD *post-hoc* test: $p = .002$). Values are mean ± SE. Sample size per group: n = 4-10.

Figure 4. Protein content of inducible catalytic β subunits in WT and L7M1 mice with denervation.

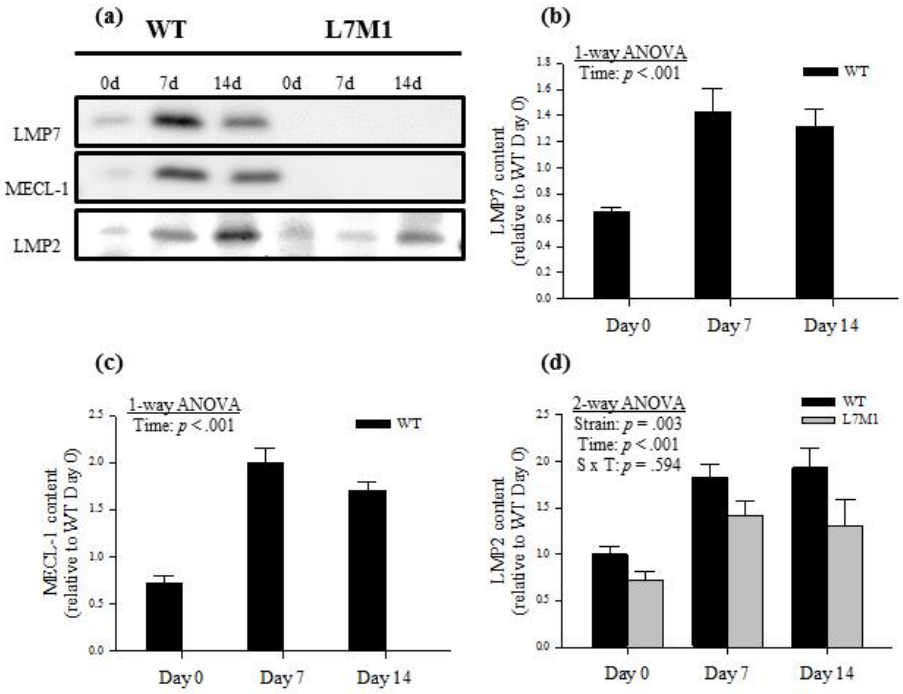

Representative Western blots from GAS muscles of WT and L7M1 mice at 0, 7 and 14 days (0d, 7d, and 14d) of denervation. Consistent with the genetic ablation of the *lmp7* and *mecl-1* genes, no protein for these subunits was detected in L7M1 muscles. (b-d) Results of densitometry are presented as the fold change compared to WT Day 0 for each respective protein. For (b) LMP7 content and (c) MECL-1 content, the one-way ANOVA statistical comparison showed a significant denervation (time) effect in LMP7 and MECL-1 content ($p < .001$). (d) For LMP2 content: The two-way ANOVA result is shown in this panel. Statistical comparison showed a significant denervation (time) effect ($p < .001$) and strain effect ($p = .003$) in LMP2 content. Values are mean ± SE. Sample size per group: n = 5-10.

Figure 5. Proteasome enzymatic activities in WT and L7M1 mice with denervation.

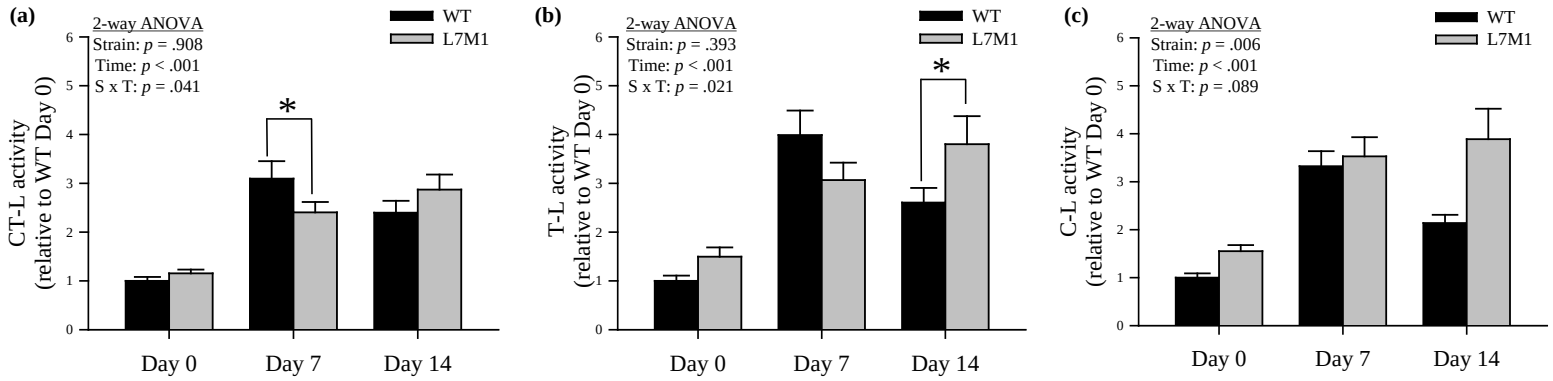

Results are presented as the fold change compared to WT Day 0 for proteasome enzymatic activity in each experimental group. Two-way ANOVA was used to detect the effect of strain (WT vs. L7M1) and time (Day 0, 7, and 14) for (a) Chymotrypsin- like (CT-L) activity, (b) Trypsin- like (T-L), and (c) Caspase- like (C-L) activity. When an effect of interaction was detected, a Fisher's LSD *post-hoc* test was performed to compare differences between strains at each time point (* indicates L7M1 is significant different from WT at that given time point, $p \leq .05$). Statistical comparison showed a significant denervation (time) effect in all proteasome activities ($p < .001$). No strain effect was detected in either CT-L or T-L activities; whereas the C-L activity showed significant strain difference ($p = .01$). (a) CT-L activity was significantly higher in the WT at day 7 compared to L7M1 (S x T, $p = .04$, LSD *post-hoc* test: $p = .04$). (b) T-L activity was significantly lower in the WT at day 14 compared to L7M1 (S x T, $p = .02$, LSD *post-hoc* test: $p = .03$). Values are mean ± SE. Sample size per group: n = 7-10.

Figure 6. Protein content of autophagy markers LC3 in WT and L7M1 mice with denervation.

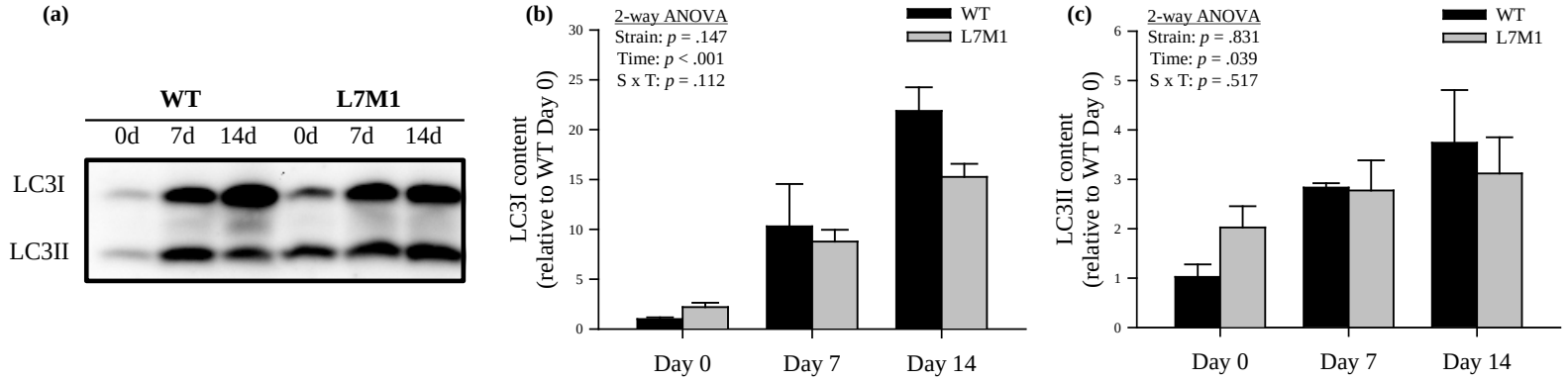

(a) Representative Western blot from GAS muscles of WT and L7M1 mice at 0, 7 and 14 days (0d, 7d, 14d) of denervation. Each panel contains results of two-way ANOVA that was used to detect the effect of strain (WT vs. L7M1) and time (Day 0, 7, and 14) for (b) LC3I and (c) LC3II. Statistical comparison showed a significant denervation (time) effect in both LC3I and LC3II content ($p < .04$). No strain effect or interaction was found. Values are mean ± SE. Sample size per group: n = 3-5.

Table 1. Antibodies used for Western blotting.

Table 1. Antibodies used for Western blotting.

Antibody	Type	Host	Dilution	Protein load (µg)	Company for primary antibody	Secondary antibody dilution
Proteasome subunit α7	M	M	1:1000	4	Enzo Life Sciences, Farmingdale, NY	1: 16,000
Proteasome 20S Y (β1)	P	R	1:1000	10	Thermo Scientific, Rockford, IL	1: 16,000
Proteasome 20S X (β5)	P	R	1:1000	10	Thermo Scientific, Rockford, IL	1: 12,000
Proteasome 20S Z (β2)	P	R	1:500	30	Thermo Scientific, Rockford, IL	1: 20,000
Proteasome subunit LMP2	M	M	1:500	26	Enzo Life Sciences, Farmingdale, NY	1: 12,000
Proteasome subunit LMP7	P	R	1:1000	22	Enzo Life Sciences, Farmingdale, NY	1: 16,000
Proteasome subunit MECL-1	P	R	1:500	26	Enzo Life Sciences, Farmingdale, NY	1: 12,000
19S (PA700)/Rpt1	P	M	1:1000	15	Enzo Life Sciences, Farmingdale, NY	1: 10,000
PA28α	P	R	1:1000	15	Enzo Life Sciences, Farmingdale, NY	1: 10,000
LC3B	P	R	1:500	30	Novus Biologicals, Littleton, CO	1: 10,000

All antibodies were isotype IgG. Monoclonal (M), polyclonal (P), host species mouse (M), host species rabbit (R).

INTERLUDE II

In the previous chapter we showed an activation of the proteasome in conjunction with significant muscle atrophy that was equivalent in both WT and L7M1 mice following 7 and 14 days of denervation. Our results indicate that the significant amount of muscle atrophy is primarily due to the ubiquitin-proteasome system through the standard 26S proteasome. The immunoproteasome has a role in influencing the composition of the proteasome subunits and the proteasome activity but does not appear to be essential for protein degradation during denervation-induced atrophy.

As we learned from Chapter II, the 26S proteasome does not work alone in the ubiquitin-proteasome system. E3 ligases and ubiquitins are required to dissemble and ubiquitinate the contractile proteins. There is ~40% muscle loss after 14 days of denervation suggesting massive degradation of myosin and actin. This massive loss in muscle mass likely to changes in muscle contractility [53,128]. As aforementioned in Chapter II 2.1., muscle function can be affected by any alteration in actin and myosin. Based on the large decrease in muscle size it is clear there is protein degradation (quantity); but it is possible that the activation of the ubiquitin-proteasome system may also modify the function of contractile proteins (quality). Hence, the next question asked was: *If there is a decrease in force generation, is the decrease due to a change in muscle quantity and/or a change muscle quality?*

In the following Chapter, Chapter IV: "Denervation-induced activation of the ubiquitin-proteasome system reduces skeletal muscle quantity not quality", is focused on the denervation-induced muscle contractility changes in conjunction with ubiquitin-proteasome system, which has been less reported in the literature [22,129]. Therefore, the study had two goals: first was to document how the ubiquitin-proteasome system responds following denervation; second, to identify muscle quantity (muscle size) and muscle quality (specific force) as consequences of these changes.

The research design is described in **Figure 1**. In brief, three experimental groups based on different denervation days: control, 7 day or 14 day denervation. Denervation was

achieved using tibial nerve transection and the rationale has been described in the previous Chapter. For this study, the soleus muscle was used for muscle morphological changes (CSA), biochemical analyses (Western blot), and whole muscle physiology. For the CSA and muscle physiology, we only analyzed groups of control and 14-day denervation because the goal of this study was to assess function shortly after the ubiquitin-proteasome system was activated, which we determined via Western blot analysis. The details in this study including the results and discussion are presented in Chapter IV.

Figure 1. Research design for the study in Chapter IV.

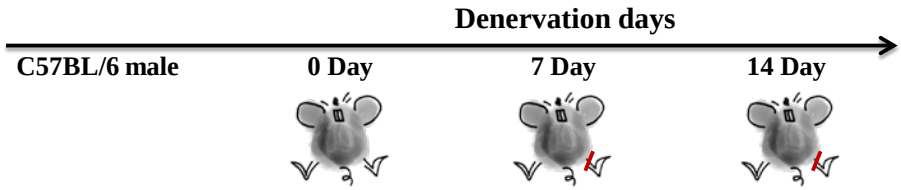

Morphological changes
- Cross-sectional area: H&E stain (control vs. 14 Day, n = 6-7)

Contractile function
- Silver stain (MyHC/actin, n = 5-7); whole muscle physiology (control vs. 14 Day, n = 6-8)

Ubiquitin-proteasome system, metabolic and cytoskeletal markers
- Western blot (n = 5-7)

Statistics
- An independent (two groups) t-test or one-way ANOVA (three groups)

*Soleus muscles were used for all analyses

CHAPTER IV. DENERVATION-INDUCED ACTIVATION OF THE UBIQUITIN-PROTEASOME SYSTEM REDUCES SKELETAL MUSCLE QUANTITY NOT QUALITY

The content in this chapter is from the manuscript submitted to Journal of Applied Physiology.

Denervation-induced Activation of the Ubiquitin-proteasome System Reduces Skeletal Muscle Quantity not Quality

Cory W. Baumann, Haiming Liu, and LaDora V. Thompson

Department of Physical Medicine and Rehabilitation, University of Minnesota, Minneapolis, Minnesota

CORRESPONDENCE

LaDora V. Thompson, Ph.D.
Department of Physical Medicine and Rehabilitation
University of Minnesota, Medical School, Minneapolis, Minnesota
Phone: 612-626-5271
Email: thomp067@umn.edu

- I was the second author of the manuscript and I assisted with the experimental design, data collection and analysis, and scientific review.
- Dr. Cory Baumann was the primary author of the manuscript and responsible for the experimental design, data collection and analysis.
- Dr. LaDora Thompson was the guarantor of study, assisted in study design and data interpretation, major contribution to manuscript writing, scientific review, and funding.

SUMMARY OF CHAPTER IV

It is well known the ubiquitin-proteasome system is activated in response to skeletal muscle wasting and that these changes are responsible for degrading contractile proteins. The loss of these proteins inevitably reduces skeletal muscle size (i.e., quantity). However, it is currently unknown whether activation of this pathway also affects function by impairing the muscle's intrinsic ability to produce force (i.e., quality). Therefore, the purpose of this study was twofold, 1) document how the ubiquitin-proteasome system responds to denervation and, 2) identify the physiological consequences of these changes. To induce soleus muscle atrophy, C57BL6 mice underwent tibial nerve transection of the left hindlimb for 7 or 14 days (n=6-8/group). At these time points, content of several proteins within the ubiquitin-proteasome system were determined via Western blot, while *ex vivo* whole muscle contractility was specifically analyzed at day 14. Denervation temporarily increased several key proteins within the ubiquitin-proteasome system, including the E3 ligase MuRF1 and the proteasome subunits 19S, α7 and β5. These changes were accompanied by reductions in absolute peak force and power, which were offset when expressed relative to physiological cross-sectional area. Contrary to peak force, absolute and relative force at submaximal stimulation frequencies was significantly greater following 14 days of denervation. These findings suggest, 1) activation of the ubiquitin-proteasome system is associated with reductions in skeletal muscle quantity rather than quality and, 2) shortly after denervation the muscle appears to undergo a transient remodeling phase to compensate for the loss of neural activity.

Keywords: atrophy, degradation, force, function, proteolysis, remodeling

New and Noteworthy: Upregulation of the ubiquitin-proteasome system is commonly observed following various models of skeletal muscle wasting. It is well established that in these situations, activation of the ubiquitin-proteasome system impairs the muscle's ability to generate force and by extension, its functional capacity. Here, we show that the ubiquitin-proteasome system reduces function by decreasing muscle size (i.e., quantity) rather than the muscle's intrinsic force producing properties (i.e., quality).

INTRODUCTION

Skeletal muscle atrophy can occur from a variety of stressors, which include inflammation, mechanical unloading, metabolic stress and neural inactivity. These stressors are often a result of clinical conditions or chronic diseases such as limb immobilization, bed rest, cachexia, neurodegeneration and aging [4,24,115,130]. Under these situations, there is an imbalance between anabolic and catabolic processes with protein breakdown (i.e., proteolysis) exceeding protein synthesis [55,77]. Consequently, muscle mass is reduced due to the net loss of myofibrillar and soluble proteins, organelles and the cytoplasm, all of which alter muscle function either metabolically, structurally or physiologically. The increased rate of proteolysis is mediated through the autophagy-lysosome and ubiquitin-proteasome systems [4,10,69], with the latter reported to be the primary degradation pathway in skeletal muscle [131,132].

The ubiquitin-proteasome system is a complex pathway in skeletal muscle that consists of several components [24,115,133,134]. Briefly, proteins destined for degradation are conjugated to multiple molecules of ubiquitin by an ubiquitin ligase enzyme (E3). One of the main E3 ligases in skeletal muscle is the muscle RING finger 1 (MuRF1) due to the fact many of its substrates are sarcomeric proteins. Thus far, MuRF1 has been observed to ubiquitinate/interact with troponin I [135], actin [136], myosin binding protein C [9], myosin light chains 1 and 2 [9], myosin heavy chain (MHC) [137,138] and titin [139,140]. These polyubiquitin-conjugated proteins are then recognized and subsequently degraded into peptides by the 26S proteasome. To note, the 26S proteasome is composed of a cylindrical catalytic core particle (20S) capped at one or both ends with 19S regulatory complexes (also known as PA700). These 20S particles consist of four rings that contain seven subunits each. The two outer rings are composed of α-subunits (α1 to α7) and the two inner rings of β-subunits (β1 to β7). Importantly, three of these β-subunits perform distinct proteolytic activities. Specifically, activity of β1 (PSMB6), β2 (PSMB7), and β5 (PSMB5) are classified as caspase-like, trypsin-like, and chymotrypsin-like for their cleavage of acidic, basic, and hydrophobic amino acids, respectively.

It is well established that several of these components within the ubiquitin-proteasome system increase in response to skeletal muscle wasting [22,23,36,141], and that these changes are responsible for degrading the myofibrillar proteins MHC and actin [131]. Loss of these contractile proteins inevitably reduces skeletal muscle size (i.e., quantity), but more importantly, diminishes the muscle's capacity to function. For instance, it has been reported that absolute force and power were both reduced following extended periods of denervation [142]. Interestingly, these changes were also observed when expressed relative to muscle size, indicating the muscle's intrinsic ability to contract (i.e., quality) was impaired. Although it is generally accepted loss of muscle quantity following denervation is due to the ubiquitin-proteasome system, it is currently unknown whether this pathway affects muscle quality. To date, there are a limited number of reports that have assessed skeletal muscle physiology in conjunction with the ubiquitin-proteasome system after denervation [22,143]. Moreover, these studies are often not solely focused on skeletal muscle physiology and thus, most of the contractile data is incomplete. This represents a significant gap in our current understanding of how activation of the ubiquitin-proteasome system influences skeletal muscle function.

Therefore, the goals of this study were twofold, 1) document how the ubiquitin-proteasome system responds to denervation and, 2) identify the physiological consequences of these changes. To accomplish this, we first determined when content of the ubiquitin-proteasome system returned back to resting levels in denervated skeletal muscle. At this point, we then performed *ex vivo* physiology to assess whole muscle contractility. Using this design we were able to document the changes that occurred in muscle function shortly following activation of ubiquitin-proteasome system. We hypothesized that skeletal muscle function would decline after denervation as a consequence of the ubiquitin-proteasome system reducing muscle quantity rather than quality. If correct, these findings would demonstrate the ubiquitin-proteasome system is a fine-tuned proteolytic pathway that alters muscle size without significantly affecting its intrinsic ability to generate force.

METHODS

Animals

Adult male C57BL6 mice (6.50±0.24 months old) were used in this study. Mice were housed in groups of no more than 4 animals per cage, supplied with food and water *ad libitum*, and maintained in a room at 20–23°C with a 12-h photoperiod. During the final procedure (i.e., *Ex vivo muscle preparation and contractility measurements*), mice were anesthetized by an intraperitoneal injection of ketamine/xylazine (100 mg/kg ketamine, 10 mg/kg xylazine), with supplemental doses given as required. Following the completion of this procedure, mice were euthanized by exsanguination while under anesthesia. All animal procedures were approved by the Institutional Animal Care and Use Committee at the University of Minnesota.

Experimental design

Mice were randomly assigned to one of three groups: control, 7 day denervation or 14 day denervation. The control group consisted of mice that did not receive any surgery, while mice in the denervation groups underwent tibial nerve transection of the left hindlimb and were assessed in the following 7 or 14 days. Tibial nerve transection surgery results in denervation to the gastrocnemius, plantaris and soleus muscles, and has been reported to result in significant atrophy [53,54]. However, only the soleus muscle of the left hindlimb was evaluated in this study. Biochemical analyses, which included Western blotting and silver staining were assessed for all groups, while fiber cross-sectional area (CSA) and whole muscle physiology were examined in the control and 14 day groups. Post-denervation CSA and muscle physiology were only analyzed at day 14 because the goal of this study was to assess function shortly after the ubiquitin-proteasome system was activated, which we determined via Western blot analysis (See RESULTS).

Experimental methodology

Tibial nerve transection

Tibial nerve transection was performed on the left hindlimb, similar to that previously described [52,53]. Briefly, while under anesthesia (2.5% isoflurane), an incision of ~1 cm

was made from the sciatic notch to the knee. Following this initial incision, another small incision was made through the hamstring muscles to allow access to the tibial nerve. The tibial nerve was then separated from the peroneal and sural nerve branches at the area of the popliteal fossa. Using an 8-0 sterile silk suture, knots were made around the distal and proximal ends of the tibial nerve, separated by ~5 mm. A ≥3 mm piece of nerve between the two knots was then removed and the proximal end of the tibial nerve was sutured to the biceps femoris to prevent re-innervation. After denervation, the incisions made in the muscle and skin were sutured together and glued with vet-bond. Following the surgery, mice were given 0.1 ml Buprenorphine (0.03 mg/ml) for analgesia and monitored until they were ambulatory. Mice were brought back to the laboratory at 7 or 14 days post-surgery.

Ex vivo muscle preparation and contractility measurements

The soleus muscle from the left hindlimb of an anesthetized mouse was dissected free and studied using an *ex vivo* preparation, similar to that described previously [144–146]. Following excision, the muscle was mounted in an organ bath containing a Krebs-Ringer buffer (pH 7.3) with 115 mM NaCl, 5.9 mM KCl, 1.2 mM $MgCl_2$, 1.2 mM NaH_2PO_4, 1.2 mM Na_2SO_4, 2.5 mM $CaCl_2$, 25 mM $NaHCO_3$ and 10 mM glucose, which was equilibrated with 95% O_2-5% CO_2 gas and maintained at 25°C via a circulating water system. The distal tendon was attached by a silk suture and secured to a fixed support, and the proximal tendon was attached to the lever arm of a servomotor system (300B; Aurora Scientific Inc., Aurora, ON, Canada). Optimal muscle length (L_o) in the organ bath was set with a series of twitch stimulations (0.5 ms pulse at 30 V; 701B Stimulator, software controlled with Dynamic Muscle Control version 3.2; ASI). *Ex vivo* muscle length was then measured from the proximal to the distal myotendinous junctions using a digital caliper. Three minutes after L_o was determined, the muscle performed a final twitch contraction followed by a force-frequency protocol that included five isometric contractions (900 ms train of 0.2 ms pulses at 10, 40, 80, 100 and 120 Hz), all separated with a 3 min rest period. For analysis, the final twitch was recorded as peak isometric twitch force (P_t), whereas the highest recorded force during the force-frequency protocol was defined as peak isometric tetanic force (P_o).

Force-frequency relationships were modeled with the following equation: $f(x) = \min + (\max - \min) / [1 + (x/ EC_{50})^n]$, where x is the stimulation frequency, min and max are the smallest (i.e., twitch) and largest (i.e., peak tetanic) respective estimated forces, EC_{50} is the stimulation frequency at which half the amplitude of force (max – min) is reached and n, the Hill coefficient, characterizes the slope of the curve at its midpoint.

After P_o was determined, the load clamp technique was used to determine velocity of contraction as previously described [111,147]. In brief, the muscle length was set at L_o and activated at various percentages of P_o (10, 20, 30, 40, 60, 70, 80 and 90%) using the stimulation frequency that corresponded to P_o for a 500 ms train. Once the muscle could overcome the set load (clamped at 10-90% of P_o), the muscle concentrically contracted and the distance the servomotor level arm moved was recorded. The contraction velocity for each % load of P_o was then computed and converted from millimeters per second (mm/s) to a normalized measurement of fiber lengths per second (fl/s) using a ratio of intact fiber length to muscle length of 0.69 [148]. Using a custom MATLAB (Natick, MA) program, a force-velocity curve was generated using the hyperbolic Hill equation and the maximum unloaded velocity (V_{max}) was determined by extrapolation to the zero load of the force-velocity relationship. From the force and velocity data, a force-power curve was constructed in METLAB (by fitting the data to a 5^{th} degree polynomial curve) and peak power (P_{max}) and the percentage of P_o at which P_{max} occurred (% P_o at P_{max}) were calculated.

Following the force-velocity protocol, the soleus muscle was removed, trimmed, weighed and stored at −80° C for later analysis. Physiological cross-sectional area (PCSA) was computed using the average density of skeletal muscle: PCSA (cm^2) = muscle mass (g)/[L_o (cm)*1.06 (g/cm^3)] [149]. To attain relative force and power values, all absolute values were normalized to PCSA (cm^2).

Histology

Following excision, the soleus muscle was removed, embedded in a tissue freezing medium and immediately frozen in 2-methylbutane cooled in liquid nitrogen. Transverse, serial sections at 10 μm were cut through the mid-belly of the soleus muscle using a

cryostat (Leica CM3050S, Nussloch, Germany). Sections were then processed for hematoxylin and eosin staining, dehydrated through alcohols, mounted, and visualized at 10X with a Nikon Eclipse E400 microscope (Nikon, Tokyo, Japan) as previously described [111]. The CSA of approximately 300 fibers per muscle were estimated using ImageJ analysis software (National Institutes of Health, Bethesda, MD, USA).

Western blotting

Left soleus muscles were homogenized in an ice-cold RIPA lysis and extraction buffer (Thermo Scientific, Rockford, IL) supplemented with a protease inhibitor cocktail (Thermo Scientific). Total protein content was quantified with a bicinchoninic acid (BCA) assay (Thermo Scientific) using bovine serum albumin (BSA) as a standard. A portion of the muscle homogenate was then diluted in a loading buffer and heated for 4 min. Equal amounts of protein (25 μg) were loaded onto a 10% SDS polyacrylamide gel and separated according to molecular weight (100 V for 120 min). The proteins were then transferred to a PDVF membrane using a semi-dry transfer system at 15 V for 30 min (Bio-Rad Laboratories, Hercules, CA). Membranes were allowed to dry overnight and then blocked in 5% nonfat dried milk (w/v) dissolved in tris-buffered saline with 0.1% Tween-20 (TBS-T) for 1 hour at room temperature. Following the block, the membranes were probed with an anti-MuRF1 (1:250; #32920, Santa Cruz), anti-ubiquitin (1:2000; #3933, Cell Signaling), anti-19S Rpt1/S7 subunit (referred to as 19S in the present study) (1:1000; #PW9400, Enzo Life Sciences), anti-α7 (1:1000; #PW8110, Enzo Life Sciences), anti-β5 (1:1000; #PA1-977, Thermo Scientific), anti-GAPDH (1:5000; #3683, Cell Signaling), anti-PGC1-α (1:2000; #515667, EMD Calbiotech) or an anti-α-tubulin (1:2000, #2144, Cell Signaling) primary antibody diluted in 0.2% nonfat dried milk dissolved in TBS-T for 2 h at room temperature on an orbital shaker. Following incubation in the primary antibodies, membranes were washed with TBS-T (3×5 min) and then probed with the appropriate secondary antibody (goat anti-rabbit IgG, 1:10000; Santa Cruz or goat anti-mouse IgG, 1:10000; Thermo Scientific) in 5% nonfat dried milk dissolved in TBS-T for 1 h at room temperature with shaking and washed as previously stated. Membranes were then treated with an enhanced chemiluminescent solution (Thermo Scientific) prior to detection using a BioRad ChemiDoc XRS imaging station

(Bio-Rad Laboratories) and analyzed by densitometry using QuantityOne software (Bio-Rad Laboratories). To ensure protein load was similar between samples, all membranes were stained with Ponceau S before blocking or Coomassie Blue after imaging.

Determination of contractile protein content (Silver staining)

Myosin heavy chain (MHC) and actin protein content were estimated using a gel silver staining kit (Bio-Rad) as previously described [150]. Briefly, equal amounts of protein (2 μg) were loaded onto an 8% SDS polyacrylamide gel and separated according to molecular weight (100 V for 100 min). Following electrophoresis, gels were fixed for 20 min and decanted with deionized distilled water for 20 min (2×10 min). Gels were then silver stained for 16-21 min, transferred into a 5% acetic acid solution for 15 min to stop the reaction and rinsed with deionized distilled water for 20 min (2×10 min). The stained gels were imaged using a BioRad GS-800 imager (Bio-Rad) and analyzed by densitometry using QuantityOne software (Bio-Rad).

Statistics Analysis

An independent t-test or one-way ANOVA was used to determine differences between groups when two (control vs. 14 day) or three (control vs. 7 day vs. 14 day) independent variables were selected, respectively. To assess changes between groups across force-frequency, force-velocity and force-power curves, all data (group × Hz or % P_o) was entered into a two-way repeated measures ANOVA. A Fisher's least significant difference (LSD) *post hoc* test was performed in the event of a significant ANOVA. An α-level of ≤0.05 was used for all analyses. Values are presented in mean±SEM. All statistical testing was performed using SigmaPlot version 11.0 (Systat Software, San Jose, CA).

RESULTS

Activation of the ubiquitin-proteasome system

To assess how the ubiquitin-proteasome system responded to denervation, we used Western blot analysis to determine content of several key proteins implicated in this pathway (**Figures 1 & 2**). The first protein assessed was the E3 ligase MuRF1 because it can interact with several key sarcomeric proteins. As previously reported, MuRF1 content was relatively low under basal conditions, but increased as a result of denervation [9]. By 7 days post-denervation, MuRF1 content was elevated 73% ($p=0.003$; **Figure 1A**) and was accompanied by a 42% ($p=0.008$; **Figure 2**) increase in total ubiquitin content. At day 14, MuRF1 content returned to baseline ($p=0.19$) while total ubiquitin content remained elevated (55%, $p=0.001$). At both 7 and 14 days post-denervation, most of the ubquitinated proteins were observed just above 25 kDa and between 75 to150 kDa.

Next, we assessed different components of the 26S proteasome by measuring a subunit of the 19s regulatory complex and two subunits of the 20S catalytic core, α7 and β5 (**Figure 1B-D**). The changes in proteasome content were similar to that of MuRF1 and ubiquitin at day 7. Specifically, 19S, α7 and β5 content increased 79% ($p=0.004$), 34% ($p=0.022$) and 36% ($p=0.012$), respectively. By day 14, 19S, α7 and β5 content decreased and were not different compared to control muscle ($p\geq0.32$).

Skeletal muscle atrophy and contractile function

Soleus wet weight and fiber CSA were reduced by 28% and 41% by day 14 ($p\leq0.001$; **Figure 3**), respectively. Both of which indicate myofibrillar protein content declined following denervation. Therefore, we sought to determine if these reductions were due to a preferential loss of MHC or actin. Analysis of the MHC and actin bands from silver stained gels revealed that when an equal amount of protein was loaded (2 μg), content of MHC, actin and MHC/actin remained similar between control and denervated muscle ($p\geq0.72$; **Figure 4**). This observation suggests that MHC and actin content were lost at comparable rates when assessed at 7 and 14 days post-denervation.

Due to the loss of muscle wet weight and fiber CSA observed at day 14 (**Figure 4**), it was apparent contractile function would also be impaired, particularly when expressed in

absolute terms (i.e., not relative to PCSA). As hypothesized, absolute P_o decreased 19% ($p=0.021$; **Figure 5A** and **Table 1**) while relative P_o remained unchanged ($p=0.80$; **Figure 5B** and **Table 1**).

Unexpectedly, P_t did not mimic that of P_o, as absolute and relative P_t both increased in the denervated muscle (74%, $p=0.001$ and 120%, $p\leq0.001$; **Figure 5A,B** and **Table 1**). To further assess these changes, time to P_t (TPT) and one-half relaxation time ($RT_{1/2}$) were also analyzed (**Table 1**). As with P_t, both increased at day 14 (~60% $p\leq0.001$), which indicates a slowing of the contraction after denervation.

Moreover, there was a leftward shift in the force-frequency curves following denervation, which was accompanied by reductions in EC_{50} and the Hill coefficient ($p\leq0.001$; **Figure 5A,B** and **Table 1**). Upon further analysis of the force-frequency curves, it was also apparent denervation effected absolute and relative force across several other stimulation frequencies, besides those that elicited P_t and P_o. Absolute force at 10 Hz increased ($p<0.001$) while force at 80, 100 and 120 Hz ($p\leq0.016$) decreased 14 days post-denervation. Moreover, relative force increased at 10 and 40 Hz ($p\leq0.037$) but did not differ from control muscle at higher frequencies ($p\geq0.42$).

Muscle power is the product of force and contraction velocity. Despite the changes observed in the force-frequency curves, denervation had no effect on V_{max} ($p=0.84$, **Table 1**) or the force-velocity relationship ($p=0.99$, data not presented). Peak power (P_{max}) occurred at ~26% of P_o and was not different 14 days post-denervation ($p=0.77$; **Figure 5C,D** and **Table 1**). However, absolute P_{max} decreased 25% ($p=0.050$), comparable to the 19% reduction in absolute P_o previously stated. A similar reduction was also observed at 20, 30 and 40% of absolute P_o 14 days post-denervation ($p\leq0.029$). As with relative P_o, denervation did not alter relative P_{max} ($p=0.44$) or any other relative % P_o on the force-power curve ($p=0.98$).

Altered metabolic and cytoskeletal profile

In addition to skeletal muscle atrophy, denervation has also been reported to affect metabolic and cytoskeletal protein markers [142,151–153]. Due to the plethora of proteins that could be classified under these categories, we selected three commonly used in the

literature: GAPDH, PGC1-α and α-tubulin (**Figure 6**). GAPDH and PGC1-α content did not differ from control muscle 7 days following denervation ($p \geq 0.14$); however, by day 14 both were significantly reduced. Specifically, protein content decreased 20% for GAPDH ($p = 0.001$) and 40% for PGC1-α ($p \leq 0.001$). Contrary to these reductions, α-tubulin content dramatically increased 7 days post-denervation and remained elevated through day 14 (~84%, $p \leq 0.001$).

DISCUSSION

Skeletal muscle atrophy is primarily due to the loss of myofibrillar proteins and is a hallmark outcome of many clinical conditions and chronic diseases. The increase in proteolysis is largely attributed to the ubiquitin-proteasome system, the primary pathway responsible for degrading the contractile apparatus. Despite the correlative relationship between skeletal muscle size and the ubiquitin-proteasome system, it is unclear how this pathway affects muscle quality. Therefore, we denervated mouse soleus muscle for up to 14 days and assessed activity of the ubiquitin-proteasome system, in addition to *ex vivo* whole muscle contractility. Here, we report content of several key proteins within the ubiquitin-proteasome system temporarily increased following denervation and as a result, reduced skeletal muscle size. These changes were accompanied by reductions in absolute P_o and P_{max}, which were offset when expressed relative to PCSA. However, contrary to P_o, absolute and relative P_t increased as a result of denervation. Taken together, this data represents two key findings. First, activation of the ubiquitin-proteasome system is associated with reductions in skeletal muscle quantity rather than quality. Second, despite the loss of contractile proteins, short-term denervation enhanced force at submaximal stimulation frequencies, which suggests the muscle may undergo a transient phase of remodeling to compensate for the loss of neural activity.

Denervation-induced muscle atrophy models are known to increase several components of the ubiquitin-proteasome system, including E3 ligases, content of ubiquinated proteins and several subunits of the 26S proteasome. Upregulation of the ubiquitin-proteasome system has been reported to increase as early as 2-3 days post-denervation [22,23,141] and remain elevated up to 14 days [23,36]. Due to the complexity of this pathway and the various E3 ligases and proteasome subunits present in skeletal muscle, many of these studies assessed specific parts of the ubiquitin-proteasome system rather than it as a whole. However, it is apparent that these components (i.e., E3 ligases and proteasome subunits) are regulated in a coordinated response to mediate skeletal muscle proteolysis [141] and are controlled by similar transcription factors [22,69]. Our analysis included key proteins from several different components of the ubiquitin-proteasome system: the E3 ligase MuRF1, total ubiquitin content and three subunits from different rings of the 26S proteasome (i.e., 19S, α7 and β5). As reported by others [22,36,127,141], protein content (or

mRNA expression) of the ubiquitin-proteasome system significantly increased following denervation. Specifically, MuRF1, ubiquitin, 19S, α7 and β5 content were elevated 7 days post-denervation and returned to control levels by day 14, with the exception of ubiquitin. Other E3 ligases like NEDD4 have been found to be more persistent in denervated muscle [23,54,152] and may contribute to the presence of these ubiquitinated proteins beyond day 7, after MuRF1 and proteasome content have declined.

The temporary increase in MuRF1, 19S, α7 and β5 content reduced soleus muscle wet weight and fiber CSA ≥28% by day 14. The loss in muscle size is thought to be primarily due to the proteolysis of MHC and actin by the ubiquitin-proteasome system [131]. Interestingly, both MHC and actin were degraded at a similar rate through day 14, as the ratio of MHC to actin did not change, comparable to that previously reported 10 days post-denervation [9]. In support of this, absolute P_o and P_{max} were reduced while relative P_o and P_{max} were unaffected, which suggests the muscle's intrinsic ability to generate force was not altered at day 14. Furthermore, denervation did not significantly impact V_{max} indicating the reduction in P_{max} was primarily due to P_o, or more accurately, the loss in fiber CSA. These contractile observations (i.e., P_o, P_{max} and V_{max}) confirm that of Greising et al. [53], who used tibial nerve transection and assessed mouse soleus muscle after 14 days of denervation, similar to the present study. In contrast, Agbulut et al. [142] reported V_{max} and relative P_o and P_{max} were all impaired in mouse soleus muscle one month following denervation. Taken together, these findings suggest that the loss in skeletal muscle quality after extended periods of denervation (i.e., beyond 14 days) is due to factors other than the ubiquitin-proteasome system. Although these factors were not determined in the present study, others have shown denervation inevitably effects muscle quality by reducing the fraction of CSA occupied by the contractile proteins [154–156] and through decreasing the fibers' sensitivity to Ca^{2+} [157].

In addition to these findings, our data also indicates that shortly following denervation (i.e., ~7 to 14 days) there is a temporary gain in excitation-contraction (EC) coupling. In support of this, absolute and relative submaximal force (≤10 Hz and ≤40 Hz, respectively) both increased 14 days post-denervation. When specifically assessing the twitch contraction, we observed an overall improvement of 74% in absolute force and

120% in relative force, which was accompanied by a 60% increase in TPT and $RT_{1/2}$. Although these changes (i.e., twitch parameters) have not been reported in mouse soleus muscle, they are consistent with that seen in rat soleus muscle following 7 days of denervation [158]. The fact we and others [158] show P_t was greater 7 to 14 days after denervation, despite the loss of contractile proteins, suggests sarcoplasmic reticulum (SR) Ca^{2+} release was enhanced. Some important features that develop in denervated rodent muscle, which could result in a gain of EC coupling, include increased acetylcholine receptor expression, density and sensitivity [159,160], dihydropyridine receptor expression [129,161,162] and SR Ca^{2+} loading capacity [158,163]. Interestingly, similar observations (i.e., upregulation of the acetylcholine and dihydropyridine receptors) have been reported in the days following eccentric contraction-induced injury when EC coupling failure is pervasive [145,164,165]. These changes may reflect a compensatory mechanism to offset the loss in voltage-induced SR Ca^{2+} release that occurs after eccentric contractions (i.e., 0-5 days post-injury) or denervation in skeletal muscle. However, as with relative P_o, P_t has been shown to progressively decline following denervation [142] and therefore, these compensatory mechanisms are likely short-term.

Regardless, these changes occurred in conjunction to the increases we observed in MuRF1 and proteasome protein content. This may indicate that, in addition to myofibrillar degradation, there is a transient remodeling of the EC coupling pathway after denervation. Although more data is needed to confirm this concept, the neuromuscular junction [160], blood vessels [166], extracellular matrix [154,156] and cytoskeleton [151] all have been reported to undergo remodeling following denervation. In support of the latter, content of the cytoskeletal protein α-tubulin significantly increased after denervation, similar to that observed in rat soleus muscle denervated for 3 to 15 days [151]. Denervation has also been shown to impair mitochondrial biogenesis/oxidative metabolism [142,152,167] and glycolysis [152,153], which coincides with the lower levels of PGC1-α and GAPDH we detected. It is also worth noting that α-tubulin and GAPDH are common housekeeping proteins used by many as internal controls. However, as we and others report [151–153], these proteins are significantly influenced by denervation and therefore, if set as internal controls, caution should be used.

In closing, we demonstrate that several key proteins of the ubiquitin-proteasome system including MuRF1, 19S, α7 and β5 were all upregulated in mouse soleus muscle after denervation. Content of these proteins increased in a coordinated fashion and were only temporally affected by denervation. These changes reduced soleus muscle size and maximal force, but did not appear to alter fiber quality, at least 14 days post-denervation. Contrary to these deficits, submaximal force was improved despite the loss of MHC and actin, which suggests a gain in EC coupling. Taken together, our results demonstrate the ubiquitin-proteasome system is a fine-tuned proteolytic pathway, which upon activation primarily impairs maximal force by reducing skeletal muscle size, rather than its intrinsic ability to generate force. In addition, we also suggest skeletal muscle may undergo a transient phase of remodeling in concert to the proteolysis that occurs shortly following denervation, possibly to compensate for the loss in voltage-induced SR Ca^{2+} release.

ACKNOWLEDGEMENTS

The authors would like to thank JingYing Zhang for her assistance with the Western blot preparations, and Drs. Dongmin Kwak and Russell Rogers for their review of the manuscript.

FUNDING

This study was partially supported by a NIA/NIH training grant (T32-AG029796).

DISCLOSURES

No conflicts of interest, financial or otherwise, are declared by the authors.

FIGURES AND TABLES

Figure 1. Protein content of (A) MuRF1, (B) 19S, (C) α7 and (D) β5 in Control, 7 Day or 14 Day soleus muscle.

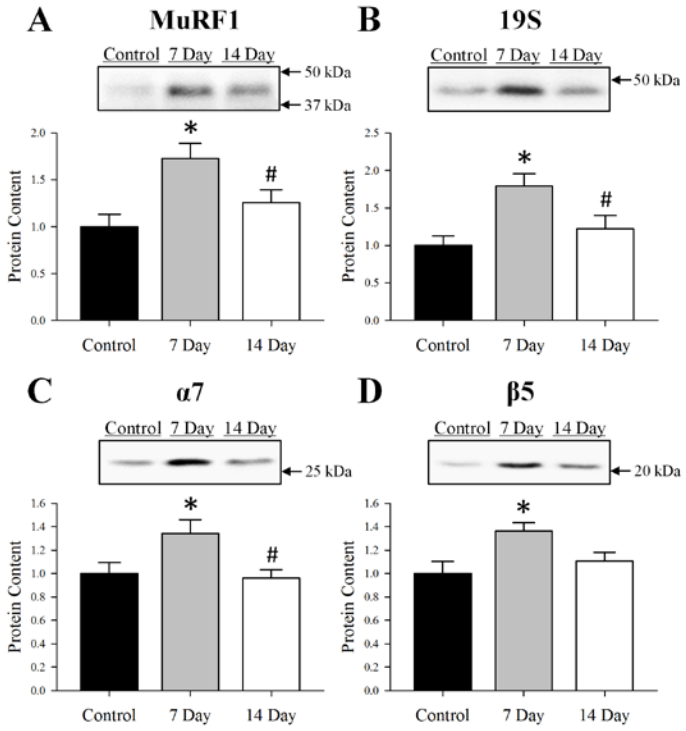

Content of each protein was determined using Western blot analysis, normalized to the Control muscle and set at 1.0 (arbitrary units). Pictured above the graphs are representative Western blots for each protein with arrows indicating molecular weight standards. Control was innervated muscle, 7 Day was denervated for 7 days and 14 Day was denervated for 14 days. Sample size per group, n=5-7. Values are mean±SEM. *Significantly different from Control ($p \leq 0.05$). #Significantly different from 7 Day ($p \leq 0.05$).

Figure 2. Total ubiquitin content in Control, 7 Day or 14 Day soleus muscle.

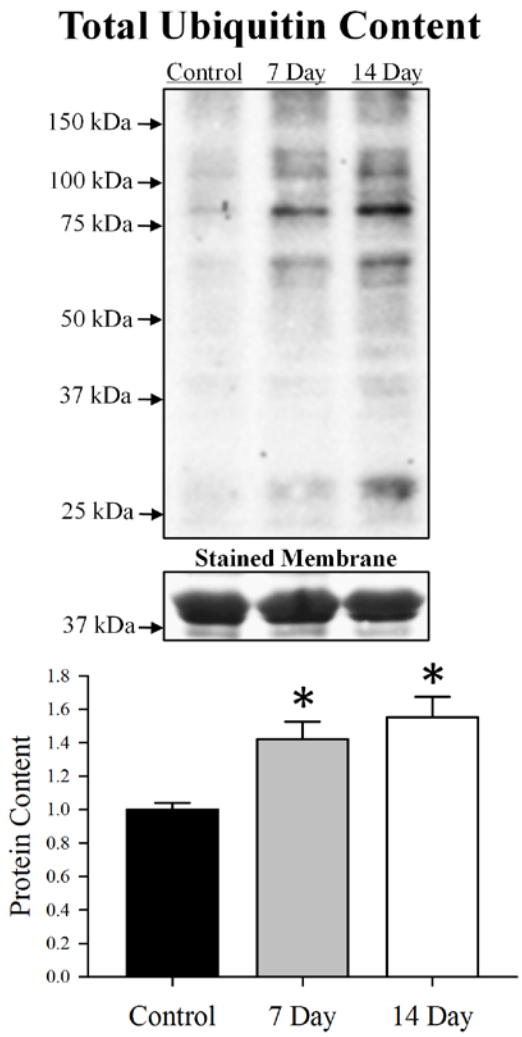

Content of each protein was determined using Western blot analysis, normalized to the Control muscle and set at 1.0 (arbitrary units). Pictured above the graph is a representative Western blot with arrows indicating molecular weight standards. The stained membrane is a representative section (above ~37 kDa) of a Coomassie Blue stained membrane. Control was innervated muscle, 7 Day was denervated for 7 days and 14 Day was denervated for 14 days. Sample size per group, n=5-7. Values are mean±SEM. *Significantly different from Control ($p \leq 0.05$).

Figure 3. Fiber (A) distribution and (B) mean cross-sectional area (CSA) in Control and 14 Day soleus muscle.

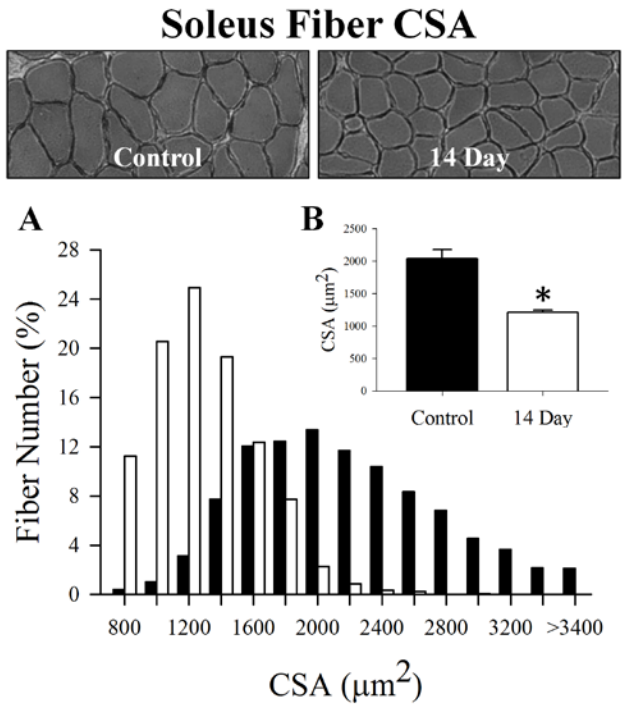

Pictured above the graphs are representative hematoxylin and eosin stains. Control was innervated muscle and 14 Day was denervated for 14 days. Sample size per group, n=6-7. Values are mean±SEM. *Significantly different from Control ($p \leq 0.05$).

Figure 4. Protein content of (A) Myosin heavy chain: MHC, (B) Actin and (C) MHC/Actin in Control, 7 Day or 14 Day soleus muscle.

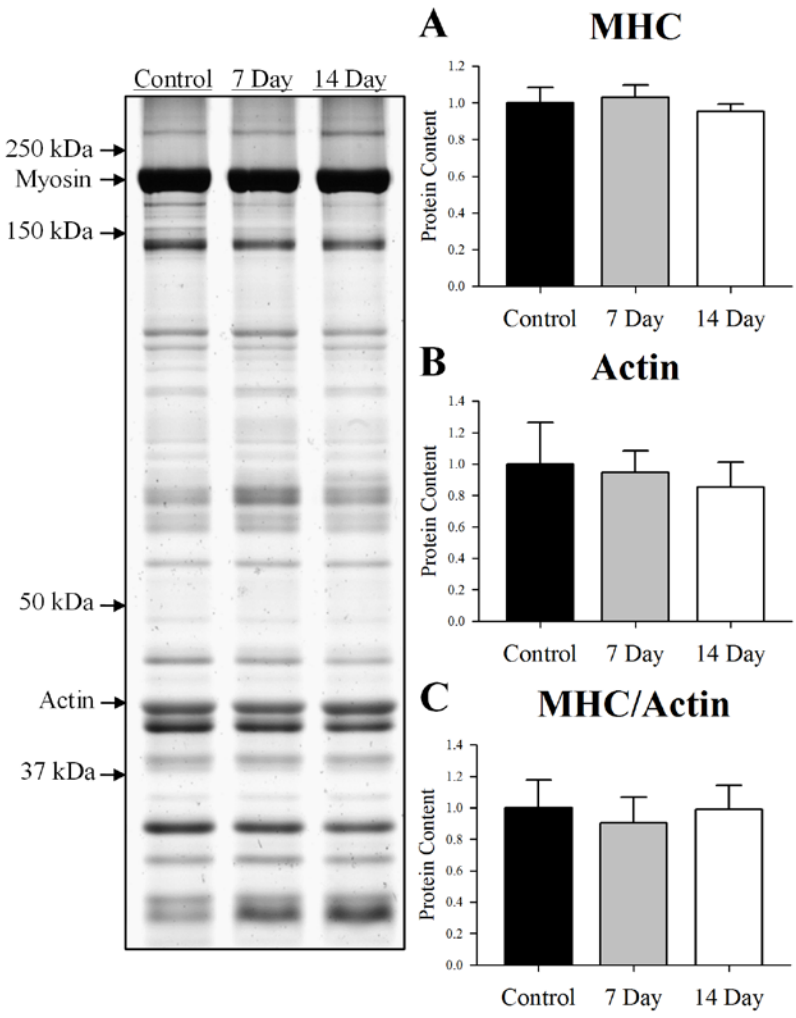

Content of each protein was determined using gel silver staining, normalized to the Control muscle and set at 1.0 (arbitrary units). Pictured to the left of the graphs is a representative silver stain with arrows indicating molecular weight standards. Control was innervated muscle, 7 Day was denervated for 7 days and 14 Day was denervated for 14 days. Sample size per group, n=5-7. Values are mean±SEM.

Figure 5. ***Ex vivo*** **(A) Absolute Force, (B) Relative Force, (C) Absolute Power and (D) Relative Power in Control and 14 Day soleus muscle.**

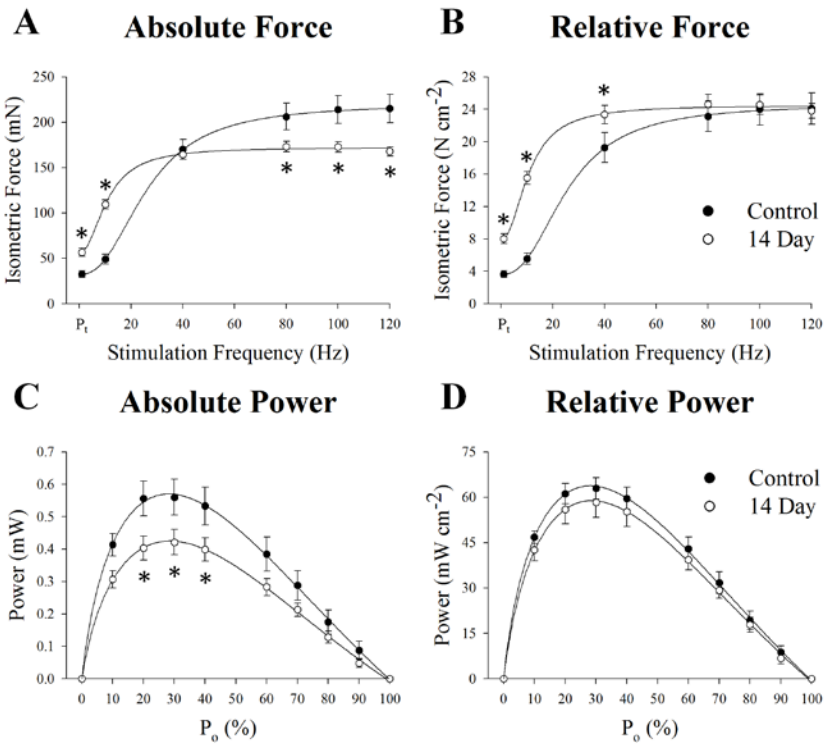

Control was innervated muscle and 14 Day was denervated for 14 days. Sample size per group, n=6-8. Values are mean±SEM. *Significantly different from Control ($p \leq 0.05$). P_t, peak isometric twitch force.

Figure 6. Protein content of (A) GAPDH, (B) PGC1-α, (C) α-tubulin in Control, 7 Day or 14 Day soleus muscle.

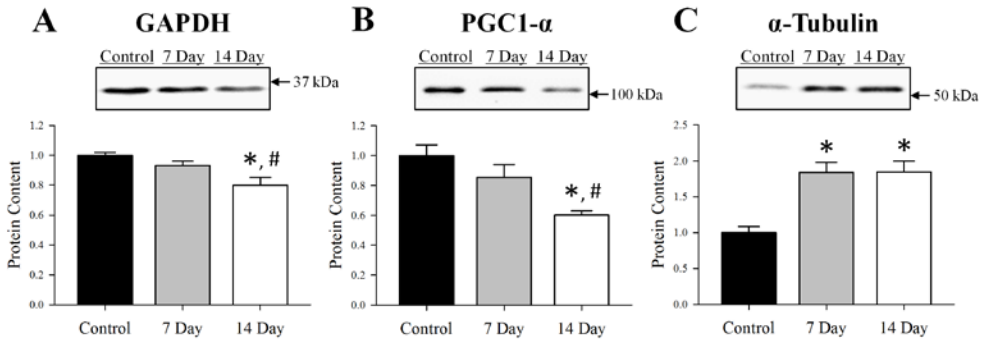

Content of each protein was determined using Western blot analysis, normalized to the Control muscle and set at 1.0 (arbitrary units). Pictured above the graphs are representative Western blots for each protein with arrows indicating molecular weight standards. Control was innervated muscle, 7 Day was denervated for 7 days and 14 Day was denervated for 14 days. Sample size per group, n=5-7. Values are mean±SEM. *Significantly different from Control ($p \leq 0.05$). #Significantly different from 7 Day ($p \leq 0.05$).

Table 1. Soleus muscle characteristics and *ex vivo* contractile parameters.

	Control	Denervated
Muscle Weight (mg)	10.76±0.51	7.72±0.25*
Histological CSA (μm^2)	2040.88±139.86	1210.32±39.66*
Muscle Length (mm)	10.82±0.33	10.60±0.44
PCSA (mm^2)	0.92±0.08	0.71±0.02*
Absolute P_t (mN)	32.59±3.64	56.73±4.56*
Absolute P_o (mN)	215.28±15.57	173.68±5.83*
Relative P_t ($N\ cm^{-2}$)	3.65±0.41	8.01±0.61*
Relative P_o ($N\ cm^{-2}$)	24.10±1.94	24.69±1.22
TPT (ms)	36.43±1.88	56.71±1.60*
$RT_{1/2}$ (ms)	40.29±1.25	66.14±5.20*
EC_{50} (Hz)	26.20±1.32	11.04±0.57*
Hill Coefficient	2.48±0.12	1.89±0.06*
V_{max} (fl/s)	4.40±0.26	4.34±0.20
Absolute P_{max} (mW)	0.57±0.05	0.43±0.04*
Relative P_{max} ($mW\ cm^{-2}$)	63.93±3.26	58.96±5.03
% P_o at P_{max} (%)	26.33±1.05	26.71±0.71

Values are means±SEM. Sample size per group, n=19-20 for Muscle Weight. For all other variables, n=6-8. The Control group consisted of soleus muscle that was innervated, while the Denervated group included soleus muscle that was denervated for 14 days. CSA, cross-sectional area; PCSA, physiological cross-sectional area; P_t, peak isometric twitch force; P_o, peak isometric tetanic force; TPT, time to P_t; $RT_{1/2}$, one-half P_t relaxation time; EC_{50}, frequency at which 50% P_o was developed; Hill Coefficient, slope coefficient of the force-frequency curve at its midpoint; V_{max}, maximum unloaded velocity; P_{max}, peak power.
*Significantly different from Control ($p \leq 0.05$).

INTERLUDE III

In the previous Chapter, 14-day tibial nerve transection induced 40% muscle loss (CSA) in soleus muscle, which is consistent with the result of gastrocnemius muscle denervation described in Chapter III. Hence, it seems 14-day denervation causes same degree of atrophy in muscles with different fiber type composition (soleus has 50% MyHC I and 50% MyHC II whereas gastrocnemius is mainly 100% MyHC II). Also, the ubiquitin-proteasome system (UPS) was activated in soleus muscle following 7 and 14-day denervation. Consistently with gastrocnemius muscle, all of the markers in UPS in the soleus muscle were upregulated in response to denervation.

Muscle contractility is also altered following 14 days of denervation. The soleus muscle's absolute force generation decreased 20% and this reduction in force generation is mainly due to a reduction of muscle quantity rather than quality. Specifically, there was a decrease in absolute force and absolute power, but the relative force and relative power (both normalized to CSA) did not decrease in response to 14-day denervation. Taken together, the second study suggests that the UPS is finely-tuned with the disassembly of the sarcomere, such that the remaining actin and myosin within the sarcomere are functional.

My second research interest is frailty, an age-related clinical syndrome, highly associated with the condition of muscle atrophy (sarcopenia). In contrast to the first two studies that investigate muscle atrophy at a cellular and molecular level, the third study was to evaluate the muscle atrophy-associated syndrome, frailty, at a physical and functional level. The long-term goal of this study is to facilitate frailty studies investigating exercise or/and pharmaceutical interventions on C57BL/6 mice (an established animal model for aging study) or other genetically-modified mice (e.g. short lived IL-$10^{tm/tm}$ mice, [106]). Ultimately, these basic bench studies may provide the foundation for translational frailty studies and eventually move to the clinical setting.

In clinical studies, there are several Frailty Indexes for the identification of frail individuals. The two most popular ones, the Frailty Phenotype Index (Fried) and the Accumulative Deficit Index (Rockwood) were introduced in Chapter II. In animal studies, Parks *et al.*, and other groups proposed several Frailty Indexes in mice, which were all based on accumulated deficits calculated from multiple invasive and noninvasive measures [104–107]. However, a clinically-relevant non-invasive Frailty Index was still lacking in animal models.

As a result, the goal of the study reported in Chapter V was to develop a clinically-relevant Frailty Index based on Fried's Frailty Phenotype Index in clinic. In brief, our Frailty Index contains four criteria: weaker grip strength (weakness), slower running speed (slowness), decreased voluntary running (low activity), and decreased endurance (poor endurance). To initiate the pilot study, we tested a cohort of eleven male C57BL/6 mice (27-28 months). Each animal was evaluated and designated a score under each criterion. Frail mice were identified with three criteria fell below the cutoff points (1.5 *SD* below the mean score); whereas the mildly frail mice were identified with two criteria presented. With this frailty index, I hypothesized that frail and mildly frail mice can be identified in the old cohort. The details in this study including the results and discussion are presented in Chapter V.

CHAPTER V. CLINICALLY-RELEVANT FRAILTY INDEX FOR MICE

The content in this chapter is minimally modified[3] *from the published journal article:*

Liu, H., Graber, T. G., Ferguson-Stegall, L., & Thompson, L. V. (2014). Clinically relevant frailty index for mice. *The Journals of Gerontology. Series A, Biological Sciences and Medical Sciences, 69*(12), 1485–91. [4]

- I was the primary author of this manuscript and responsible for the experimental design, data analysis, and the writing of the manuscript.
- Dr. Ted Graber equally contributed as the first author and participated in experimental design, data analysis and scientific review of the manuscript.
- Dr. Lisa Ferguson-Stegall was involved in data collection and review for this manuscript.
- Dr. LaDora Thompson was the guarantor of study, assisted in study design and data interpretation, major contribution to manuscript writing, scientific review, and funding.

[3] The format of figures and tables are modified to fit the content in this dissertation. The title of the Abstract was changed to Summary of Chapter V.
[4] Copyright permission is granted by the *Journals of Gerontology. Series A, Biological Sciences and Medical Sciences.*

SUMMARY OF CHAPTER V

Frailty is a clinical syndrome associated with the aging process and adverse outcomes. The purpose of this short report was to initiate the development of a Frailty Index in 27- to 28-month-old C57BL/6 mice that matched the clinical criteria used in humans (weakness, slow walking speed, low activity level, poor endurance). The selected criteria included grip strength, walking speed, physical activity and endurance. The criteria in mice were evaluated by the inverted-cling grip test, rotarod test, voluntary wheel running, and derived endurance scores. Each criterion had a designated cutoff point (1.5 *SD* below the cohort mean) to identify the mice with the lowest performance. If a mouse presented with three of the criteria scores below the cutoff points, it was identified as frail. Mild frailty was designated if two criteria were below the cutoff points. In this mouse cohort, one mouse was identified as frail and one was mildly frail. This prevalence of 9% frailty is consistent with the prevalence of frailty in humans at the same survival age. Collectively, our selected criterion, cutoff point, and Frailty Index provide a potential standardized definition for frailty in mice that is consistent with the operational definition of frailty in humans.

INTRODUCTION

Frailty is a clinical syndrome associated with the aging process, increased vulnerability, decreased physical function, and adverse outcomes (mortality, disability, and hospitalization) [1–3]. The prevalence of frailty in older populations (65 years or older) is about 9.9% [97], and this portion increases to 25%-50% in people aged 85 or older [3]. Fried and colleagues developed a physical phenotype of frailty according to a combination of weakness, slowness, physical inactivity, increased subjective exhaustion, and weight loss, where frailty was defined as the presence of three or more of the criteria [1]. This frailty definition was shown to be valid and a powerful predictor for adverse outcomes [1]. Further studies report measurements of frailty using 'Frailty Indices' focused on clinical phenotype definitions of frailty or multiple-deficits [98].

Besides the clinical studies discussed above, animal models are useful for the investigation of frailty and the mechanisms underlying frailty. Parks and coworkers proposed a Frailty Index in mice, using a well-established mouse model, C57BL/6. The Frailty Index was based on accumulated deficits calculated from 31 invasive and noninvasive measures [104]. The invasive tests required anesthetizing the animal before procedures, including body composition (fat mass and lean mass) and basic metabolic status (level of electrolytes and blood components). The non-invasive assessments included the activity analyses: move distance duration and velocity. A frailty score was generated for each mouse in order to quantify the level of frailty, which was higher in the older mice and positively correlated to the age-related cardiac myocyte changes.

Although Parks and coworkers recognized the importance of identifying frailty in rodents and provided a Frailty Index score, an index that is closely related to the clinically accepted frailty criteria and is simple to use (non-invasive) may facilitate frailty research in animal models. Moreover, the results of these animal studies would have potential to translate to clinical settings. Another advantage of a Frailty Index in mice lies in the definition of cutoff points for distinguishing between frail and non-frail mice within each criterion. The cutoff definition provides standardized assessment that has the potential to be used in every research laboratory. As a result, the purpose of this short report is to initiate the development of a Frailty Index including the identification of four criteria of

frailty, the definition of the cutoff points for each criterion, the designation of frailty, and the evaluation of the Frailty Index with old mice.

Specifically, in this short report, the Frailty Index matches the physical frailty indicators from the Fried and coworkers' study, including weakness, slow walking speed, low activity level, and poor endurance (four non-invasive criteria), and each criterion has a designated cutoff point (1.5 *SD* below the mean of the cohort). If a mouse presents with three frailty criteria, it is identified as frail.

METHODS

Animals

Eleven 27- to 28-month-old male C57BL/6 mice were purchased from the National Institute on Aging Colony and housed in specific pathogen-free facilities at the University of Minnesota. This age of mice was selected because this age represents 50% survival rate in this species [168]. The mice were fed *ad libitum* and maintained on a 12-hour light/dark cycle at 20°C. The mice underwent an acclimation period for 7 days before any experimental procedures. All procedures were performed in agreement to the University of Minnesota's guidelines on experimental animal research. Each mouse was designated a letter from A to K.

Frailty criteria

In order to develop a Frailty Index, we identified four frailty criteria including grip strength, walking speed, physical activity, and endurance. These criteria were selected because they were similar to the human clinical criteria described by Fried and coworkers (**Table 1**).

Criterion 1: grip strength. –The inverted-cling grip test was used for evaluating the grip strength of limbs and the endurance of muscles in the mouse [144]. The cage-like device had a top lid with a wire grid and a padded bottom. After placing the mouse on the top lid, the lid was immediately closed so that the mouse was inverted inside of the cage. The outcome measurement was the total time (seconds) the mouse could support itself before falling (latency to fall). Two trials were performed, with a 20-minute rest between trials. The final score (seconds) of grip strength was the average score of the two trials. In addition, this score was used for calculating the endurance score, as described in Criterion 4.

Criterion 2: walking speed. –The walking speed was evaluated using the rotarod test (Rota-Rod R/S, Lsi Letica, Cornella, Spain). The rotarod test is widely used for determining overall motor function in mice [144,169]. The rod cylinder rotates at a speed of 4 rpm and accelerates to 40 rpm over 5 minutes. The mouse is placed on the cylinder and

the rotating speed (rpm) is recorded when the mouse falls, latency to fall. In the current study, the mice practiced on the device for three days (three trials per day of various protocols) before the actual testing procedure. On the testing day (the fourth day), three trials were performed with 20 min rest between each trial. The last three trials were averaged and the average was used as the final score of walking speed. The time the mouse remained on the rotarod before falling was used for the endurance score, which will be discussed in Criterion 4.

Criterion 3: physical activity. –Voluntary wheel running was used for evaluating the daily physical activity level of each mouse. The Lafayette Activity Wheel Cages (model #80820F; Lafayette Instruments, Lafayette, IN) were used for the voluntary running procedure. The mice were individually housed in the wheel-running cages. Mice ran *ad libitum* in the wheel cages for 1 week. The running distance, in revolutions, was recorded daily at the same time (AM). The unit of revolutions was converted into kilometers for data analysis (1 revolution = 0.4m). The average daily running distance in the week was calculated (km/d) and used as the score of physical activity.

Criterion 4: endurance. –Both the grip test and the rotarod test were used to assess overall endurance [144]. In this study, an endurance score was derived from the two tests. The time of the grip test was recorded as described in Criterion 1. The duration, in seconds, the mouse remained on the rotarod was recorded as outlined in Criterion 2. The score of endurance was calculated by determining the mean time of grip test and rotarod test [Endurance score (seconds) = (Time of grip test + Time of rotarod test)/ 2].

Determination of Frailty Index

After evaluating and designating a score to each animal, the cohort mean and the *SD* were calculated for each criterion. Next, we determined a cutoff point at 1.5 *SD* below the cohort mean to identify the mice with the lowest performance. Frailty was defined if three or more of the criteria measures were below the cutoff point; whereas, mild frailty was designated if two fell below the cutoff. **Table 2** summarizes the Frailty Index.

RESULTS

Scores of Criteria

Grip strength. **–**Grip test is a measurement that assesses strength and endurance **(Figure 1).** The cohort mean of the grip test was 99 ± 14 seconds with a cutoff point at 31 seconds. Animal H (24 seconds) and G (28 seconds) were ranked below the 1.5 *SD* cutoff, which indicated weaker strength and endurance.

Walking speed. **–**Rotarod test (speed) is a measurement that identifies the slowness in the mouse **(Figure 2)**. The scores of the walking speed for the aged mice (n = 11) had a mean of 9.6 ± 0.6 rpm and a cutoff point of 6.8 rpm. Animal H showed a slower walking speed at 6.3 rpm, which was below the cutoff point.

Physical activity. **–**Voluntary wheel running assesses physical activity level **(Figure 3)**. The cohort (11 mice) mean of the daily voluntary wheel-running distance for 1 week was 1.53 ± 0.25 km/day. None of the 11 mice were below the cutoff point (0.37 km/d).

Endurance. –The endurance was determined from the mouse's performance on the grip test and the rotarod test **(Figure 4)**. The average endurance score in the cohort was 74 ± 9 seconds. Animals H (23 seconds) and G (31 seconds) were identified with poor endurance because they were below the cutoff point (33 seconds).

*Identification of Frail Mice***. –Table 3** shows all the rankings under the four criteria in the 28-month-old male C57BL/6 mouse cohort. According to the identification of Frailty Index described previously, animal H was identified as a frail mouse (more than three criteria below the cutoff points). The mouse had overall physical weakness, including weaker grip strength, slower walking speed, and less endurance in comparison to the other mice in the cohort. Animal G was identified as a mildly frail mouse (two criteria below the cutoff; **Table 2**). The main weaknesses of the animal G were strength and endurance level.

DISCUSSION

The purpose of this short report was to initiate the development of a Frailty Index in mice that is closely related to the clinically accepted frailty criteria in humans. The Frailty Index was composed of four Frailty Criteria based on the clinical frailty indicators described by Fried and coworkers [1]: weakness, slow walking speed, low activity level, and poor endurance. Frailty was defined in a mouse if three or more of the criteria measures were below the cutoff point, whereas, mild frailty was designated if two fell below the cutoff point. The cutoff point was set at 1.5 *SD* below the cohort mean of each criterion. Using this Frailty Index, one mouse was frail and one was mildly frail in the 27- to 28-month-old male C57BL/6 mouse cohort (n=11).

To our knowledge, there is one published study that reports a Frailty Index in mice and this index was based on the accumulative deficits model [104]. In order to quantify frailty, Parks and coworkers determined health related variables associated with the function of vary physiological systems that change with age (muscle, bone, and cardiovascular). In particular, 31 invasive and non-invasive variables were measured including activity levels (distance moved, duration of movement, velocity, meander, and rearing frequency), body composition (weight, bone mass density, body mineral content, body surface area, lean and fat body mass, percent body fat, and total body tissue), and hemodynamic (blood pressures, pulse pressure, heart rate, tail blood flow, and tail blood volume) and metabolic measures (the levels of sodium, potassium, chloride, pH, glucose, hematocrit, bicarbonate, hemoglobin, and urea) to generate a unique score for each mouse.

Using this Frailty Index of deficit accumulation, mice with higher frailty scores had prominent age-related cellular changes when compared with younger mice. Indeed, this Frailty Index identified the older mice; however, these measures do not coincide to the accepted measures used clinically to define frailty, and the measures required a multitude of tools. As a result, categorizing frailty by a more clinical relevant, approachable noninvasive assessment in mice is still desired.

Foremost, the criteria selected in the current short report mimicked the established-clinical indicators of frailty, so that future studies would have translational significance

(tool to identify risk for disability and mortality in mice), and secondly, the criteria use simple noninvasive measures. Finally, the four selected criteria and cutoff points identify the weak individuals in the cohort.

The Four Selected Criterion

We found a 9% prevalence of frailty using the selected criteria in 27- to 28-month-old males, an age group that is comparable with an 80-year-old humans [170]. This finding is consistent with the 11% prevalence of frailty using Fried's criteria of frailty in age at 76-84 years old [1]. This finding suggests that the selected criteria used in these old mice (grip strength, walking speed, physical activity, and endurance) are good choices for the Frailty Index.

Grip strength. –Grip strength of the dominant hand is one of the criteria used in identifying frailty [1] because it is able to predict adverse health outcomes when combined with other outcome measures [171]. The equivalent criterion in the mouse is the inverted-cling grip test, a functional test for assessing the strength and the endurance. In this test, the mouse is required to activate the limb muscles to hold their body weight (strength) as long as possible (endurance). Based on the individual values, which range from 24 sec to 171 seconds (4-fold), it is likely the inverted-cling grip test alone would not be able to predict adverse function. However, because it is an easy, reliable assessment, and the potential of combining this assessment with the other frailty criteria, the inclusion of the inverted-cling grip test in the Frailty Index is necessary.

Walking speed.- In the human Frailty Index, the criterion of walking speed is determined by the 15' walking test [1]. This test is selected because walking speed is an assessment of physical function, especially mobility [172]. Slower walking speed represents a functional limitation [173,174] and it has been used as a predictor of poor geriatric outcomes, such as risk of fall, institutionalization, and mortality [175,176]. In mice, rotarod is a commonly used device for testing overall motor function (balance, coordination, endurance), seems to be a good match to the 15' walking test, and performance on the rotarod decreases with age [144,169,177,178]. Specifically, the rotarod test measures two parameters, speed and latency to fall. Although both parameters are valid, we selected the speed of the rotarod test for the

frailty criterion because it is a direct measurement of maximal walking speed before the mouse falls.

Physical activity. –The frailty criterion for activity levels is evaluated by the short version of the Minnesota Leisure Time Activity questionnaire, which covers most of the daily activities and estimates the calorie expenditure during 1 week [1]. To match this criterion, the physical activity of the mouse was determined by the daily voluntary wheel-running distance because it is an assessment widely used for quantifying the locomotor activity level [177,179]. Moreover, this measurement is a close match to the human physical activity measure because when a running wheel is provided in a mouse cage, the main energy expenditure is attributed to the voluntary running [179,180]. In this short report, this criterion did not independently identify an animal as frail using the designated cutoff point. Further evaluation of this criterion within the Frailty Index is needed because the activity levels were very low (0.51-2.93 km/d) in these 27- to 28-month-old mice compared with 19 months old (3.9 km/day) [181]. Moreover, it may be necessary to adjust the cutoff points such that each criterion has its own specific cutoff point, which is consistent with Fried's Frailty Index.

Endurance. –Another criterion in the Frailty Index by Fried's group is related to exhaustion or poor endurance. Exhaustion is determined by the self-reported CES-D Depression Scale (a valid questionnaire and an indicator for VO_2 max level and cardiovascular diseases) [1]. To match the clinical study, this short report used a derived endurance score from rotarod (duration in seconds the mouse stayed on the rotarod) and grip test, which is objective and measurable (impossible to ask a mouse if it is exhausted). Indeed, a biasing may exist in this criterion because the grip test is the same as the strength criterion. To avoid the potential for bias in the future, other behavioral measures might be considered such as running to exhaustion.

In summary, the four criteria we selected for the mouse Frailty Index functioned well because they are established measures of mouse physical functions and also match corresponding human criteria.

Frailty Index

Strengths of the identified Cutoff points. –In the study of Fried and coworkers, the lowest 20% in the cohort (bottom quintile) was used for most of the criteria (grip strength, walking speed, and activity level). These cutoff points are reasonable for the population investigated because they have been shown to predict hospitalization, mortality, first fall, worsening activities of daily living disability, and worsening morbidity disability. Because of our small sample size, using 20% of the cohort as our cutoff point was not reasonable and would likely identify a mouse as frail incorrectly. Therefore, we chose a more conservative primary cutoff point, 1.5 *SD* below the mean, because 1 *SD* is usually considered within the normal range (the main population, 68%). The 1.5 *SD* identifies the lowest 7%, a much more stringent percentile than the clinical measure (20%).

Definition of frail.- In the human Frailty Index designed and tested by Fried and coworkers, the frail identification (three or more criteria presented) has high predictive power for physical limitation, first hospitalization, first fall, worsening activities of daily living disability, and worsening mobility disability. In contrast, the presence of two criteria is identified as prefrail with significant prediction of outcomes, but with lower association [1].

Consistent with the human Frailty Index, the Frailty Index for mice included the presence of three or more of the criteria as frail and two criteria as mildly frail. However, this definition of frail is more conservative than that provided by Fried and coworkers because there are only four criteria (with a much lower cutoff point of the bottom 7%) and may underestimate the true number of frail or mild frail mice. In order to improve the identification of frail mice, the inclusion of another criterion would be beneficial. In summary, the selection of the cutoff point as 1.5 *SD* below the mean and the method of identifying frail or mildly frail mice match the human study, although being more conservative.

The frailty criteria demonstrated in this short report used the classic clinical frailty indicators; however, other frailty criteria require consideration, such as impaired cognition, balance, and gait patterns. These indicators have established protocols such as

objective recognition tests (cognition), raised beam test (balance), foot print analysis (gait), and dual-energy X-ray absorptiometry (body composition) ([182,183],[104]). This report is the beginning of Frailty Indices for mice. In order to test the validity of this Frailty Index, a longitudinal study is required with different ages, both genders, and short-lived and long-lived mouse strains. Moreover, the molecular and cellular mechanisms underlying frailty also need to be investigated in the future study.

Collectively, our Frailty Index provides a potential standardized definition for frailty in mice that is consistent with the operational definition of frailty in humans. The Frailty Index, thus, has potential use in future studies in molecular and cellular mechanisms underlying the process of frailty.

Funding

This study was supported by the National Institute of Aging at National Institutes of Health (R01 AG017768 to L.V.T, and T32 AG029796 and F31AG044108 to T.G.G.) and the University of Minnesota Center for Excellence in Critical Care Center grant (to L.V.T).

Acknowledgements

The authors thank Dr. Walter C. Low of the Department of Neurosurgery and Briana K. Jones of the Program in Physical Therapy (DPT) at University of Minnesota.

L.F.S. is now an Assistant Professor of Biology at Hamline University in St Paul, Minnesota.

FIGURES AND TABLES

Figure 1. Criterion 1: grip strength.

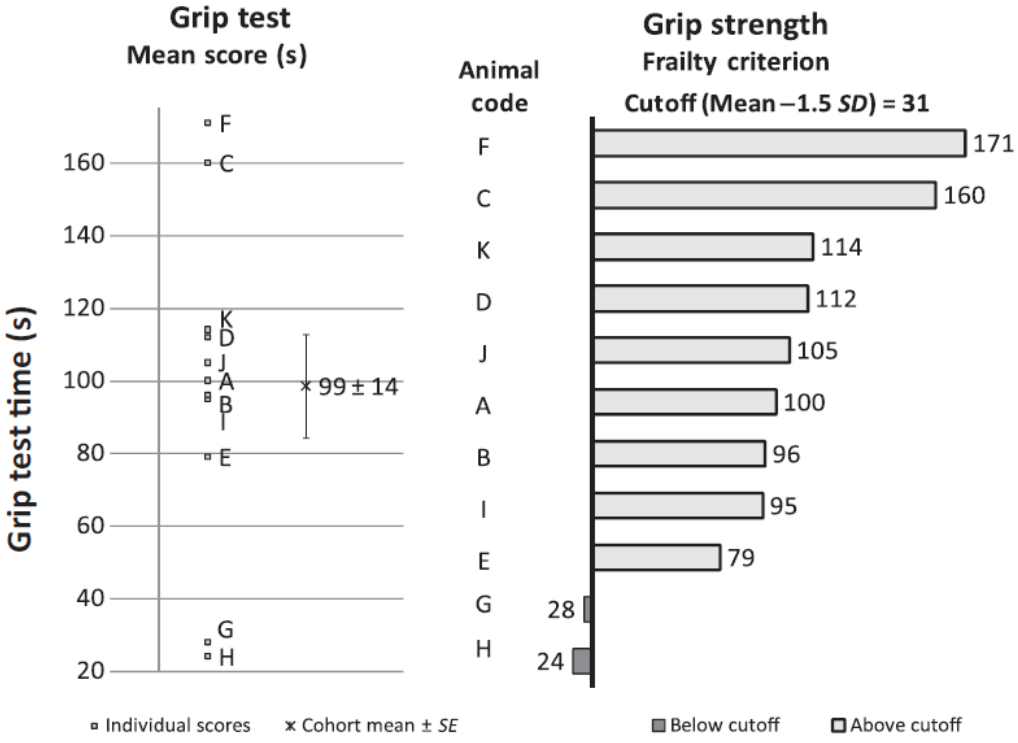

Left: A–K were individual grip test scores, in seconds, for each animal. The cohort mean of the grip test was 99±14 seconds. Right: the frailty criterion of the grip strength. Animals A–K were ranked from high to low (top to the bottom). The cutoff point was 31 seconds, 1.5 *SD* below the mean. The grip strength scores of animal H (24 seconds) and G (28 seconds) were below the 1.5 *SD* cutoff point (dark bars), whereas the remaining animals were above the cutoff point (light bars).

Figure 2. Criterion 2: walking speed.

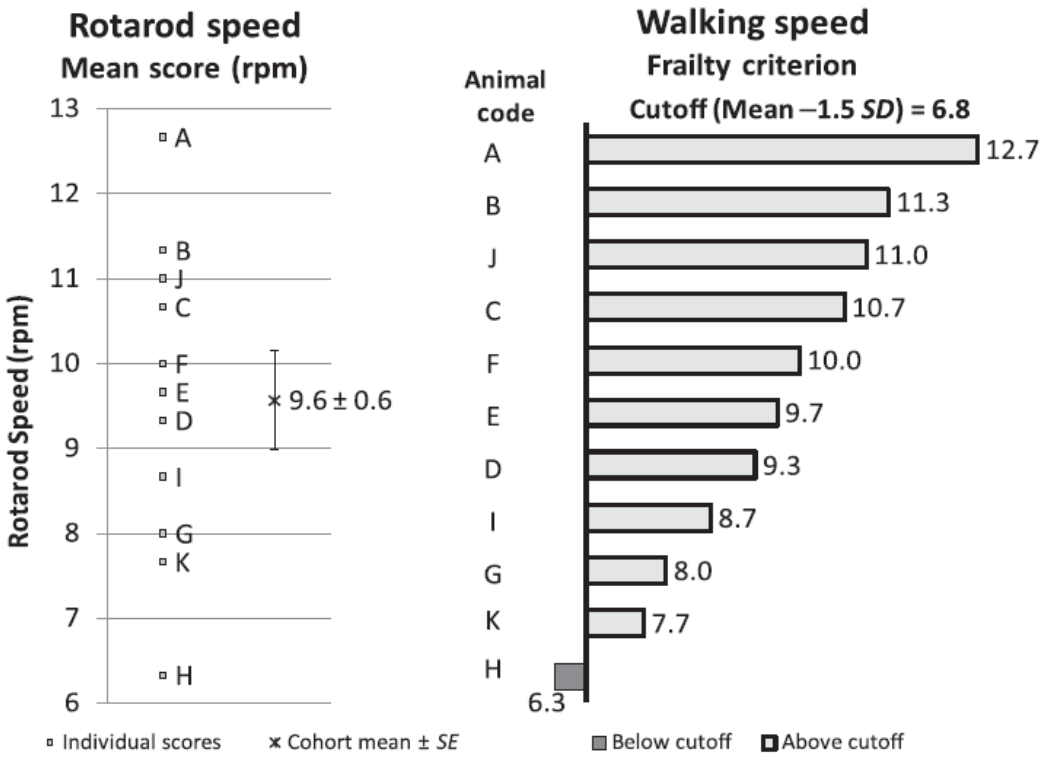

Left: A–K were individual rotarod speed, in rpm, for each animal. The cohort mean of the rotarod test was 9.6±0.6rpm. Right: the frailty criterion of walking speed. Animals A–K were ranked from high to low (top to the bottom). The cutoff point was 6.8rpm, 1.5 *SD* below the mean. The walking speed score of animal H (6.3rpm) was below the 1.5 *SD* cutoff point (dark bar), whereas for the remaining animals, it is above the cutoff point (light bars).

Figure 3. Criterion 3: physical activity.

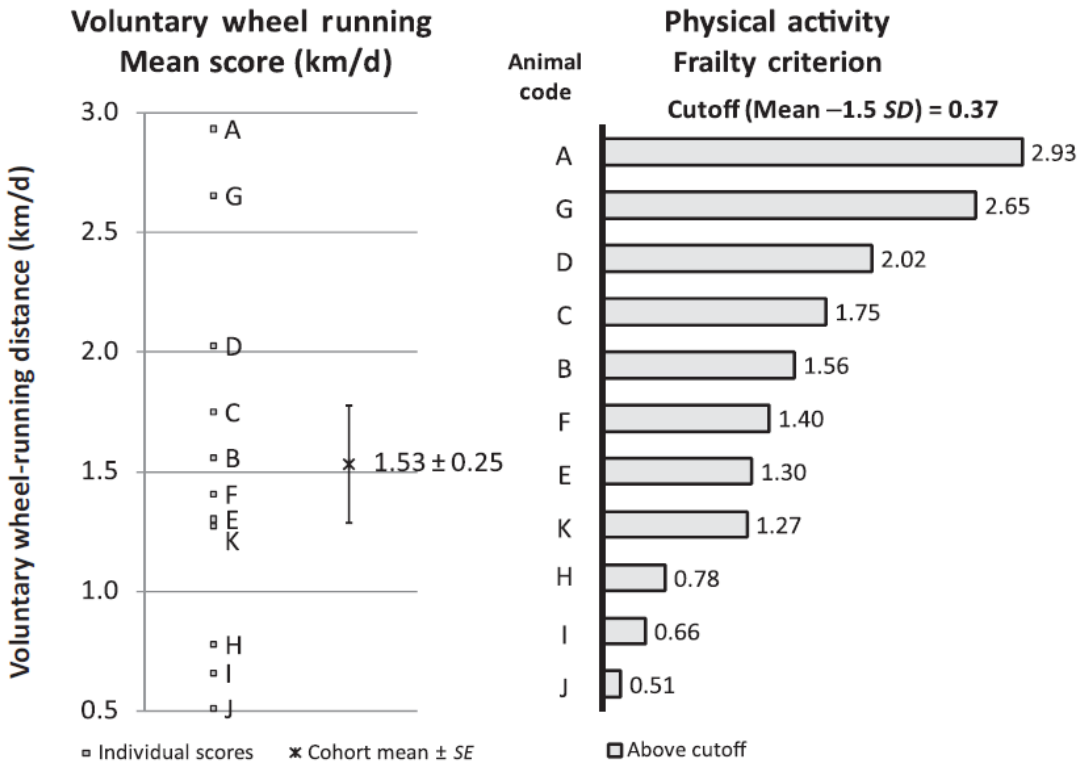

Left: A–K were individual voluntary wheel-running distances, in km/d, for each animal. The cohort mean of the voluntary wheel running was 1.53±0.25 km/d. Right: the frailty criterion of physical activity. Animals A–K were ranked from high to low (top to the bottom). The cutoff point was 0.37 km/d, 1.5 *SD* below the mean. The physical activity score of each mouse within our cohort was above the cutoff point (light bars).

Figure 4. Criterion 4: endurance.

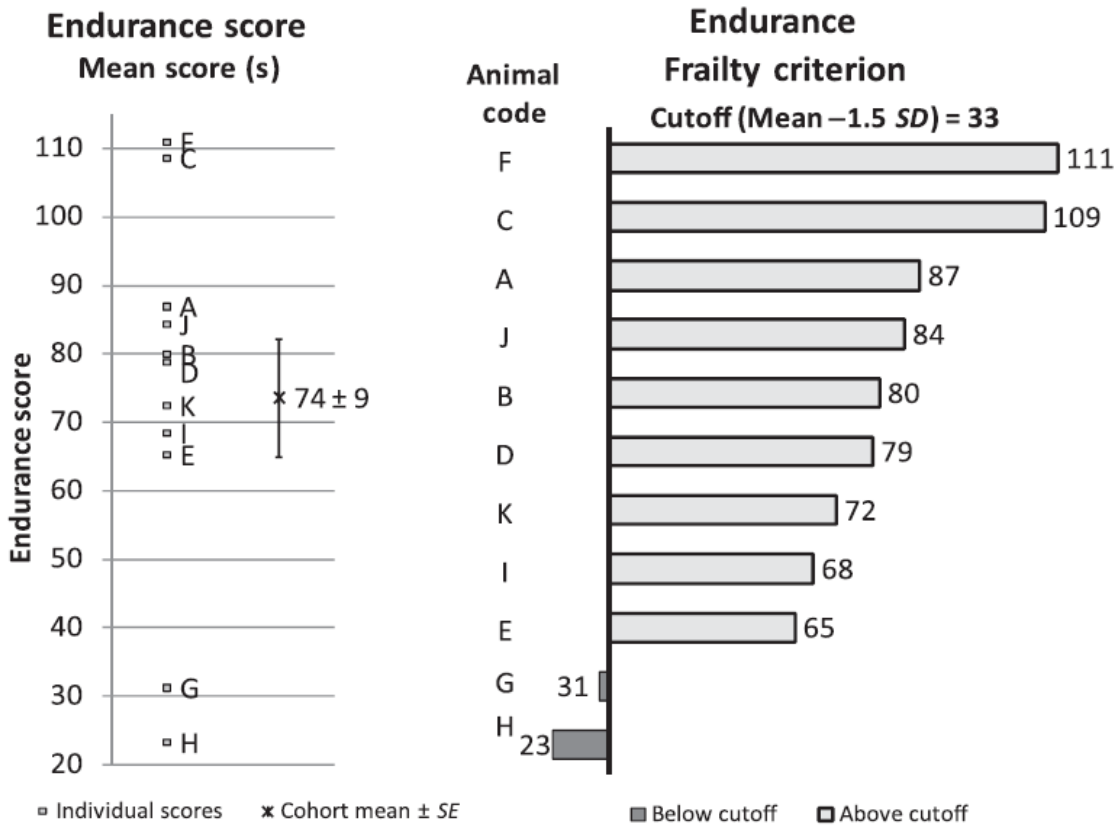

Left: A–K were individual endurance scores, in seconds, for each mouse. The cohort mean of the endurance score was 74±9 seconds. Right: the frailty criterion of endurance score. Mice A–K were ranked from high to low (top to the bottom). The cutoff point was 33 seconds, 1.5 *SD* below the mean. The endurance scores of mouse H (23 seconds) and mouse G (31 seconds) were below the 1.5 *SD* cutoff point (dark bars), whereas the remaining mice were above the cutoff point (light bars).

Table 1. Frailty Criteria.

Table 1. Frailty Criteria

Clinical Frailty Criteria*	Mouse Frailty Criteria	Approach
Weakness	Grip strength	Grip test (s)
Slowness	Walking speed	Rotarod test (revolution/min)
Low activity	Physical activity	Voluntary wheel running (km/d)
Poor endurance	Endurance	Grip test + rotarod (s)

Note: Each of the four frailty criteria identified by *Fried and coworkers (2001) is matched to a criterion for the mouse with the corresponding experimental approach.

Table 2. Determination of Frailty.

Table 2. Determination of Frailty

Cutoff Points of Each Criterion	Number of Criteria Below the Cutoff Point in Each Mouse		
Primary (1.5 *SD* below the mean)	≥3	2	None
Degree of frailty	Frail	Mildly frail	Nonfrail

Notes: The performance of each mouse is tested across the four criteria (described in Table 1) and designated a score for each criterion. For each criterion, a cutoff point, at 1.5 *SD* below the mean, was set to define frailty. A mouse was identified as frail if three or more of the criteria measures were below the cutoff point, whereas, mild frailty was designated if two fell below the cutoff.

Table 3. Frailty Identification.

Table 3. Frailty Identification

Criteria	Grip Strength (s)	Walking Speed (rpm)	Physical Activity (km/d)	Endurance (s)
Ranked from high to low	F	A	A	F
	C	B	G	C
	K	J	D	A
	D	C	C	J
	J	F	B	B
	A	E	F	D
	B	D	E	K
	I	I	K	I
	E	G	H	E
	G*	K	I	G*
	H*	H*	J	H*

Notes: The animals were ranked, by the scores of each criterion, from high to low. Animals were coded A–K.

*The score of the animals that fell below the 1.5 *SD* of the cohort specific criterion mean. These animals were identified as frail or mildly frail based on the determination of frailty (Table 2). Specifically, animal H was frail with three criteria below the cutoff points (grip strength, walking speed, and endurance). Animal G was mildly frail with two criteria below the cutoff points (grip strength and endurance).

CHAPTER VI. SUMMARY AND CONCLUSION

There are many clinical conditions where the patients have muscle atrophy such as peripheral nerve injury, immobilization, aging, cachexia and malnutrition. Muscle atrophy, a loss of muscle mass, occurs when protein degradation exceeds protein synthesis [4]. Muscle atrophy is associated with decreased muscle strength, which has potential to impair physical activities and the quality of life for individuals. Thus, understanding the cellular mechanisms behind the protein degradation may facilitate future pharmaceutical interventions.

Denervation (tibial nerve transection) is one of the most commonly used atrophy models in animal studies because it causes atrophy within a short period of time and the extent of atrophy is predictable. So far, several proteolytic systems have been characterized in response to denervation, including ubiquitin-proteasome system (UPS), autophagy/lysosomal, cathepsin L, and calpain etc. Because skeletal muscle is composed primarily of contractile proteins, the UPS has been the target of investigations. In the UPS, the proteasome functions like a "garbage disposal" for the contractile proteins (after ubiquitination). Briefly, proteasome is composed of regulatory complex and 20S core; whereas, the catalytic β subunits are the "choppers" for protein degradation via proteasome activities.

The studies reported in Chapter III demonstrate the major role of the proteasome in protein degradation following denervation.

The immunoproteasome, an inducible form of proteasome, has been less studied during conditions of muscle atrophy. The results in Chapter III demonstrate an increase in the immunoproteasome subunits (LMP2, LMP7, and MECL-1) following denervation; however, using immunoproteasome deficient mice (L7M1) the immunoproteasome was not essential for protein degradation. This finding did not support the stated hypothesis. The discussion highlights the potential physiological role of the immunoproteasome subunits during protein degradation. In particular, the composition of the subunits within

the 20S core appears to be influenced by deletion of the two immunoproteasome subunits. Future investigations are required to tease out the function of the immunoproteasome in subunit incorporation.

In Chapter IV, we focused on a bigger picture, muscle function and the UPS in response to denervation at 14 days. Muscle force production is reduced with denervation and this reduction is related to changes in the size of the muscle rather than protein quality. These findings support the role of UPS in protein quality surveillance.

Taken together, the first study demonstrated the insight of the standard and immuno-proteasome in protein degradation following denervation. It provides the evidences of immunoproteasome's functions in skeletal muscle atrophy. The second study described the upregulation of UPS and the associated muscle weakness following denervation, where the muscle quantity was affected rather than the quality. In summary, these two studies help us have a better understanding of the protein degradation system under the condition of loss of neural activity.

In Chapter V, frailty is the focus. Frailty is a clinical syndrome with multiple physiological and physical deficits that is highly associated with the age-related muscle atrophy (sarcopenia). In the population older than 80 years, the prevalence of frailty and sarcopenia are 22% and 23%, respectively [79,98]. To prevent and treat frailty in the older adult, it requires animal studies to bring the research from the bench to the bedside. However, in the field, few studies demonstrate a mouse frailty index closely-relevant to the clinical phenotype index. Thus, the third study in this dissertation is a report on developing a Frailty Index for mice. With this Frailty Index, the frail and mildly frail mice can be identified by assessing the physical and functional deteriorations within an old cohort. Using this Frailty Index, we found a 9% frailty prevalence in our old mice that is similar to the prevalence in age-equivalent humans (80-year old). Moreover, this finding provides a potential standardized definition for frailty in mice that is consistent with the operational definition of frailty in humans. To test the validity of this Frailty Index, future studies are required with different ages, both genders, and short-lived and long-lived mouse strains. In summary, our study on developing a clinically-relevant

Frailty Index provides the foundation for scientific studies in frail mice that will be translated into clinical settings eventually.

BIBLIOGRAPHY

1. Fried, L. P. *et al.* Frailty in older adults: evidence for a phenotype. *J. Gerontol. A. Biol. Sci. Med. Sci.* **56,** M146–56 (2001).

2. Rockwood, K., Stadnyk, K. & MacKnight, C. A brief clinical instrument to classify frailty in elderly people. *Lancet* **353,** 205–206 (1999).

3. Clegg, A., Young, J., Iliffe, S., Rikkert, M. O. & Rockwood, K. Frailty in elderly people. *Lancet* **381,** (2013).

4. Fanzani, A., Conraads, V. M., Penna, F. & Martinet, W. Molecular and cellular mechanisms of skeletal muscle atrophy: an update. *J. Cachexia. Sarcopenia Muscle* **3,** 163–79 (2012).

5. Cohen, S., Nathan, J. a. & Goldberg, A. L. Muscle wasting in disease: molecular mechanisms and promising therapies. *Nat. Rev. Drug Discov.* **14,** 58–74 (2014).

6. Tintignac, L. A., Brenner, H.-R. & Rüegg, M. A. Mechanisms Regulating Neuromuscular Junction Development and Function and Causes of Muscle Wasting. *Physiol. Rev.* **95,** 809–852 (2015).

7. Pennefather, P. & Quastel, D. M. Relation between subsynaptic receptor blockade and response to quantal transmitter at the mouse neuromuscular junction. *J Gen Physiol* **78,** 313–344 (1981).

8. Thompson, L. V. Age-related muscle dysfunction. *Exp. Gerontol.* **44,** 106–111 (2009).

9. Cohen, S. *et al.* During muscle atrophy, thick, but not thin, filament components are degraded by MuRF1-dependent ubiquitylation. *J. Cell Biol.* **185,** 1083–95 (2009).

10. Bonaldo, P. & Sandri, M. Cellular and molecular mechanisms of muscle atrophy. *Dis. Model. Mech.* **6,** 25–39 (2013).

11. Graber, T. G., Kim, J. H., Grange, R. W., McLoon, L. K. & Thompson, L. V. C57BL/6 life span study: Age-related declines in muscle power production and contractile velocity. *Age (Omaha).* **37,** (2015).

12. Romanick, M., Thompson, L. V. & Brown-Borg, H. M. Murine models of atrophy, cachexia, and sarcopenia in skeletal muscle. *Biochim. Biophys. Acta - Mol. Basis Dis.* **1832,** 1410–1420 (2013).

13. Masiero, E. *et al.* Autophagy is required to maintain muscle mass. *Cell Metab.* **10,** 507–15 (2009).

14. Lecker, S. H. *et al.* Multiple types of skeletal muscle atrophy involve a common program of changes in gene expression. *FASEB J.* **18,** 39–51 (2004).

15. Bardag-Gorce, F. Effects of ethanol on the proteasome interacting proteins. *World J. Gastroenterol.* **16,** 1349 (2010).

16. Husom, A. D. *et al.* Altered proteasome function and subunit composition in aged muscle. *Arch. Biochem. Biophys.* **421,** 67–76 (2004).

17. Ferrington, D. A., Husom, A. D. & Thompson, L. V. Altered proteasome structure, function, and oxidation in aged muscle. *FASEB J.* **19,** 644–6 (2005).

18. Bodine, S. C. *et al.* Identification of ubiquitin ligases required for skeletal muscle atrophy. *Science* **294,** 1704–8 (2001).

19. Gomes, M. D., Lecker, S. H., Jagoe, R. T., Navon, A. & Goldberg, A. L. Atrogin-1, a muscle-specific F-box protein highly expressed during muscle atrophy. *Proc. Natl. Acad. Sci. U. S. A.* **98,** 14440–5 (2001).

20. Reed, S. A., Sandesara, P. B., Senf, S. M. & Judge, A. R. Inhibition of FoxO transcriptional activity prevents muscle fiber atrophy during cachexia and induces hypertrophy. *FASEB J.* **26,** 987–1000 (2012).

21. Egerman, M. a & Glass, D. J. Signaling pathways controlling skeletal muscle mass.

Crit. Rev. Biochem. Mol. Biol. **49,** 59–68 (2014).

22. Milan, G. *et al.* Regulation of autophagy and the ubiquitin–proteasome system by the FoxO transcriptional network during muscle atrophy. *Nat. Commun.* **6,** 6670 (2015).

23. Gomes, A. V *et al.* Upregulation of proteasome activity in muscle RING finger 1-null mice following denervation. *FASEB J.* **26,** 2986–99 (2012).

24. Bodine, S. C. & Baehr, L. M. Skeletal Muscle Atrophy and the E3 Ubiquitin Ligases, MuRF1 and MAFbx/Atrogin-1. *Am. J. Physiol. Endocrinol. Metab.* **95616,** (2014).

25. Baehr, L. M., Furlow, J. D. & Bodine, S. C. Muscle sparing in muscle RING finger 1 null mice: response to synthetic glucocorticoids. *J. Physiol.* **589,** 4759–76 (2011).

26. Centner, T. *et al.* Identification of muscle specific ring finger proteins as potential regulators of the titin kinase domain. *J. Mol. Biol.* **306,** 717–726 (2001).

27. Lagirand-Cantaloube, J. *et al.* The initiation factor eIF3-f is a major target for Atrogin1/MAFbx function in skeletal muscle atrophy. *EMBO J.* **27,** 1266–1276 (2008).

28. Goodman, C. A., Mayhew, D. L. & Hornberger, T. A. Recent progress toward understanding the molecular mechanisms that regulate skeletal muscle mass. *Cell. Signal.* **23,** 1896–906 (2011).

29. Foletta, V. C., White, L. J., Larsen, A. E., Léger, B. & Russell, A. P. The role and regulation of MAFbx/atrogin-1 and MuRF1 in skeletal muscle atrophy. *Pflügers Arch. Eur. J. Physiol.* **461,** 325–35 (2011).

30. Glass, D. J. Signaling pathways perturbing muscle mass. *Curr. Opin. Clin. Nutr. Metab. Care* **13,** 225–229 (2010).

31. Tintignac, L. a *et al.* Degradation of MyoD mediated by the SCF (MAFbx) ubiquitin ligase. *J. Biol. Chem.* **280,** 2847–56 (2005).

32. Lokireddy, S. *et al.* Myostatin induces degradation of sarcomeric proteins through a Smad3 signaling mechanism during skeletal muscle wasting. *Mol. Endocrinol.* **25,** 1936–49 (2011).

33. Lokireddy, S. *et al.* Identification of atrogin-1-targeted proteins during the myostatin-induced skeletal muscle wasting. *AJP Cell Physiol.* **303,** C512–C529 (2012).

34. Sha, Z., Peth, A. & Goldberg, A. L. Keeping proteasomes under control--a role for phosphorylation in the nucleus. *Proc. Natl. Acad. Sci. U. S. A.* **108,** 18573–4 (2011).

35. Ferrington, D. a & Gregerson, D. S. Immunoproteasomes: structure, function, and antigen presentation. *Prog. Mol. Biol. Transl. Sci.* **109,** 75–112 (2012).

36. Furuya, N. *et al.* PARK2/Parkin-mediated mitochondrial clearance contributes to proteasome activation during slow-twitch muscle atrophy via NFE2L1 nuclear translocation. *Autophagy* **10,** 631–41 (2014).

37. Jamart, C. *et al.* Regulation of ubiquitin-proteasome and autophagy pathways after acute LPS and epoxomicin administration in mice. *BMC Musculoskelet. Disord.* **15,** 166 (2014).

38. Chen, C.-N. J., Graber, T. G., Bratten, W. M., Ferrington, D. A. & Thompson, L. V. Immunoproteasome in animal models of Duchenne muscular dystrophy. *J. Muscle Res. Cell Motil.* **35,** 191–201 (2014).

39. Fanin, M., Nascimbeni, A. C. & Angelini, C. Muscle atrophy in Limb Girdle Muscular Dystrophy 2A: A morphometric and molecular study. *Neuropathol. Appl. Neurobiol.* **39,** 762–771 (2013).

40. Angeles, A., Fung, G. & Luo, H. Immune and non-immune functions of the

immunoproteasome. *Front. Biosci. (Landmark Ed.* **17,** 1904–16 (2012).

41. Muchamuel, T. *et al.* A selective inhibitor of the immunoproteasome subunit LMP7 blocks cytokine production and attenuates progression of experimental arthritis. *Nat. Med.* **15,** 781–7 (2009).

42. Seifert, U. *et al.* Immunoproteasomes preserve protein homeostasis upon interferon-induced oxidative stress. *Cell* **142,** 613–24 (2010).

43. Arima, K. *et al.* Proteasome assembly defect due to a proteasome subunit beta type 8 (PSMB8) mutation causes the autoinflammatory disorder, Nakajo-Nishimura syndrome. *Proc. Natl. Acad. Sci. U. S. A.* **108,** 14914–9 (2011).

44. Kitamura, A. *et al.* A mutation in the immunoproteasome subunit PSMB8 causes autoinflammation and lipodystrophy in humans. *J. Clin. Invest.* **121,** 4150–60 (2011).

45. Zu, L. *et al.* Evidence for a role of immunoproteasomes in regulating cardiac muscle mass in diabetic mice. *J. Mol. Cell. Cardiol.* **49,** 5–15 (2010).

46. De, M. *et al.* B2 Subunit Propeptides Influence Cooperative Proteasome Assembly. *J. Biol. Chem.* **278,** 6153–6159 (2003).

47. Groettrup, M., Standera, S., Stohwasser, R. & Kloetzel, P. M. The subunits MECL-1 and LMP2 are mutually required for incorporation into the 20S proteasome. *Proc. Natl. Acad. Sci. U. S. A.* **94,** 8970–8975 (1997).

48. Hussong, S. a, Kapphahn, R. J., Phillips, S. L., Maldonado, M. & Ferrington, D. a. Immunoproteasome deficiency alters retinal proteasome's response to stress. *J. Neurochem.* **113,** 1481–90 (2010).

49. Schuld, N. J. *et al.* Immunoproteasome Deficiency Protects in the Retina after Optic Nerve Crush. *PLoS One* **10,** e0126768 (2015).

50. Opitz, E. *et al.* Impairment of immunoproteasome function by β5i/LMP7 subunit

deficiency results in severe enterovirus myocarditis. *PLoS Pathog.* **7,** e1002233 (2011).

51. Kingsbury, D. J., Griffin, T. A. & Colbert, R. A. Novel propeptide function in 20 S proteasome assembly influences ?? subunit composition. *J. Biol. Chem.* **275,** 24156–24162 (2000).

52. Batt, J. A. E. & Bain, J. R. Tibial Nerve Transection - A Standardized Model for Denervation-induced Skeletal Muscle Atrophy in Mice. *J. Vis. Exp.* (2013). doi:10.3791/50657

53. Greising, S. M. *et al.* Estradiol's beneficial effect on murine muscle function is independent of muscle activity. *J. Appl. Physiol.* **110,** 109–15 (2011).

54. Nagpal, P. *et al.* The ubiquitin ligase Nedd4-1 participates in denervation-induced skeletal muscle atrophy in mice. *PLoS One* **7,** e46427 (2012).

55. Jackman, R. W. & Kandarian, S. C. The molecular basis of skeletal muscle atrophy. *Am. J. Physiol. Cell Physiol.* **287,** C834–43 (2004).

56. Tang, H. *et al.* A Histone Deacetylase 4/Myogenin Positive Feedback Loop Coordinates Denervation-dependent Gene Induction and Suppression. *Mol. Biol. Cell* **20,** 1120–1131 (2009).

57. Cohen, T. J. *et al.* The histone deacetylase HDAC4 connects neural activity to muscle transcriptional reprogramming. *J. Biol. Chem.* **282,** 33752–33759 (2007).

58. Moresi, V. *et al.* Myogenin and Class II HDACs Control Neurogenic Muscle Atrophy by Inducing E3 Ubiquitin Ligases. *Cell* **143,** 35–45 (2010).

59. Tajrishi, M. M., Shin, J., Hetman, M. & Kumar, A. DNA Methyltransferase 3a and Mitogen-activated Protein Kinase Signaling Regulate the Expression of Fibroblast Growth Factor-inducible 14 (Fn14) during Denervation-induced Skeletal Muscle Atrophy. *J. Biol. Chem.* **289,** 19985–19999 (2014).

60. Choi, M.-C. *et al.* A direct HDAC4-MAP kinase crosstalk activates muscle atrophy program. *Mol. Cell* **47,** 122–32 (2012).

61. Zanelli, E., Zhou, P., Cao, H., Smart, M. K. & David, C. S. Genomic organization and tissue expression of the mouse proteasome gene Lmp-7. *Immunogenetics* **38,** 400–7 (1993).

62. Zhou, P., Zanelli, E., Smart, M. & David, C. Genomic organization and tissue expression of mouse proteasome gene Lmp-2. *Genomics* **16,** 664–8 (1993).

63. Tang, H. *et al.* mTORC1 Promotes Denervation-Induced Muscle Atrophy Through a Mechanism Involving the Activation of FoxO and E3 Ubiquitin Ligases. *Sci. Signal.* **7,** ra18 (2014).

64. Zhang, Y. & Manning, B. D. mTORC1 signaling activates NRF1 to increase cellular proteasome levels. *Cell Cycle* **14,** 2011–2017 (2015).

65. Pickering, A. M., Linder, R. a, Zhang, H., Forman, H. J. & Davies, K. J. a. Nrf2-dependent induction of proteasome and Pa28αβ regulator are required for adaptation to oxidative stress. *J. Biol. Chem.* **287,** 10021–31 (2012).

66. Sha, Z. & Goldberg, A. L. Proteasome-Mediated Processing of Nrf1 Is Essential for Coordinate Induction of All Proteasome Subunits and p97. *Curr. Biol.* **24,** 1573–1583 (2014).

67. Sandri, M. Protein breakdown in muscle wasting: role of autophagy-lysosome and ubiquitin-proteasome. *Int. J. Biochem. Cell Biol.* **45,** 2121–9 (2013).

68. O'Leary, M. F. N., Vainshtein, A., Carter, H. N., Zhang, Y. & Hood, D. a. Denervation-induced mitochondrial dysfunction and autophagy in skeletal muscle of apoptosis-deficient animals. *Am. J. Physiol. Cell Physiol.* **303,** C447–54 (2012).

69. Zhao, J. *et al.* FoxO3 Coordinately Activates Protein Degradation by the Autophagic/Lysosomal and Proteasomal Pathways in Atrophying Muscle Cells. *Cell Metab.* **6,** 472–483 (2007).

70. Moresi, V. *et al.* Histone deacetylases 1 and 2 regulate autophagy flux and skeletal muscle homeostasis in mice. *Proc. Natl. Acad. Sci.* **109,** 1649–1654 (2012).

71. Furuno, K., Goodman, M. N. & Goldberg, A. L. Role of different proteolytic systems in the degradation of muscle proteins during denervation atrophy. *J. Biol. Chem.* **265,** 8550–8557 (1990).

72. Bechet, D., Tassa, A., Taillandier, D., Combaret, L. & Attaix, D. Lysosomal proteolysis in skeletal muscle. *International Journal of Biochemistry and Cell Biology* **37,** 2098–2114 (2005).

73. Mayer, R. J. The meteoric rise of regulated intracellular proteolysis. *Nat. Rev. Mol. Cell Biol.* **1,** 145–148 (2000).

74. Lowell, B. B., Ruderman, N. B. & Goodman, M. N. Evidence that lysosomes are not involved in the degradation of myofibrillar proteins in rat skeletal muscle. *Biochem. J.* **234,** 237–240 (1986).

75. Nedergaard, A., Karsdal, M. A., Sun, S. & Henriksen, K. Serological muscle loss biomarkers: an overview of current concepts and future possibilities. *J. Cachexia. Sarcopenia Muscle* **4,** 1–17 (2013).

76. Yamazaki, Y. *et al.* The cathepsin L gene is a direct target of FOXO1 in skeletal muscle. *Biochem. J.* **427,** 171–8 (2010).

77. Sacheck, J. M. *et al.* Rapid disuse and denervation atrophy involve transcriptional changes similar to those of muscle wasting during systemic diseases. *FASEB J.* **21,** 140–155 (2007).

78. Huang, J. & Forsberg, N. E. Role of calpain in skeletal-muscle protein degradation. *Proc. Natl. Acad. Sci. U. S. A.* **95,** 12100–12105 (1998).

79. Rolland, Y. *et al.* Sarcopenia: its assessment, etiology, pathogenesis, consequences and future perspectives. *J. Nutr. Health Aging* **12,** 433–50 (2008).

80. Lexell, J. Human aging, muscle mass, and fiber type composition. *J. Gerontol. A. Biol. Sci. Med. Sci.* **50 Spec No,** 11–6 (1995).

81. Marzetti, E. & Leeuwenburgh, C. Skeletal muscle apoptosis, sarcopenia and frailty at old age. *Exp. Gerontol.* **41,** 1234–8 (2006).

82. Deschenes, M. R. Effects of aging on muscle fibre type and size. *Sports Med.* **34,** 809–24 (2004).

83. Walston, J. D. Sarcopenia in older adults. *Curr. Opin. Rheumatol.* **24,** 623–7 (2012).

84. Williams, G. N., Higgins, M. J. & Michael, D. Aging Skeletal Muscle : Physiologic. 62–68 (2002).

85. Chai, R. J., Vukovic, J., Dunlop, S., Grounds, M. D. & Shavlakadze, T. Striking denervation of neuromuscular junctions without lumbar motoneuron loss in geriatric mouse muscle. *PLoS One* **6,** (2011).

86. Joseph, A.-M. *et al.* The impact of aging on mitochondrial function and biogenesis pathways in skeletal muscle of sedentary high- and low-functioning elderly individuals. *Aging Cell* **11,** 801–9 (2012).

87. Beyer, I., Mets, T. & Bautmans, I. Chronic low-grade inflammation and age-related sarcopenia. *Curr. Opin. Clin. Nutr. Metab. Care* **15,** 12–22 (2012).

88. Narici, M. V. & Maffulli, N. Sarcopenia: Characteristics, mechanisms and functional significance. *British Medical Bulletin* **95,** 139–159 (2010).

89. Verdijk, L. B. *et al.* Satellite cell content is specifically reduced in type II skeletal muscle fibers in the elderly. *Am. J. Physiol. Endocrinol. Metab.* **292,** E151–E157 (2007).

90. Clark, B. C. & Manini, T. M. What is dynapenia? *Nutrition* **28,** 495–503 (2012).

91. Brooks, S. V & Faulkner, J. A. Contractile properties of skeletal muscles from

young, adult and aged mice. *J. Physiol.* **404,** 71–82 (1988).

92. Russ, D. W., Gregg-Cornell, K., Conaway, M. J. & Clark, B. C. Evolving concepts on the age-related changes in 'muscle quality'. *Journal of Cachexia, Sarcopenia and Muscle* **3,** 95–109 (2012).

93. Bigland-Ritchie, B. Muscle fatigue and the influence of changing neural drive. *Clin. Chest Med.* **5,** 21–34 (1984).

94. Lowe, D. a, Thomas, D. D. & Thompson, L. V. Force generation, but not myosin ATPase activity, declines with age in rat muscle fibers. *Am. J. Physiol. Cell Physiol.* **283,** C187–92 (2002).

95. Andersson, D. C. *et al.* Ryanodine receptor oxidation causes intracellular calcium leak and muscle weakness in aging. *Cell Metab.* **14,** 196–207 (2011).

96. Umanskaya, A. *et al.* Genetically enhancing mitochondrial antioxidant activity improves muscle function in aging. *Proc. Natl. Acad. Sci. U. S. A.* **111,** 15250–5 (2014).

97. Collard, R. M., Boter, H., Schoevers, R. a & Oude Voshaar, R. C. Prevalence of frailty in community-dwelling older persons: a systematic review. *J. Am. Geriatr. Soc.* **60,** 1487–92 (2012).

98. Morley, J. E. *et al.* Frailty consensus: a call to action. *J. Am. Med. Dir. Assoc.* **14,** 392–7 (2013).

99. Rockwood, K. *et al.* A global clinical measure of fitness and frailty in elderly people. *CMAJ* **173,** 489–95 (2005).

100. Mitnitski, A. *et al.* Age-related frailty and its association with biological markers of ageing. *BMC Med.* **13,** 161 (2015).

101. Rowlatt, C., Chesterman, F. C. & Sheriff, M. U. Lifespan, age changes and tumour incidence in an ageing C57BL mouse colony. *Lab. Anim.* **10,** 419–42 (1976).

102. Turturro, A., Duffy, P., Hass, B., Kodell, R. & Hart, R. Survival characteristics and age-adjusted disease incidences in C57BL/6 mice fed a commonly used cereal-based diet modulated by dietary restriction. *J. Gerontol. A. Biol. Sci. Med. Sci.* **57,** B379–89 (2002).

103. Turturro, A. *et al.* Growth curves and survival characteristics of the animals used in the Biomarkers of Aging Program. *J. Gerontol. A. Biol. Sci. Med. Sci.* **54,** B492–501 (1999).

104. Parks, R. J. *et al.* A procedure for creating a frailty index based on deficit accumulation in aging mice. *J. Gerontol. A. Biol. Sci. Med. Sci.* **67,** 217–27 (2012).

105. Howlett, S. E. & Rockwood, K. Factors that influence reliability of the mouse clinical frailty index. *J. Gerontol. A. Biol. Sci. Med. Sci.* **70,** 696 (2015).

106. Walston, J. *et al.* The physical and biological characterization of a frail mouse model. *J. Gerontol. A. Biol. Sci. Med. Sci.* **63,** 391–8 (2008).

107. Whitehead, J. C. *et al.* A clinical frailty index in aging mice: comparisons with frailty index data in humans. *J. Gerontol. A. Biol. Sci. Med. Sci.* **69,** 621–32 (2014).

108. Beharry, A. W. *et al.* HDAC1 activates FoxO and is both sufficient and required for skeletal muscle atrophy. *J. Cell Sci.* **127,** 1441–53 (2014).

109. Ferrington, D. a *et al.* Immunoproteasome responds to injury in the retina and brain. *J. Neurochem.* **106,** 158–69 (2008).

110. Maldonado, M. *et al.* Immunoproteasome deficiency modifies the alternative pathway of NFκB signaling. *PLoS One* **8,** e56187 (2013).

111. Graber, T. G., Ferguson-Stegall, L., Liu, H. & Thompson, L. V. Voluntary Aerobic Exercise Reverses Frailty in Old Mice. *Journals Gerontol. Ser. A Biol. Sci. Med. Sci.* **70,** 1–15 (2014).

112. Bonaldo, P. & Sandri, M. Cellular and molecular mechanisms of muscle atrophy.

Dis. Model. Mech. **6,** 25–39 (2013).

113. Loos, B., du Toit, A. & Hofmeyr, J.-H. S. Defining and measuring autophagosome flux-concept and reality. *Autophagy* **8627,** 37–41 (2014).

114. Lira, V. a *et al.* Autophagy is required for exercise training-induced skeletal muscle adaptation and improvement of physical performance. *FASEB J.* **27,** 4184–93 (2013).

115. Lecker, S. H., Solomon, V., Mitch, W. E. & Goldberg, A. L. Muscle Protein Breakdown and the Critical Role of the Ubiquitin- Proteasome Pathway in Normal and Disease States. *J. Nutr.* **129,** 227s–237s (1999).

116. Ostrowska, H., Kruszewski, K. & Kasacka, I. Immuno-proteasome subunit LMP7 is up-regulated in the ischemic kidney in an experimental model of renovascular hypertension. *Int. J. Biochem. Cell Biol.* **38,** 1778–85 (2006).

117. Quy, P. N., Kuma, A., Pierre, P. & Mizushima, N. Proteasome-dependent activation of mammalian target of rapamycin complex 1 (mTORC1) is essential for autophagy suppression and muscle remodeling following denervation. *J. Biol. Chem.* **288,** 1125–34 (2013).

118. Ju, J. S., Varadhachary, A. S., Miller, S. E. & Weihl, C. C. Quantitation of ‘autophagic flux’ in mature skeletal muscle. *Autophagy* **6,** 929–935 (2010).

119. Kisselev, A. F., Akopian, T. N., Castillo, V. & Goldberg, A. L. Proteasome active sites allosterically regulate each other, suggesting a cyclical bite-chew mechanism for protein breakdown. *Mol. Cell* **4,** 395–402 (1999).

120. Gomes-Marcondes, M. C. C., Smith, H. J., Cooper, J. C. & Tisdale, M. J. Development of an in-vitro model system to investigate the mechanism of muscle protein catabolism induced by proteolysis-inducing factor. *Br. J. Cancer* **86,** 1628–1633 (2002).

121. Raule, M., Cerruti, F. & Cascio, P. Enhanced rate of degradation of basic proteins

by 26S immunoproteasomes. *Biochim. Biophys. Acta - Mol. Cell Res.* **1843,** 1942–1947 (2014).

122. Walsh, M. E., Bhattacharya, A., Liu, Y. & Van Remmen, H. Butyrate prevents muscle atrophy after sciatic nerve crush. *Muscle Nerve* **52,** 859–868 (2015).

123. Dahlmann, B., Ruppert, T., Kuehn, L., Merforth, S. & Kloetzel, P. M. Different proteasome subtypes in a single tissue exhibit different enzymatic properties. *J. Mol. Biol.* **303,** 643–53 (2000).

124. Heinemeyer, W., Fischer, M., Krimmer, T., Stachon, U. & Wolf, D. H. The active sites of the eukaryotic 20 S proteasome and their involvement in subunit precursor processing. *J. Biol. Chem.* **272,** 25200–25209 (1997).

125. Arendt, C. S. & Hochstrasser, M. Identification of the yeast 20S proteasome catalytic centers and subunit interactions required for active-site formation. *Proc. Natl. Acad. Sci. U. S. A.* **94,** 7156–7161 (1997).

126. Cui, Z., Hwang, S. M. & Gomes, A. V. Identification of the immunoproteasome as a novel regulator of skeletal muscle differentiation. *Mol. Cell. Biol.* **34,** 96–109 (2014).

127. Gomes, A. V *et al.* Contrasting proteome biology and functional heterogeneity of the 20 S proteasome complexes in mammalian tissues. *Mol. Cell. Proteomics* **8,** 302–15 (2009).

128. Schiaffino, S., Dyar, K. A., Ciciliot, S., Blaauw, B. & Sandri, M. Mechanisms regulating skeletal muscle growth and atrophy. *FEBS J.* **280,** 4294–4314 (2013).

129. Magnusson, C., Svensson, A., Christerson, U. & Tågerud, S. Denervation-induced alterations in gene expression in mouse skeletal muscle. *Eur. J. Neurosci.* **21,** 577–80 (2005).

130. Jagoe, R. T. & Goldberg, A. L. What do we really know about the ubiquitin-proteasome pathway in muscle atrophy? *Curr. Opin. Clin. Nutr. Metab. Care* **4,**

183–190 (2001).

131. Solomon, V. & Goldberg, A. L. Importance of the ATP-ubiquitin-proteasome pathway in the degradation of soluble and myofibrillar proteins in rabbit muscle extracts. *J. Biol. Chem.* **271,** 26690–7 (1996).

132. Tawa, N. E., Odessey, R. & Goldberg, A. L. Inhibitors of the proteasome reduce the accelerated proteolysis in atrophying rat skeletal muscles. *J. Clin. Invest.* **100,** 197–203 (1997).

133. Attaix, D. *et al.* Mechanisms of ubiquitination and proteasome-dependent proteolysis in skeletal muscle. *Mol. Nutr.* 219–235 (2003).

134. Saeki, Y. & Tanaka, K. Assembly and function of the proteasome. *Methods Mol. Biol.* **832,** 315–337 (2012).

135. Kedar, V. *et al.* Muscle-specific RING finger 1 is a bona fide ubiquitin ligase that degrades cardiac troponin I. *Proc. Natl. Acad. Sci. U. S. A.* **101,** 18135–40 (2004).

136. Polge, C. *et al.* Muscle actin is polyubiquitinylated in vitro and in vivo and targeted for breakdown by the E3 ligase MuRF1. *FASEB J.* **25,** 3790–802 (2011).

137. Clarke, B. A. *et al.* The E3 Ligase MuRF1 Degrades Myosin Heavy Chain Protein in Dexamethasone-Treated Skeletal Muscle. *Cell Metab.* **6,** 376–385 (2007).

138. Fielitz, J. *et al.* Myosin accumulation and striated muscle myopathy result from the loss of muscle RING finger 1 and 3. *J. Clin. Invest.* **117,** 2486–95 (2007).

139. McElhinny, A. S., Kakinuma, K., Sorimachi, H., Labeit, S. & Gregorio, C. C. Muscle-specific RING finger-1 interacts with titin to regulate sarcomeric M-line and thick filament structure and may have nuclear functions via its interaction with glucocorticoid modulatory element binding protein-1. *J. Cell Biol.* **157,** 125–136 (2002).

140. Gregorio, C. C., Perry, C. N. & McElhinny, A. S. Functional properties of the

titin/connectin-associated proteins, the muscle-specific RING finger proteins (MURFs), in striated muscle. *J. Muscle Res. Cell Motil.* **26,** 389–400 (2005).

141. Medina, R., Wing, S. S. & Goldberg, A. L. Increase in levels of polyubiquitin and proteasome mRNA in skeletal muscle during starvation and denervation atrophy. *Biochem. J.* **307 (Pt 3,** 631–7 (1995).

142. Agbulut, O. *et al.* Slow myosin heavy chain expression in the absence of muscle activity. *Am. J. Physiol. Cell Physiol.* **296,** C205–14 (2009).

143. Paul, P. K. *et al.* Targeted ablation of TRAF6 inhibits skeletal muscle wasting in mice. *J. Cell Biol.* **191,** 1395–1411 (2010).

144. Graber, T. G., Ferguson-Stegall, L., Kim, J.-H. & Thompson, L. V. C57BL/6 Neuromuscular Healthspan Scoring System. *Journals Gerontol. Ser. A Biol. Sci. Med. Sci.* **68,** 1326–1336 (2013).

145. Baumann, C. W., Rogers, R. G., Gahlot, N. & Ingalls, C. P. Eccentric contractions disrupt FKBP12 content in mouse skeletal muscle. *Physiol. Rep.* **2,** 1–12 (2014).

146. Baumann, C., Rogers, R., Otis, J. & Ingalls, C. Recovery of strength is dependent on mTORC1 signaling after eccentric muscle injury. *Muscle Nerve (In Press.* (2016).

147. Graber, T. G., Kim, J.-H., Grange, R. W., McLoon, L. K. & Thompson, L. V. C57BL/6 life span study: age-related declines in muscle power production and contractile velocity. *Age (Dordr).* **37,** 9773 (2015).

148. Brooks, S. V & Faulkner, J. A. Contractile properties of skeletal muscles from young, adult and aged mice. *J. Physiol.* **404,** 71–82 (1988).

149. Mendez, J. & Keys, A. Density and Composition of Mammalian Muscle. *Metabolism* **9,** 184–188 (1960).

150. Thompson, L. V, Durand, D., Fugere, N. a & Ferrington, D. a. Myosin and actin

expression and oxidation in aging muscle. *J. Appl. Physiol.* **101,** 1581–1587 (2006).

151. Boudriau, S. *et al.* Remodeling of the cytoskeletal lattice in denervated skeletal muscle. *Muscle Nerve* **19,** 1383–90 (1996).

152. Batt, J. *et al.* Differential gene expression profiling of short and long term denervated muscle. *FASEB J.* **20,** 115–7 (2006).

153. Nakao, R., Yamamoto, S., Yasumoto, Y., Kadota, K. & Oishi, K. Impact of denervation-induced muscle atrophy on housekeeping gene expression in mice. *Muscle and Nerve* **51,** 276–281 (2015).

154. Salonen, V., Lehto, M., Kalimo, M., Penttinen, R. & Aro, H. Changes in intramuscular collagen and fibronectin in denervation atrophy. *Muscle Nerve* **8,** 125–31 (1985).

155. Viguie, C. A., Lu, D. X., Huang, S. K., Rengen, H. & Carlson, B. M. Quantitative study of the effects of long-term denervation on the extensor digitorum longus muscle of the rat. *Anat Rec* **248,** 346–354 (1997).

156. Ozawa, J. *et al.* Regulation of connective tissue remodeling in the early phase of denervation in a rat skeletal muscle. *Biomed. Res.* **34,** 251–8 (2013).

157. Patterson, M. F., Stephenson, G. M. M. & Stephenson, D. G. Denervation produces different single fiber phenotypes in fast- and slow-twitch hindlimb muscles of the rat. *Am. J. Physiol. Cell Physiol.* **291,** C518–28 (2006).

158. Midrio, M., Danieli-Betto, D., Megighian, A. & Betto, R. Early effects of denervation on sarcoplasmic reticulum properties of slow-twitch rat muscle fibres. *Pfl*[illegible]*gers Arch. Eur. J. Physiol.* **434,** 398–405 (1997).

159. Goldman, D., Brenner, H. R. & Heinemann, S. Acetylcholine receptor alpha-, beta-, gamma-, and delta-subunit mRNA levels are regulated by muscle activity. *Neuron* **1,** 329–33 (1988).

160. Yampolsky, P., Pacifici, P. G. & Witzemann, V. Differential muscle-driven synaptic remodeling in the neuromuscular junction after denervation. *Eur. J. Neurosci.* **31,** 646–658 (2010).

161. Shih, H. T., Wathen, M. S., Marshall, H. B., Caffrey, J. M. & Schneider, M. D. Dihydropyridine receptor gene expression is regulated by inhibitors of myogenesis and is relatively insensitive to denervation. *J. Clin. Invest.* **85,** 781–789 (1990).

162. Radzyukevich, T. L. & Heiny, J. a. Regulation of dihydropyridine receptor gene expression in mouse skeletal muscles by stretch and disuse. *Am. J. Physiol. Cell Physiol.* **287,** C1445–52 (2004).

163. Midrio, M. The denervated muscle: Facts and hypotheses. A historical review. *European Journal of Applied Physiology* **98,** 1–21 (2006).

164. Warren, G. L., Ingalls, C. P., Shah, S. J. & Armstrong, R. B. Uncoupling of in vivo torque production from EMG in mouse muscles injured by eccentric contractions. *J Physiol* **515 (Pt 2,** 609–619 (1999).

165. Ingalls, C. P., Warren, G. L., Zhang, J.-Z., Hamilton, S. L. & Armstrong, R. B. Dihydropyridine and ryanodine receptor binding after eccentric contractions in mouse skeletal muscle. *J. Appl. Physiol.* **96,** 1619–25 (2004).

166. Borisov, A. B., Huang, S. K. & Carlson, B. M. Remodeling of the vascular bed and progressive loss of capillaries in denervated skeletal muscle. *Anat. Rec.* **258,** 292–304 (2000).

167. Nemeth, P. M., Meyer, D. & Kark, R. A. Effects of denervation and simple disuse on rates of oxidation and on activities of four mitochondrial enzymes in type I muscle. *J. Neurochem.* **35,** 1351–60 (1980).

168. Aged Rodent Colonies Handbook | National Institute on Aging. at <http://www.nia.nih.gov/research/dab/aged-rodent-colonies-handbook/strain-survival-information>

169. Ingram, D. K. & Reynolds, M. A. Assessing the predictive validity of psychomotor tests as measures of biological age in mice. *Exp. Aging Res.* **12,** 155–62 (1986).

170. Arias, E. National Vital Statistics Reports. *Natl. Vital Stat. Syst.* **59,** (2011).

171. Syddall, H., Cooper, C., Martin, F., Briggs, R. & Aihie Sayer, A. Is grip strength a useful single marker of frailty? *Age Ageing* **32,** 650–6 (2003).

172. Whetstone, L. M. *et al.* The Physical Functioning Inventory: Procedure for Assessing Physical Function in Adults. *J. Aging Health* **13,** 467–493 (2001).

173. Bandeen-Roche, K. *et al.* Phenotype of Frailty: Characterization in the Women's Health and Aging Studies. *Journals Gerontol. Ser. A Biol. Sci. Med. Sci.* **61,** 262–266 (2006).

174. Woo, J., Ho, S. C. & Yu, A. L. Walking speed and stride length predicts 36 months dependency, mortality, and institutionalization in Chinese aged 70 and older. *J. Am. Geriatr. Soc.* **47,** 1257–1260 (1999).

175. Woo, J., Leung, J. & Morley, J. E. Comparison of frailty indicators based on clinical phenotype and the multiple deficit approach in predicting mortality and physical limitation. *J. Am. Geriatr. Soc.* **60,** 1478–86 (2012).

176. Viccaro, L. J., Perera, S. & Studenski, S. a. Is timed up and go better than gait speed in predicting health, function, and falls in older adults? *J. Am. Geriatr. Soc.* **59,** 887–92 (2011).

177. Brooks, S. P. & Dunnett, S. B. Tests to assess motor phenotype in mice: a user's guide. *Nat. Rev. Neurosci.* **10,** 519–29 (2009).

178. Ingram, D. K., Archer, J. R., Harrison, D. E. & Reynolds, M. A. Physiological and behavioral correlates of lifespan in aged C57BL/6J mice. *Exp. Gerontol.* **17,** 295–303 (1982).

179. Harri, M. *et al.* Effect of access to a running wheel on behavior of C57BL/6J mice.

Lab. Anim. Sci. **49,** 401–5 (1999).

180. Novak, C. M., Burghardt, P. R. & Levine, J. a. The use of a running wheel to measure activity in rodents: relationship to energy balance, general activity, and reward. *Neurosci. Biobehav. Rev.* **36,** 1001–14 (2012).

181. van Praag, H., Shubert, T., Zhao, C. & Gage, F. H. Exercise enhances learning and hippocampal neurogenesis in aged mice. *J. Neurosci.* **25,** 8680–5 (2005).

182. Sternberg, S. S. A., Schwartz, A. W., Karunananthan, S., Bergman, H. & Mark Clarfield, A. The identification of frailty: a systematic literature review. *J. Am. Geriatr. Soc.* **59,** 2129–2138 (2011).

183. Fahlström, A., Yu, Q. & Ulfhake, B. Behavioral changes in aging female C57BL/6 mice. *Neurobiol. Aging* **32,** 1868–80 (2011).